NIST United States Department of Commerce
National Institute of Standards and Technology

NIST
PUBLICATIONS

NIST Technical Note 1287

High Resolution Diffraction Imaging of Crystals Grown in Microgravity and Closely Related Terrestrial Crystals

B. Steiner, R. Dobbyn, D. Black, H. Burdette, M. Kuriyama,
R. Spal, L. van den Berg, A. Fripp, R. Simchick, R. Lal,
A. Batra, D. Matthiesen, and B. Ditchek

QC
100
.U5753
#1287
1991
C.2

QC100
.U5753
#1287
1991
c.2

NIST Technical Note 1287

High Resolution Diffraction Imaging of Crystals Grown in Microgravity and Closely Related Terrestrial Crystals

B. Steiner
R. Dobbyn
D. Black
H. Burdette
M. Kuriyama
R. Spal

National Institute of Standards and Technology
Gaithersburg, MD 20899

August 1991

L. van den Berg
EG&G Energy Measurements

A. Fripp
R. Simchick*
NASA Langley Research Center

R. Lal
A. Batra
Alabama A&M University

D. Matthiesen
B. Ditchek
GTE Laboratories

* Lockheed Engineering and Sciences Co.
Hampton, VA

U.S. Department of Commerce
Robert A. Mosbacher, Secretary

National Institute of Standards and Technology
John W. Lyons, Director

National Institute of Standards
and Technology
Technical Note 1287
Natl. Inst. Stand. Technol.
Tech. Note 1287
162 pages (Aug. 1991)
CODEN: NTNOEF

U.S. Government Printing Office
Washington: 1991

For sale by the Superintendent
of Documents
U.S. Government Printing Office
Washington, DC 20402

EXECUTIVE SUMMARY

This paper reports on irregularities found in three crystals grown in space, in four crystals grown entirely on the ground, and compares the two sets. Irregularities have been observed in mercuric iodide, lead tin telluride, triclycine sulfate, and gallium arsenide by high resolution synchrotron x-radiation diffraction imaging.

Radiation detectors made from mercuric iodide crystals grown in microgravity have been reported to perform far better than conventional detectors grown from the same material under full gravity. Effort is now underway to reproduce these "space" crystals, optimize their properties, and extend comparable superiority to other types of material.

Interest in space crystals arises in another way as well. Increase in the local regularity of protein crystals through growth in space would lead to more precise knowledge of their chemical structure. This, in turn, would provide greatly increased efficiency in the tailoring of drugs specifically designed to interact with particular chemical groups.

For advances both in superior devices and in tailored drugs, observation of crystal irregularity is essential, first to provide fundamental scientific insight, then to optimize expensive space growth, and ultimately to establish superior growth conditions in far less extreme and more economical environments.

Determination of the specific factors responsible for the extraordinary character of space crystals thus should have far-reaching scientific, industrial, and health implications. Insight into characteristic irregularities is essential to the predictable growth of optimum crystals, both in space and on the ground. What is required is determination of the specific nature of the mesoscopic irregularities in these crystals, their level of incidence, and their distribution.

Recent advances in diffraction imaging with highly parallel monochromatic synchrotron x-radiation now offer the chance to take major steps toward these ends. We find ourselves in a position, given suitable samples, to develop comprehensive understanding both of the nature of the special structures associated with crystals grown in space and of their genesis and control.

In order to accelerate the realization of these opportunities, long term collaboration has been initiated between investigators

associated with the NASA Microgravity Sciences and Applications Division and synchrotron radiation scientists in the NIST Materials Science and Engineering Laboratory. This collaboration is designed to accomplish three specific goals:

1) Establishment of a base line of mesoscopic structural information on those crystals of greatest importance to the space program;

2) Correlation of observed variation in characteristics with observed features in the mesoscopic structure;

3) Determination of conditions optimum for growth, both on the ground and in microgravity.

At the request of the Microgravity Sciences and Applications Division, the effort the first year focused on three distinct activities. The first of these established a systematic approach to the achievement of these ends through dialogue with each of 49 principal investigators in the NASA Microgravity Program directly related to crystal growth. The second activity inaugurated collaborative research on four materials of particular urgency. The third activity advanced the capability of quasi-real-time diffraction imaging.

Systematic interaction with the various principal investigators was required because of the large number of crystal growth factors to which diffraction imaging might contribute. As a result of this dialogue, areas that should benefit most from information on mesoscopic structural irregularity have been delineated and planning initiated. Through this dialogue, we have confirmed the promise of high-resolution mesoscopic structural information for each of the 13 projects in which the successful growth of extensive high-quality monolithic crystals is an immediate goal. Another 15 investigators want to explore the applicability of high resolution diffraction imaging to the novel systems on which they are working; these would require extension of high resolution diffraction imaging techniques, which to date have addressed relatively large, monolithic, high-quality crystals.

These 28 projects and their requirements for mesoscopic structural information are identified here. Most of the members of this large group consider the information of such central value to their research programs that their commitment extends beyond the offer of characteristic samples to active participation in the diffraction imaging experiments. This interest should ensure that full advantage of the diffraction imaging is achieved. However, the number of technical questions on which work is contemplated is clearly larger than can be accommodated within the scope of the current program.

As a result of the initial dialogue with NASA and its crystal growers, seven crystals were selected from four different materials for immediate imaging. Important, unanticipated observations have been made on each of the four. For two of these, mercuric iodide and lead tin telluride, more than one phase (an array of non diffracting inclusions) was observed in terrestrial samples; but the formation of these multiple phases appears to have been strongly suppressed in the comparable crystals grown in microgravity. The third terrestrial material examined, triglycine sulfate, displayed an unexpected layered structure. The fourth terrestrial material, gallium arsenide, revealed a mesoscopic structure substantially different from that of the seed.

These differences, varying in fundamental ways from material to material, are described in section VII. The reduction in multiphase formation in microgravity appears to be associated in one of the two cases with gradual changes in the lattice over a distance of millimeters. These results together support independent observations that extreme lattice regularity may be less important in influencing device performance than other factors: multiple phases may limit this performance severely. The passage of 5 years since the growth of the space crystals that have been observed and the fabrication of a device from one of these may have influenced some of these observations, however. Important thrusts of further investigation clearly would address questions of aging and the role of device fabrication.

In addition to our observation of crystals grown 5 years ago, we have observed also two recently grown crystals for subsequent comparison with crystals to be grown in flight experiments scheduled for this fall. Results on one of these coincide with the recent observation that increases in purity can dramatically improve device performance.

Immediate examination of all seven crystals that we have examined has proved to be especially valuable for the guidance that it provides for the suitable treatment of materials to be grown in subsequent flights as well as for the fundamental insights into the nature, the genesis, and the importance of various irregularities. The wisdom of an accelerated pace for the first experimental phase of this collaboration thus has been borne out.

CONTENTS

I. INTRODUCTION

A. The Work Covered in this Study

This paper reports on irregularities found in three crystals grown in space, in four crystals grown entirely on the ground, and compares the two sets. Irregularities have been observed in mercuric iodide, lead tin telluride, triclycine sulfate, and gallium arsenide by high resolution synchrotron x-radiation diffraction imaging.

B. Crystal Growth in Microgravity

The performance of materials is determined by their structure; in this performance, irregularity typically plays a leading role. The growth of materials in microgravity has long been of interest because of the anticipation that reduction in gravitational forces would strongly affect crystal growth and therefore the nature of the resulting irregularity. Both buoyancy-driven convection and loading on the warm boule are of potential importance[1][2]. Reports of early space crystal growth experiments indeed bore out this expectation; mercuric iodide crystals grown in microgravity were found to be so superior to comparable crystals grown on the ground [1][2] that reproduction and optimization of the properties of these crystals and the extension of these advantages to other types have stimulated great interest.

However, because many factors affect crystal growth, and because these can interact strongly with one another, the understanding of the structural variation necessary for its effective exploitation has not yet been achieved. Determination of the specific factors responsible for the reported superiority of some crystals grown in space remains an exciting challenge, with far-reaching scientific, industrial, and health implications. Knowledge of the irregularities in these materials, developed in conjunction with an understanding of their genesis and detailed affects on properties, would be an important intellectual achievement. Such knowledge is expected also to contribute to dramatically improved single crystal production, both in space and on the ground.

C. Types of Interest

Interest in "space" crystals arises in two distinct ways. In some instances, the performance of devices made from space-grown crystals has been reported to be far superior to similar devices made from similar ground-grown material. One example has just been noted. In x-ray and gamma-ray detectors made from mercuric iodide, the mobility of charge carriers in detectors made from space-grown crystals was at least six times as high as that for similar detectors made from ground-grown crystals [1][2]. This is expected to lead to increased energy resolution in radiation detectors made from this material.

In other instances, crystallographers have found dramatic increases in the regularity and in the morphology and size of crystals grown in space [3], which promise more precise knowledge of the chemical structure of complex proteins. This, in turn, should provide greatly increased efficiency in the fabrication of drugs designed to interact with particular chemical groups. In principle, the requisite knowledge of structural chemistry can be achieved through crystallographic structural determination of high-quality protein specimens. However, this work has been seriously impeded by the absence of specimens with sufficient regularity for effective structural analysis. Growth of proteins in space promises to address this difficulty and thus to accelerate substantially the realization of effective drugs.

Two events have led to widespread optimism that this promise will be realized. Several years ago, liquid-liquid diffusion experiments carried out in Spacelab I produced larger crystals than crystals grown on the ground by the same technique [4]. More recently, vapor diffusion growth of isocitrate lyase on space shuttle flight STS 26 achieved a dramatic increase in the regularity of the crystal morphology. This flight produced prism-like crystals, while material grown in a similar manner on the ground forms only dendritic clusters [3]. Moreover, two of the crystals obtained on this flight were substantially larger than those produced in any ground experiments. Most important, the quality of crystals from this flight is such that they diffract "to higher resolution than the best crystals obtained under similar conditions on Earth" [3]. Improvement in the regularity of such proteins through growth in microgravity thus is expected to facilitate greatly the determination of their chemical structure. The saving in time and effort in the testing of potential new drugs that can be achieved by precise structural chemical knowledge of the active protein sites has led to experimentation in the growth of exceptionally regular proteins in space.

In summary, the design both of better devices and of more effective drugs requires knowledge of crystal regularity. Irregularity in these materials is of great interest, first for the

scientific insight that it presages, then for the optimization of expensive space growth, and ultimately for the establishment of desirable growth conditions in far less extreme and expensive environments.

D. Mesoscopic Structure

Determination of the specific nature of the mesoscopic irregularities in these materials, their level of incidence, and their distribution in space-grown and comparable terrestrial materials is now required. Fortunately, recent technical advances in diffraction imaging with high resolution monochromatic synchrotron x-radiation present a timely opportunity to achieve all of these ends [5][6][7].

The appeal of high-resolution synchrotron radiation diffraction imaging of proteins is further enhanced by the fact that the "performance parameter" of particular interest in these proteins is their structural diffraction pattern in synchrotron x-ray beams. The question naturally arises, "Can high-resolution synchrotron diffraction imaging of x-radiation contribute to the improvement of the best methods of chemical structure determination, which also utilize diffraction of synchrotron radiation?"

Structural irregularity in all of these materials need to be observed, interpreted, and understood in terms of the various stages of crystal growth so that growth can be controlled in a more reliable fashion. These structural variations must then be correlated with observed anomalies in the characteristics of the crystals so that the new control that is achieved can be guided in an effective way.

The requirements for obtaining such structural information are reviewed in section II. The recently developed ability to meet these requirements is reviewed in section III. As a result of our current capability, we are in a position, given suitable samples, to develop a comprehensive understanding of the nature of the special structures associated with materials grown in space and their genesis and control.

The current collaboration between investigators associated with the National Aeronautics and Space Administration (NASA) Microgravity Sciences and Applications Division and synchrotron radiation scientists in the National Institute of Standards and Technology (NIST) Materials Science and Engineering Laboratory has been initiated in order to provide this information in a timely and systematic way. Specific areas for this collaboration have been defined and effort in several of these inaugurated. This work is geared to the following goals [8]:

1) Establishment of a reference base line of structural information on crystals of particular importance to the space program;

2) Correlation of observed differences in performance with mesoscopic structure;

3) Determination of conditions optimum for growth, both on the ground and in microgravity.

E. Initial Program Foci

Under the direction of the Microgravity Sciences and Applications Division, the collaborative effort in its first year has been focused on three activities. The first of these established a systematic approach to the ends just enumerated, through dialogue with each of NASA's principal investigators working on crystal growth. These scientists are addressing a comprehensive variety of crystal growth factors, including both space growth and terrestrial growth. As a result they have broad interest in the determination of mesoscopic structural irregularity. Following the dialogue that has now been established, specific areas for the exploration of irregularity have been defined (sec. IV); planning and the preparation of suitable samples have been initiated.

The second activity initiated imaging of four materials for which samples were already available and which were considered most urgent by the NASA Microgravity Sciences and Applications Division. These four materials are described in section V; they include early space-grown crystals and closely related crystals of particular interest, which had been retained in anticipation of just such an opportunity.

The first two inorganic crystals grown in space and comparable ground controls present interesting mesoscopic differences, shown in section VI. These differences are profound in the case of mercuric iodide, and more subtle, but perhaps equally important, in the case of lead tin telluride. One space-grown organic crystal, triglycine sulfate, was also examined and found to have been seeded by a nominally monolithic crystal layered in a manner not previously observed. The passage of time since the growth of these crystals, about 5 years, and the fabrication of a device from one of these, may have played a crucial role in some of these observations. Implications of the diffraction images are discussed in section VII. Further investigation is clearly required in order to separate questions on aging and the role of device fabrication from those of initial crystal growth and subsequent handling.

In preparation for flights scheduled for this fall, we have observed also two crystals for comparison with crystals to be grown then: one, mercuric iodide; and the other, gallium arsenide. Images of these crystals are included also in sections VI and VII, where the implications of their observed structure are discussed. Another crystal of importance for the fall flight schedule, triglycine sulfate, was made available by the crystal grower, but arrived too late for examination in the current series of experiments.

The effectiveness of future work in high resolution diffraction imaging will be substantially enhanced by the application of recently available image magnifiers and detectors. Increase in spatial resolution below 1μm is now feasible in quasi-real-time and would permit greatly increased effectiveness in the study of specific details of particular interest to the crystal grower. This capability would also greatly accelerate various stages of the analysis and permit electronic image manipulation as well. Realization of these goals requires more sensitive sample control. These improvements are described in section VIII.

F. Guidance for Future Work

Issues central to future activity are discussed in section IX. Our initial examination of crystals at this particular time has proven to be especially valuable because of the important guidance that it provides for the suitable treatment of crystals to be grown this fall and in subsequent flights.

II. IMAGING REQUIREMENTS

A. General Considerations

X-Ray topography has long promised the type of information on structural irregularities that is required both for fundamental insight into the nature of performance anomalies and for development of understanding of the origins of these irregularities in crystal growth. However, if this information had indeed been accessible it would already have permitted optimization of the various performance parameters that are accorded high priority.

A principal impediment has been x-ray beam divergence. Individual irregularities and the immediately surrounding matrix in a typical crystal are illuminated by laboratory x-ray sources over an angular range measured in arc minutes. The divergence of this incoming beam (at a given point on the sample) unfortunately supports diffraction simultaneously from many irregularities along with that from the surrounding regular regions. The spread in wavelength in white beam synchrotron radiation also supports diffraction simultaneously from irregular and regular regions. In both instances, contrast that would otherwise be present is severely reduced or eliminated entirely. Even where some contrast remains, the spatial information contained is convoluted in a way that will not permit unfolding and subsequent detailed analysis.

Lattice deviations influencing diffraction by seconds of arc, which are frequently critical to satisfactory interpretation and understanding of mesoscopic irregularity, are rendered visible in diffraction only by a source of monochromatic radiation parallel within an arc second. In such a beam, spatial fidelity also is preserved at the micrometer level. The recent availability of such a source of x-radiation thus now permits the realization of the long term promise of x-ray topography.

Where such a beam is available, the complete analysis of a crystal depends on the unobstructed observation of diffraction in Bragg and Laue geometries in all critical diffraction orientations. Such observation, in turn, places several requirements on the sample itself:

* The *thickness* of the crystal may limit observation in Laue geometry. Successful diffraction from a typical, optically thick crystal in Laue geometry depends on anomalous transmission by means of dynamical diffraction

which is determined by the crystal quality. For high-quality crystals, thickness of the order of a half millimeter is suitable.

* The *orientation* of the sample surfaces may restrict observation in either Bragg of Laue geometry. If the surface orientation is not close to a low index crystallographic plane, it can severely restrict the accessibility of diffraction critical to effective analysis and thus the detailed strain visibility analysis that can be carried out.

* The *condition of the surface* can limit the analysis of growth related irregularity even when diffraction is observed. While the residual strain from scratches can provide useful orientation in the comparison of images, where such strains dominate an image only a restricted analysis of growth-related features is possible. Crystal growers are sometimes surprised and distressed to observe the amount of residual strain from such scratches that is revealed by high-resolution diffraction imaging.

* The principal remaining requirement is that the various irregularities not interfere severely with one another. This requirement places a limit on the *density of irregularities*, although this limit depends strongly on the particular nature of the irregularities that are present, to which we turn now.

B. Lattice Orientation and Strain

Of the various types of irregularity in high-quality crystals, perhaps the most pervasive is gradual change in the lattice. The orientation of the lattice or the magnitude of the lattice parameter, or both, may vary. For any one orientation of the crystal with respect to the diffracting beam, such variation results in diffraction only from a portion of a single grain.

In some systems, such as the Czochralski growth of doped material, this variation is oscillatory, leading to striations in diffraction images of crystals cut obliquely to the local growth direction and oriented slightly off of the Bragg condition. Contrast is inverted on opposite sides of the Bragg peak. Like tree rings, these striations record, not only variation in chemical composition but, taken together, also the shape of the crystal at various stages in its growth; they can be deciphered in a somewhat similar if more complex and sophisticated manner [5][9].

Diffraction from grains whose lattice orientation or parameter varies monotonically or aperiodically yields images of restricted regions of a single grain. The part of such a grain that is in diffraction shifts as the crystal is rotated in the Bragg direction. The moving edge of this image is characteristically soft and relatively indistinct.

C. Grain and Subgrain Boundaries

Sharp contrast in the image of a crystal can delineate homogeneous grains or subgrains. In contrast to the preceding case, the boundaries of such an image do not move as the crystal is rotated in the Bragg direction. Where the lattice orientation of a pair of such homogeneous grains differs by rotation in the diffraction plane by more than the acceptance angle, only one of these grains (or subgrains) will diffract at a time; and, if it is not strained, it does so in its entirety. Variations in real-time images of such a crystal permit rapid and detailed assessment of the relative misorientation (in the Bragg direction) of the various grains and subgrains with respect to one another.

Where the lattice orientation of a pair of such contiguous grains differs in a direction orthogonal to the plane of diffraction, both grains may appear in diffraction simultaneously, but the resulting images are displaced with respect to one another in this direction. The pair of these images is either separated or overlapped, depending on the relative inclination of the two lattices.

The boundary of an individual grain or subgrain may end up strained with respect to the interior of the grain. In this case, diffraction from the boundary will generally contrast with that from the bulk grain, permitting the boundary image to be distinguished from that of the grain.

D. Dislocations

Dislocations typically appear in diffraction images taken in Laue geometry (transmission) as linear features that are broader at one end than the other. The broadening of one end of such a feature arises from scattering deep within the crystal, while the sharp end locates the intersection of the dislocation with the x-ray exit surface of the crystal. The orientation of a dislocation can be determined with high precision for those cases in which the intersection of the dislocation with both entrance and exit faces is distinct in the diffraction image.

Variation in the visibility of such a line feature in successive diffraction images indicates the direction of atomic displacement associated with the dislocation, which is parallel to its Burgers vector. However, since the visibility of such a dislocation varies relatively slowly, that is, as the cosine of the angle between the Burgers vector and the diffraction vector, the determination of this direction is most precise when contrast can be observed to disappear. When the direction of diffraction is oriented normal to the atomic displacement, such a feature vanishes from the diffraction image.

E. Phase Domain Boundaries

Twins are distinguished normally by absence of diffraction from regions between sharp, parallel boundaries visible in some diffraction directions but not in others. The contrast in the latter, when observed by high-resolution beams, may be affected by very slight differences in lattice alignment.

With angular collimation of the order of an arc second, the images of other boundaries recorded in Laue geometry may also become visible when the diffraction vector falls along the boundary. Such boundaries are visible even under these restrictive conditions only when they separate atomically coherent regions differing by an atomic phase shift [10][11]. Those boundaries that have been observed to date to fulfill these conditions appear to separate antiphase domains. Radiation with a divergence of the order of a second of arc or less is necessary to image such boundaries.

F. Additional Phases

The absence of diffraction from particular regions of a crystal under all diffraction conditions supporting diffraction from the rest of the crystal strongly suggests the presence of a second phase, although in principle the non diffracting regions may simply be misoriented with respect to the rest. In stoichiometric materials, the boundaries of two phases are sharply delineated. In alloys, this sharpness is vitiated by the gradual changes in composition that may be permitted.

G. Surface Scratches

The strain associated with surface scratches is linear, but sometimes gently curved, and typically non crystallographic in orientation. The images of scratches typically are distinguished also by three other characteristics: 1) uniform width, 2) sharp edges, and 3) contrast reversal either laterally, longitudinally, or both, particularly as the Bragg peak is scanned.

III. RESULTING CAPABILITY

A. Storage Ring

Suitable synchrotron radiation sources now offer opportunities to fulfill the long awaited promise of x-ray topography; but the degree of success in their realization depends upon the particular parameters of the storage ring and its beam lines. Since the precise orientation of the x-radiation at individual points on the sample is crucial to the analysis, the vertical source size, together with the distance of the sample from the tangent point on the ring, may limit the potential utility of the images produced.

The x-ray storage ring of the National Synchrotron Light Source at Brookhaven National Laboratory offers the most suitable combination of characteristics of any existing ring, providing an unusually bright beam whose degree of vertical convergence on a point on a sample mounted in front of the monochromator on beam line X-23A3 is 1.5 arc seconds.

B. Optics

Although this 1.5 arc second beam provides a considerable improvement over other sources, it is not yet sufficient for diffraction imaging with maximum sensitivity to defects. For maximum useful sensitivity to irregularities, which requires further improvement in beam divergence by another order of magnitude, i.e., 0.1 arc second, the optics of the monochromator are crucial. Such a beam is necessary for rendering critical features visible, for preservation of the spatial information in the image within the plane of diffraction, and for displaying essential clues to the strains upon which the success or failure of detailed analysis can depend [6].

C. Resulting Performance

With such a resulting, dedicated 0.1 arc second monochromatic capability, however, which is available on a routine basis only on Beam Line X-23A3 at the National Synchrotron Light Source, the detection and interpretation of irregularities are limited

principally by the quality of the crystals undergoing study. Irregularities can be recorded photographically with a spatial resolution of 1 μm. Observation with an x-ray vidicon and charge coupled device (ccd) cameras readily provides complementary information with a spatial resolution of 35 μm with intermediate sensitivity in real-time, and 20 μm with shot noise limited sensitivity in quasi real-time.

D. High Spatial Resolution in Real-time

Data collection and optimization would be facilitated by reduction of the 35 μm spatial resolution of real-time or quasi real-time observation toward the one micron resolution of film. An extremely promising approach, which would greatly facilitate the application of diffraction imaging, is the use of an x-ray image magnifier in conjunction with a sensitive ccd. We have thus devoted considerable effort to the application and demonstration of this capability.

IV. PRINCIPAL AREAS FOR INVESTIGATION

A. Survey

Since there are 49 principal investigators in the crystal growth program of the NASA Microgravity Sciences and Applications Division, important tasks for us at the outset were to formulate those questions that might be addressed, establish a systematic program for addressing them, and determine initial priorities.

The process to carry out these tasks was initiated by Robert A. Schmitz, who wrote to each of the principal investigators identified in the Appendix on 8 March 1990 describing the collaborative effort and soliciting expressions of interest and other comment [8]. NIST was then asked to confer directly with each of the investigators to determine the nature of individual interests and the availability of suitable samples. Although the survey was to include only NASA Microgravity funded activity, the investigators included a major fraction of the American crystal growth community. The results of this survey should therefore be of more than routine interest.

The investigators fall into three groups. Thirteen investigators are pursuing the growth of highly regular but otherwise traditional macroscopic monolithic crystals and an understanding of the factors affecting crystal regularity. All of these investigators are interested in high-resolution diffraction imaging of their crystals. Most want also to take an active role in the experimentation and analysis, which demonstrates the seriousness of their commitment to the growth of the highest quality crystals. Moreover, this interest illustrates the promise of high-resolution diffraction imaging to realization of this end.

Fifteen investigators are pursuing the growth of novel materials that would extend the utility of high-resolution diffraction imaging beyond the traditional macroscopic monolithic crystals, for which it has already proved to be of value. All of these investigators are interested in the successful application of these techniques to the systems on which they are working. In addition, many of these investigators also want to participate actively in the imaging and detailed analysis. The degree of success that can be anticipated in each of these exploratory cases is discussed below.

The remaining 21 investigators are working in areas to which diffraction imaging is irrelevant, either because the systems that they are addressing are intrinsically unsuitable or because they are working with a single, restrictive aspect of the growth to which diffraction imaging would not contribute in a substantial way.

The interest of 28 investigators in collaboration is much larger than can be accommodated in the immediate future. Thus priorities must be weighed very carefully. The following synopsis summarizes the information that provides a basis for these priorities.

B. Traditional Materials

1. Binary Inorganic Crystals

a. Gallium Arsenide

Two pairs of closely related experiments are being carried out on the growth of gallium arsenide. Among other issues, these experiments seek to determine the influence of gravity on the morphology of the solid/liquid interface during solidification. Each pair of experiments will compare growth involving periodic Peltier marking with comparable growth without marking. Brian Ditchek has designed one pair of "Get Away Special" (GAS can) experiments for flight STS 40, originally scheduled for August 1990. David Matthiesen is designing a pair of USML 1 experiments, scheduled initially for March 1992, which will be based on the results of the STS 40 experiments and complementary terrestrial experiments. Both flight experiments involve selenium doped growth from a Czochralski seed.

Twenty-six terrestrial experiments related to the GAS can experiments are scheduled for the study of growth under various combinations of gravitational and magnetic fields as part of this effort. An extensive array of characterization experiments is also planned with which the diffraction imaging can be very usefully compared.

Dr. Matthiesen has posed a variety of fundamental questions to be addressed by diffraction imaging: propagation of defects from the seed; influence of interface shape; extent of crystallographic matching between seed and new growth; nucleation of defects at the growth interface; influence of the Peltier demarcation; inauguration of polycrystalline breakdown; and the influence of gravity on each of these. He looks forward to active participation in the experiments providing the answers to these questions.

Although a number of terrestrial samples comparable to those expected from the next STS experiment were available for immediate analysis, only one of these was thin enough to present the hope for observation of diffraction in Laue geometry. We have obtained images of this sample, presented in section VI, which contain an immediate answer to one of the questions that Dr. Matthiesen had posed. Implications for growth in microgravity are discussed in section VII.

b. Gallium Antimonide

August Witt is conducting two matrices of terrestrial Czochralski growth experiments under NASA auspices and is prepared to conduct heat pipe experiments in space when suitable flight hardware becomes available. The first matrix of experiments involves the growth of gallium antimonide. In this matrix, four material variations are planned, one undoped, and three doped respectively with tellurium, zinc, and tin. Experiments are planned both with and without the imposition of magnetic fields. The second matrix is similar to the first but uses a ternary including indium rather than gallium antimonide. The flight experiments involve the growth of germanium in heat pipes. In these experiments the appearance of line defects, clusters, point defects, precipitates, and other more gradual strains is anticipated.

The rapid scheduling of many such experiments arranged in a large matrix and the interrelationships among such successive, closely spaced experiments challenge in the following way the extensive time typically taken for a comprehensive analysis with diffraction imaging. Because of the number of steps involved in such an analysis: orientation of the sample, the recording and enlargement of visual data, complex subsequent analysis frequently encompassing further enlargement and detailed comparison and study of the results, weeks or months elapse from the onset of a series of experiments to its completion. This delay is incompatible with timely feedback into an elaborate series of experiments scheduled a week or two apart.

In order to provide essential information on a time scale of a week or so, substantially different operating procedures would have to be developed. First, very specific questions would have to be posed, so that the analysis could be restricted to a few highly specific issues. Second, utilization of the real-time, high spatial resolution imaging capability that has been developed recently would permit one to obtain the structural information in essentially real-time rather than after a long wait for travel between Brookhaven and Washington, several stages of photographic development, and the exploration of various models in order to describe in a comprehensive manner what is observed. Finally, active participation of crystal growers in the data acquisition on the beam line would assume even more importance than is normally the case.

c. Mercuric Iodide

The results of mercuric iodide growth on Spacelab III by physical vapor transport [1][2] have already proved to be of major interest, and another set of microgravity experiments has been scheduled for December 1990 on IML 1. Laboratory topography has shown some correlation between grain structure and the performance of detectors, but only in the relatively extreme cases [12]. Unexplained cellular structure with a characteristic dimension of 2-6 μm has been observed in all mercuric iodide by scanning cathodoluminescence microscopy [13]. Previous exploratory high-resolution diffraction imaging of terrestrial mercuric iodide on the beam line [7] suggested that high-resolution imaging of additional crystals might prove to be extraordinarily interesting and fruitful in wrestling with these questions.

Therefore, Lodewijk van den Berg provided immediately three crystals: one grown in Spacelab III, a comparable terrestrial crystal grown about the same time, and a new, higher purity crystal grown from material to be used on IML 1. He planned also to participate in the imaging on the beam line, which would have been highly desirable. However, the extremely tight beam line schedule and Dr. van den Berg's travel schedule proved at the last minute to be incompatible.

Our previous examination had led us to anticipate that the extreme softness of this material, its high atomic number, and its extremely interesting defect structure together would prevent immediate observation in Laue geometry. In the current set of experiments, therefore, we have restricted ourselves to observation in Bragg geometry, shown in section VI. The results of this imaging, described in section VII, are so interesting that extraordinary effort to thin samples of this material and to support them rigidly in innovative ways in future work seems now to be justified.

d. Cadmium Telluride, Cadmium Sulfide, and Lead Selenide

Bridgman and vapor growth of cadmium telluride and cadmium sulfide are under study in terrestrial experiments by Sandor Lehoczky. A discussion of diffraction imaging of these materials is covered under closely related ternary materials in space, described in the next two sections.

2. Ternary Inorganic Crystals

a. Cadmium Telluride Ternaries

The growth of ternaries of cadmium telluride is being studied by four principal investigators. Sandor Lehoczky and Frank Szofran are undertaking growth of mercury cadmium telluride on USML 1, scheduled for March of 1992. David Larson is planning experiments

on zinc and selenium ternaries of cadmium telluride, while Ratnakar Neurgaonkar is planning experiments on the vanadium ternary. Growth of some or all of these latter materials is also being scheduled for USML 1. We expect that Dr. Larson and his staff would join us in work on the beam line, as they have in the past, and would participate actively in the analysis.

These investigators clearly recognize the fundamental challenges presented by the growth of these ternaries, a principal one of which is a steady shift in chemical composition during growth. A variety of characterization approaches are being contemplated, and investigators are intrigued by the opportunity to push the limits of diffraction imaging with several samples of these materials and related binaries and ternaries.

b. Mercury Zinc Telluride

Sandor Lehoczky is planning growth of mercury zinc telluride on USMP 2, scheduled for February 1993. Diffraction imaging of this and related material is covered in the preceding section.

c. Lead Tin Telluride

Roger Crouch and Archibald Fripp grew lead tin telluride on STS 61A, and have been awaiting for several years the opportunity for synchrotron examination of this and related terrestrial samples. Several examples of each were provided by Richard Simchick, who participated in the imaging on the beam line and initial analysis, sections VI and VII. He has also provided extremely useful auxiliary chemical data central to that analysis.

Archibald Fripp is designing a second flight experiment, which he would like to carry out on USMP 2, scheduled for February 1993. Examination of crystals of this and related terrestrial growth should prove to be particularly valuable after the collaborative imaging experiments on the beam line reported below.

d. Indium Gallium Antimonide

William Wilcox is studying the directional solidification of alloys of indium antimonide and gallium antimonide. He would like to use high-resolution diffraction imaging to observe compositional inhomogeneities as well as grain and twin orientation. Professor Wilcox and a student have spent substantial time on the beam line with us in the past. We anticipate that they would continue to participate actively.

3. Low Molecular Weight Organic Crystals

a. Triglycine Sulfate

Ravindra Lal grew triglycine sulfate from solution on Spacelab III and has been scheduled for a second growth experiment on IML 1 in December 1990. He has supplied a sample from the Spacelab III growth, which we examined at the very end of the current series of experiments, section VI. The extraordinarily interesting results are in summarized in section VII.

Professor Lal is particularly anxious that we examine potential seed materials, thus helping him to select the most promising seed crystals for the IML 1 experiments. This would simultaneously provide comparable terrestrially grown material for later comparison with that grown in microgravity. These experiments will include both (010)- and (001)-seeded growth, and we all anticipate that diffraction imaging would be particularly helpful in a comprehensive comparison of the two types of growth.

b. l-Arginine Phosphate

Marcus Vlasse is growing highly regular and optically featureless crystals of l-arginine phosphate, the study of which by diffraction imaging would be of great interest. Dr. Vlasse would like to participate actively in the imaging experiments.

c. Benzil

Sindo Kou is in the early stages of growing benzil. He would be interested both in determining the extent of defect structure in his material and in detailed correlation of this information with his strategy for crystal improvement.

C. Novel Materials

1. Epitaxial Systems

a. General Considerations

Epitaxial systems, in a manner fundamentally similar to more conventional seeded crystal growth, present opportunities for diffraction imaging in the examination of the degree of lattice matching and the propagation of strains within a layer (or new growth) from the substrate (or seed). Such effects are frequently magnified in epitaxial systems by the thinness of the epitaxial layer and by deliberate changes in the chemistry between successive layers. One will observe irregularity at the interface, however, only to the extent permitted by the internal regularity of the various layers of the completed crystal. Although diffraction from

various layers has been observed, the analysis of previous high-resolution images has been severely limited by the regularity of the layers [5].

b. Mercury Cadmium Telluride on Cadmium Telluride

Heribert Wiedemeier is scheduled for vapor growth of mercury cadmium telluride, epitaxially on cadmium telluride, on USML 1 in March 1992. He would like to use diffraction imaging in order to optimize growth conditions. He would participate both in data acquisition and in subsequent analysis.

This prospective intensive collaboration, and its explicit goal of optimization of the flight program appear to make such a study unusually productive. Past diffraction imaging of cadmium telluride grown by Bridgman techniques has shown a high degree of irregularity. A principal challenge in the imaging of epitaxial samples, therefore, will be to locate substrates that are good enough not to obscure information on structure of the interface.

c. Zinc Germanium Phosphide on Gallium Phosphide

Klaus Bachmann is motivated more by the cleanliness of space processing than by the reduction in gravity to grow high-purity multiple quantum well structures by organometallic molecular beam epitaxy. The effects of this purity on the strain structure should be interesting to observe in the 0.1% lattice matched systems that he is contemplating. The opportunity for close collaboration with those using transmission electron microscopy that is presented here would make such diffraction imaging experiments unusually interesting.

d. Silicon on Germanium

Randall German and Krishna Rajan are focusing on the detailed nature of the interface structure in dissimilar, non lattice-matched systems. Their interests span a range from germanium/silicon bicrystals, through solidification, to sintering. They are focusing on local strain gradients and their effects on solute diffusion. Thus their interest in crystal regularity derives from the sophisticated knowledge of interfaces that they want to acquire, rather than the formation and study of generally more regular crystals. The use of complementary electron microscopy, which is characteristic of their work, would make collaboration with them in high-resolution diffraction imaging unusually valuable.

2. Proteins

a. General Considerations

The strong interest in protein crystal regularity arising from the promised improvement of crystallographic structural determination was summarized in section I. Diffraction imaging of proteins has not been attempted, however; and suggestions that it be tried lead to several important questions, which we now address. Both those issues noted by potential collaborators and additional issues that we view with concern are identified here and examined.

i. Relevance of the mesoscopic regularity observed in diffraction imaging to the order required for structural determination. A perfect single crystal is not required for structural determination. Indeed, dynamical diffraction from a perfect crystal can complicate the analysis of kinematic scattering used in structural determination. Nevertheless, crystals that diffract more effectively have been observed to display superior morphology as well [3]. If this proves to be true of proteins in general, then any guidance from diffraction imaging that would assist in the achievement of superior morphology may well contribute to success in the determination of crystal structure.

ii. Substantial mesoscopic irregularity in the crystallization of organic molecules in general and of protein molecules in particular. One of the conditions already identified for successful diffraction imaging is the presence of sufficiently small numbers of irregularities that their interpretation is not obscured by scattering from adjacent features. Pervasive irregularity even that characteristic of a specimen that could prove ideal for the determination of crystal structure, may well constrain the amount of useful information in a diffraction image. This is perhaps the most serious source of concern in anticipating the utility of diffraction imaging of protein systems. The relative importance of this factor can be determined only empirically. This means that the ultimate extent of high-resolution diffraction imaging may be established only by trial. Initial attempts clearly should focus on the most promising, that is the most regular, protein crystals.

iii. Change in regularity of crystals grown in space on return to earth. Changes in the regularity observed in space-grown crystals in the days following return to earth [14] raise some question about the long-term stability of their structure. However, rapid diffraction imaging during the period of instability might prove to be exceptionally interesting.

iv. The necessity to keep good protein crystals in contact with their mother liquor. The presence of a liquor around the crystal to be analyzed presents two challenges. The first is the necessity to surround the crystal by a vial to contain the liquor. Diffraction through such a vial could prove extremely challenging

in practice. The presence of the liquor, moreover, could well interfere with the firm orientation of the sample as it is tilted for diffraction in various directions. Since useful crystallographic patterns have been obtained of such systems, this would not appear to be an absolute limitation. But successful imaging of a crystal swimming in its liquor could prove to be very difficult.

v. The destructive power of x rays in systems with low atomic number. Substantial crystal damage has been observed in proteins after crystallographic study with high intensity x-ray beams, which often contain a full white radiation spectral distribution. Indeed, a principal advantage of synchrotrons for this analysis is the high flux that they deliver. The resulting useful exposure time is sufficiently short that relatively slow damage processes are completed only after the exposure. The focused beams used in these crystallography experiments deposit orders of magnitude more energy on the sample than do high-resolution diffraction imaging beams, for which the desired improvement in collimation and monochromatization severely reduces the irradiance of the magnified probe beam. The hope that proteins will withstand the lower irradiance levels characteristic of high-resolution diffraction imaging is difficult to evaluate quantatively. The extent of damage will depend partly on the length of time required for diffraction imaging, which depends on many factors.

vi. The low x-ray scattering power of organic molecules in general and of protein molecules in particular: possible low contrast in the images. The kinematic scattering responsible for the diffraction spots used for crystallography is certainly strong enough to support structural analysis. Individual spots indeed contain structure as well [15]. We report in section VI on the diffraction imaging of triglycine sulfate. Contrast thus does not appear to be an insurmountable problem in the diffraction imaging of proteins.

vii. Complexity in the analysis of diffraction images because of the mixture of kinematic as well as dynamical scattering expected from the small optical thickness of such materials. Crystallography depends on kinematic scattering from adjacent atoms or groups of atoms. Diffraction imaging of the characteristic optically thick crystals to which it is applied is most successful under conditions that suppress such scattering in favor of perfect crystal dynamical scattering. In proteins and other organic materials consisting largely of "low Z" atoms, however, we anticipate that both kinematic and dynamical scattering will coexist, as is observed later in this report in triglycine sulfate. The interpretation of such mixed images may well be complicated and possibly limited by the simultaneous occurrence of both types of scattering.

b. Interest in the Imaging of Proteins

Six of the nine principal investigators working with protein growth: Robert Feigelson, Daniel Carter, Charles Bugg, Larry DeLucas, Franz Rosenberger, and Donald Voet, are interested in exploring the relevance of diffraction imaging to the growth of better crystals for crystallography. Of these, Charles Bugg and Larry DeLucas have performed a number of space experiments and are actively planning a number of new ones, with particular emphasis on USML 1 scheduled for March 1992. The views of the other three are reviewed below in section D.

All nine investigators would very much like to succeed in the growth of more regular crystals for crystallographic analysis, but are sensitive to the preceding set of issues that may restrict the utility of the results of diffraction imaging for protein crystal growth. It seems fair to say that all would approach the imaging of protein crystals with preparation that is at least as thorough as that which should precede the diffraction imaging of any prospective system. Perhaps the principal initial practical issue is the establishment of a consensus on a promising system for exploratory experiments.

3. Other Systems

a. Whiskers

Herman Hobbs is studying the evolution of whiskers with characteristic dimensions of 1 square micrometer by 1 centimeter. He observes that critical changes in the structure occur when the whisker thickness has grown to about 5 μm, so that the imaging of whiskers as they approach this size might prove to be unusually interesting. He would like to collaborate actively in such a project; and this collaboration should contribute to the chances for success.

However, the current spatial resolution in real-time is 30 μm; the comparable resolution is 1 μm for nuclear emulsion plates. Thus whiskers of the size that is most interesting would strain these spatial resolution limits severely. Extension of the real-time capability toward 1 μm should improve the chances for success in such experiments.

b. Small Particles

William Hofmeister is working on the containerless growth of high temperature 1-2-3 superconductors in a similar size range, 20-100 μm. The challenge in the diffraction imaging of such materials is increased by the known propensity of these materials to twin. As with the whiskers, the prospects for success in working with micrometer size materials should be increased substantially by the extension of the real-time capability toward 1 micrometer.

c. Polygrain Growth by Physical Vapor Transport

Elmer Anderson is investigating the polygrain growth of zinc selenide by physical vapor transport. He achieves clusters of single crystals and large twinned boules, and would like to minimize the irregularity in optical materials. He is interested in exploring the applicability of diffraction imaging to such polygrained systems and would join us actively in such experiments, which would contribute to the prospects for success. The principal question here is whether the crystals have sufficient regularity and size to lend themselves to successful high-resolution analysis.

d. Rapid Solidification

Robert Schiffman is studying the establishment of properties in microgravity in real-time, for example following rapid solidification by quenching from very high temperature. Although he is interested in collaboration with us, the utility of high-resolution diffraction imaging for these systems may depend ultimately on the observation of longer duration changes, changes in properties at least over several days following return to full gravity.

e. Liquid Encapsulated Melt Zone

Reza Abbaschian is planning the liquid encapsulated melt zone growth of bismuth doped with tin on USMP 2, scheduled for February 1993. He anticipates analysis by a variety of techniques among which he will consider diffraction imaging.

f. Convective Effects

Singh is planning the growth of lead bromide on USML 2, scheduled for March 1994, and IML 3, scheduled for April 1995. His primary interest is in the study of convective effects. The utility of high-resolution diffraction imaging will depend on the particular nature of the convective effects.

D. Materials Not Relevant to this Study

1. Glass Formation

a. Oxide Glasses

George Neilson, Chandra Ray, and Michael Weinberg are each working in the area of glass formation. Without a crystal structure, glasses are not candidates for diffraction imaging, high or low resolution.

b. Metglasses

William Johnson is working on metglasses, which also, by definition, are not candidates for diffraction imaging.

2. Fine Particles

a. Rapid Solidification

Merton Flemings and Carl Koch are studying rapid solidification leading to submicrometer crystallites. The required resolution would be substantially less than their size, say of the order of a nanometer. This is below the best current spatial resolution available with diffraction imaging.

b. Diamond Films

John Margrave is studying the formation of diamond films. The crystallographic perfection of individual diamond crystallites is not of immediate interest in this work. Moreover, the submicrometer particle size would require resolution of the order of a nanometer, which is below that accessible with current diffraction imaging.

3. Specific Stages of Growth

a. Seeding

Frederick Carlson is studying the role of seeding, particularly in conjunction with modeling. Although diffraction imaging is able to shed light on some aspects of seeding, other analytic information is likely to be more useful to this modeling effort.

b. Transport in Alloys

Martin Glicksman, John Perepzko, Robert Bayuzick, and Eugene Trinh are each engaged in the study of various effects of transport on the solidification of alloys. The information provided by diffraction imaging is not immediately relevant to these studies focussing on dendritic growth.

c. Ostwald Ripening

Peter Voorhees is focusing on the Ostwald ripening of alloys. Although he and NIST scientists have carried out white beam diffraction imaging and radiography on such systems [16], diffraction imaging is not immediately relevant to his current activity.

d. Magnetostriction

Julian Szekely is studying the magnetostrictive levitation of liquid metal droplets. They are clearly not accessible to diffraction imaging.

e. Proteins

Our survey indicates that three principal investigators, Ponzy Lu, Alexander McPherson, and Marc Pusey are focusing on aspects of protein science to which diffraction imaging is not likely to contribute.

4. Model Systems

a. Ammonium Chloride

Mary McCay is planning experiments on the holographic observation of diffusion of ammonium chloride on IML 1, scheduled for March 1992. These experiments do not produce "returnable" crystals.

b. Organic Analogues of Metal Systems

Barry Andrews is observing the solidification of transparent organic analogues of immiscible alloys. The degree of perfection of these materials is not a principal factor in this work.

5. Diagnostic Techniques

a. Acoustic Techniques

Martin Barnatz is applying acoustic techniques to the sintering of ceramics. Crystal perfection is irrelevant.

b. Dynamic Measurements

Ared Cezairliyan is making dynamic measurements on systems that do not result in the growth of high-quality crystals.

V. MATERIALS IN THE CURRENT EFFORT

A. Selection Considerations

The large number of systems and questions identified in the preceding section, suggests both the importance of careful sample selection and the complexity of carrying it out. The proximity of space flights scheduled for crystal growth (table 1) introduces urgency as an additional factor. Realization of the three goals of the imaging program identified in section IV: establishment of a baseline of image data, correlation with performance, and optimization of growth experiments, required an immediate start for this work.

In work toward each of these goals, optimization of the scientific value of diffraction images requires that samples have the four characteristics identified in section II. However, the desirability of starting on the structural base line before the next scheduled flights dictated that work this first year be limited to samples already at hand. The definition of our initial activity thus required some compromises in the crystals observed.

The first crystals selected included three early examples of space growth, i.e. mercuric iodide, lead tin telluride, and triglycine sulfate, and comparable terrestrial samples of each. The comparison crystal for the space-grown triglycine sulfate was actually the seed used for the space growth, so that a separate sample was not required. We also observed two terrestrial samples for later comparison with crystals to be grown in space this fall: mercuric iodide and gallium arsenide.

The resulting images and what we have learned from them, although not optimized in terms of the detailed interpretation that might come from specially prepared samples, are of such far-reaching consequence to the future program that they support the wisdom of the decision to observe immediately those high-priority crystals already available.

TABLE 1: Flight PI samples anticipated

	89-90	90-91	91-92
Many flights:			
Bugg (protein)	0	0	0
STS 40 (August 1990):			
Ditchek (GaAs)	3-6	2-4	2-4
IML 1 (December 1990):			
van den Berg (HgI_2)	3-6	6-8	6-8
Lal (TGS)	2	4	2
McPherson (protein)	0	0	0
USML 1 (March 1992):			
Matthiesen (GaAs)	0	2	2
Wiedemeier (HgCdTe)	0	2	2
Larson (CdXTe)	0	3	3
Carlson (CdTe)	0	0	0
Neurgaonkar (CdVTe)	0	3-4	3-4
Lehoczky (HgCdTe)	0	3	3
DeLucas (protein)	0	0	0
USMP 2 (February 1993):			
Fripp (PbSnTe incl. sg)	2	2	4
Abbaschian (Bi(Sn))	0	0	1
Lehoczky (HgZnTe)	0	2	2
USML 2 (March 1994):			
Singh ($PbBr_2$)	0	0	X
IML 3 (April 1995):			
Singh ($PbBr_2$)	0	0	0
TOTALS	10-16	31-36	32-37

B. Mercuric Iodide

Mercuric iodide was given high priority for several reasons. The extraordinary charge carrier mobility displayed by a mercuric iodide crystal grown by physical vapor transport in Spacelab III has been noted in the Introduction. This improvement over comparable terrestrially grown crystals is particularly noteworthy because the intrinsic advantages of mercuric iodide radiation detectors, high quantum efficiency with high energy resolution [17], have typically been compromised by marked variation in energy resolution within a single detector and by low yield [18]. Crystalline imperfections, chemical and crystallographic, have been shown to degrade the energy resolution [12][19][20][21], and these can arise either during crystal growth or in subsequent processing into a device [22][23][24].

Previous collaboration in high-resolution diffraction imaging of terrestrial mercuric iodide with Lodewijk van den Berg [7], who had grown this material himself in space, had verified the prominence in this material of individual grains, as reported following neutron and gamma-ray diffraction [25] and x-ray topography [12][26]. A 2-6 μm cellular structure had also been reported [13]. However, neither the origin of the grains nor that of the cellular structure had been identified.

The unusual performance of space-grown material, the active collaboration of the grower, and the opportunity to incorporate what was to be learned in scheduled space growth all ensured that progress on these questions would exert maximum scientific leverage. Only conflicting schedules at the last minute prevented Dr. van den Berg's joining us on the diffraction imaging synchrotron beam line for the imaging itself.

We observed three mercuric iodide crystals: 1) the crystal grown on Spacelab III, which had been made into a detector by the application of graphite electrodes, which were not expected to interfere directly with the observation; 2) a terrestrial control grown about the same time and from similar material; and 3) a terrestrial sample recently grown from new, high-purity material comparable to that to be used in the IML 1 flight scheduled for December 1990. The terrestrial samples were selected on the basis of the regularity of their Laue spot patterns from two samples of each that were made available.

The high atomic number of the constituents and the interesting structure observed in earlier work indicated that samples of mercuric iodide much thinner than a millimeter would be required for observation in Laue geometry. The extraordinary softness of the material, however, suggested that the achievement of sufficient thinning without deformation would require a special research project that would seriously delay the imaging. In any event, it

seemed inadvisable to carry out thinning research on a rare space sample. We therefore elected to focus these initial experiments on an evaluation of the general nature of the crystals by imaging them in Bragg geometry, solidly mounted so that deformation on thinning would not interfere, and to save until later experiments with extreme thinning and mounting procedures if the present results of the imaging in Bragg geometry indicated that a special effort might prove worthwhile.

C. Lead Tin Telluride

A crystal of lead tin telluride grown by Bridgman techniques on STS 61A [27] and a comparable terrestrial sample were studied in order to explore any additional effects that previous space growth had on a ternary and to provide a foundation for the analyis of new growth experiments on USMP 2, scheduled for February 1993. This ternary is of particular interest for growth in microgravity because its growth is thermo-solutally unstable in a terrestrial environment [27].

The presence for the imaging on the beam line of Richard Simchick, who participated in the growth of these crystals and had carried out chemical analyses of them, ensured that the results of these experiments would be optimized and would exert maximum influence on subsequent growth of this material. Both samples were selected on the basis of the regularity of their Laue spot patterns from two samples of each type.

In planning these imaging experiments, we recognized that existing samples of this material also were too thick to support diffraction in Laue geometry. The irregularity that we anticipated by itself would require severe thinning for successful transmission. This requirement for thinning would be amplified by the high atomic number of the constituents. Because of the undesirability of unnecessary handling of a space-grown crystal before examining it, we elected not to thin them at this juncture. We thus minimized the effect of surface treatment in this initial analysis.

D. Triglycine Sulfate

Triglycine sulfate $(NH_2CH_2COOH)_3H_2SO_4$, a ferroelectric material, is a good model crystal for solution crystal growth. It is pyroelectric below 49 ^{0}C. It has a monoclinic crystal structure with a (010) cleavage plane normal to the pyroelectric axis. Interest in TGS for thermal imaging and detection devices, space-borne radiometry, and sensing high energy pulse lasers has led to a search for crystals of high optical quality and improved pyro-

electric properties. In Spacelab III, two TGS growth experiments were carried out. In both, disc-shaped (001)-oriented seed crystals were used. In one of these (FES-3, cell # 204) the growth conditions were $T_{st} = T_{sl} < T_{sa}$, where T_{st}, T_{sl}, and T_{sa} are the temperatures of the sting (crystal), solution, and saturation, respectively. For characterization, slices perpendicular to the [001] growth direction were cut, lapped, and polished.

One of these slices was examined as part of the current effort. In this case, the terrestrial seed acted as its own internal control. The regularity of this material has been shown to be extremely sensitive to the growth rate, growth regularity including temperature stability, and purity, provided that the seed is sufficiently regular [28][29]. In addition to the opportunity to survey marked anomalies in early space growth, the immediate influence that results might have on the IML 1 growth, originally scheduled for December 1990, was an important factor in the selection of this crystal. Additional factors were the active collaboration of Ravindra Lal and his associates and the anticipation, in light of earlier collaboration with Professor Lal, that diffraction from these crystals in Laue geometry would be accessible.

E. Gallium Arsenide

Finally, although gallium arsenide has not yet been grown in the NASA space program, two Bridgman-growth experiments are now planned: one by Brian Ditchek in the STS 40 GAS can flight, originally scheduled for August 1990, and one by David Matthiesen on USML 1, originally scheduled for March 1992. One comparable terrestrial crystal on hand was thin enough to offer a chance to observe diffraction in Laue geometry, so this was selected.

Additional factors supporting its selection were the potential technological importance of gallium arsenide, the availability of infrared images that could be compared directly with diffraction images, the active collaboration of David Matthiesen in the selection of fundamental issues to be addressed and in planning the experiments, and the anticipation that he would join us on the beam line. Unfortunately that proved at the last minute not to be possible.

VI. THE DIFFRACTION IMAGES

A. Mercuric Iodide

1. Terrestrial Crystal Compared with Spacelab III Crystal

While the terrestrial mercuric iodide crystal grown from the same source material as the Spacelab III crystal diffracts over a range of one half degree, a large central portion is sufficiently regular to diffract only within a few minutes of arc. Full high-resolution diffraction images of this terrestrial crystal appear in figures 1-6, and enlarged portions of these in figures 7-25.

Most of the central portion of the crystal is in diffraction in the (1 1 12) and (1 1 10) images in figures 1 and 2, respectively, indicating lattice regularity with respect to rotation around a [1$\bar{1}$0] axis of the order of a few arc seconds. However, the absence of diffraction in a wide [110] (vertical) stripe in the center of figures 1 and 2 indicates that the lattice is deformed by a sharp twist of about 10 minutes of arc around an axis defined by this stripe. The extent of this twist is determined from the 100 μm width of the stripe in figures 1 & 2, and the knowledge that the photographic plate was located about 3.5 centimeters from the crystal. The twist of the crystal lattice is evident indirectly also in the (0 1 10) and (0 1 11) diffraction images, figures 3-6, for which the crystal was rotated azimuthally 45°. In this orientation, the misalignment of the two parts of the crystal precludes bringing them simultaneously into diffraction. Examination of the full images, figures 1-6, and of a sequence of real-time images of the (008) diffraction, for which the acceptance angle is narrower than for that in the printed images, indicates that the principal lattice twist axis itself bends through several minutes of arc, differing slightly in the two subgrains.

The other principal large feature of the full images of this crystal in figures 1-6 is a set of textural stripes, which are oriented in the [1$\bar{1}$0] direction. The enlargements in figures 7-25 show these stripes to consist of a relatively high density of discrete features, typically out of diffraction in these images and therefore ascribed to one or more additional phases. Some of these features take the form of thin {100}-oriented stripes a few micrometers wide; they are sometimes crossed. The others are more irregular, globular particles, 1-60 μm in diameter. These may differ completely from the stripes, but may simply represent similar stripes normal to the (001) image and projected on it.

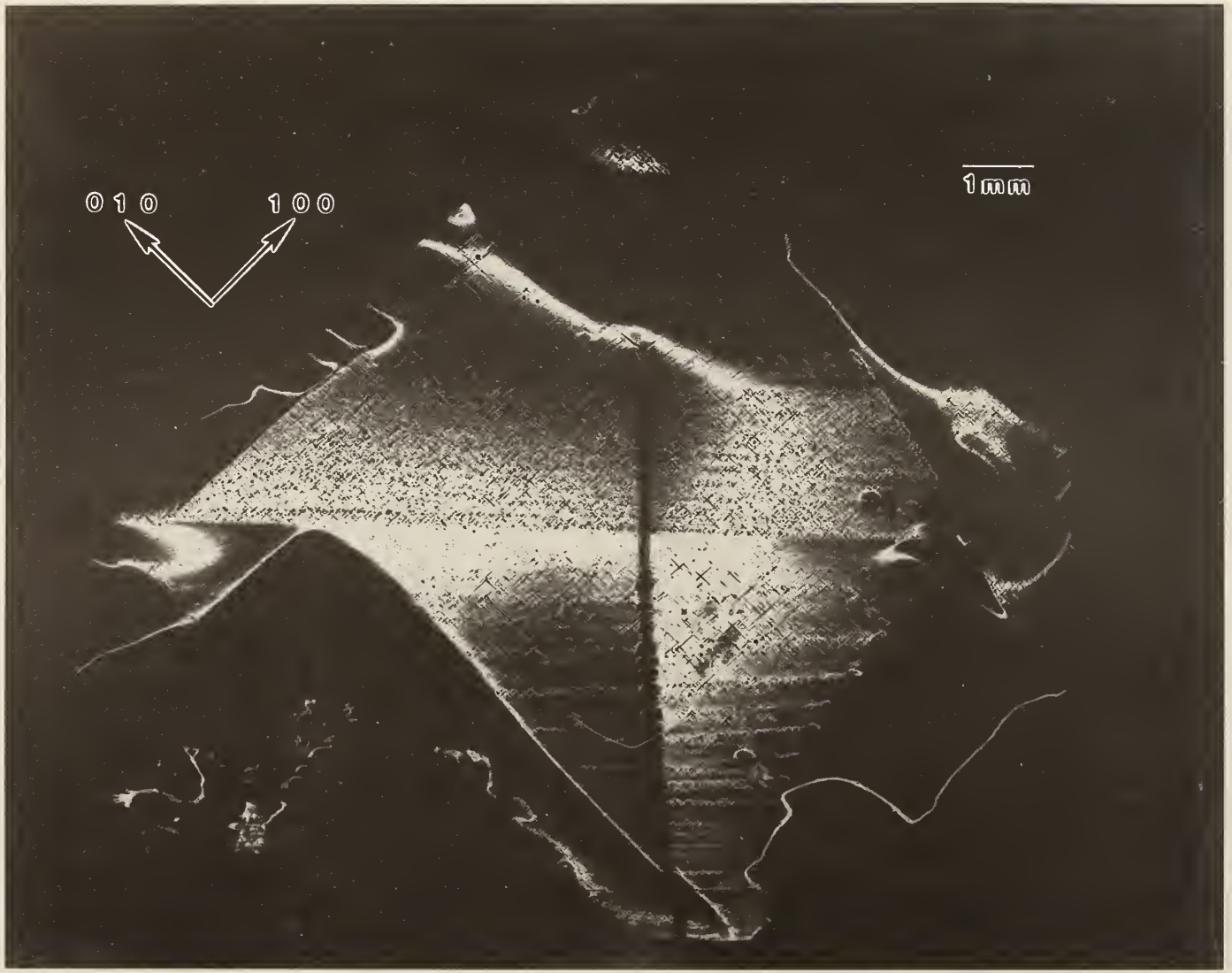

Figure 1. High-resolution (1 1 12) 8 keV diffraction image in Bragg geometry of (001) surface of terrestrial HgI_2 crystal 116, comparable to that grown on Spacelab III. Lighter areas diffract more strongly.

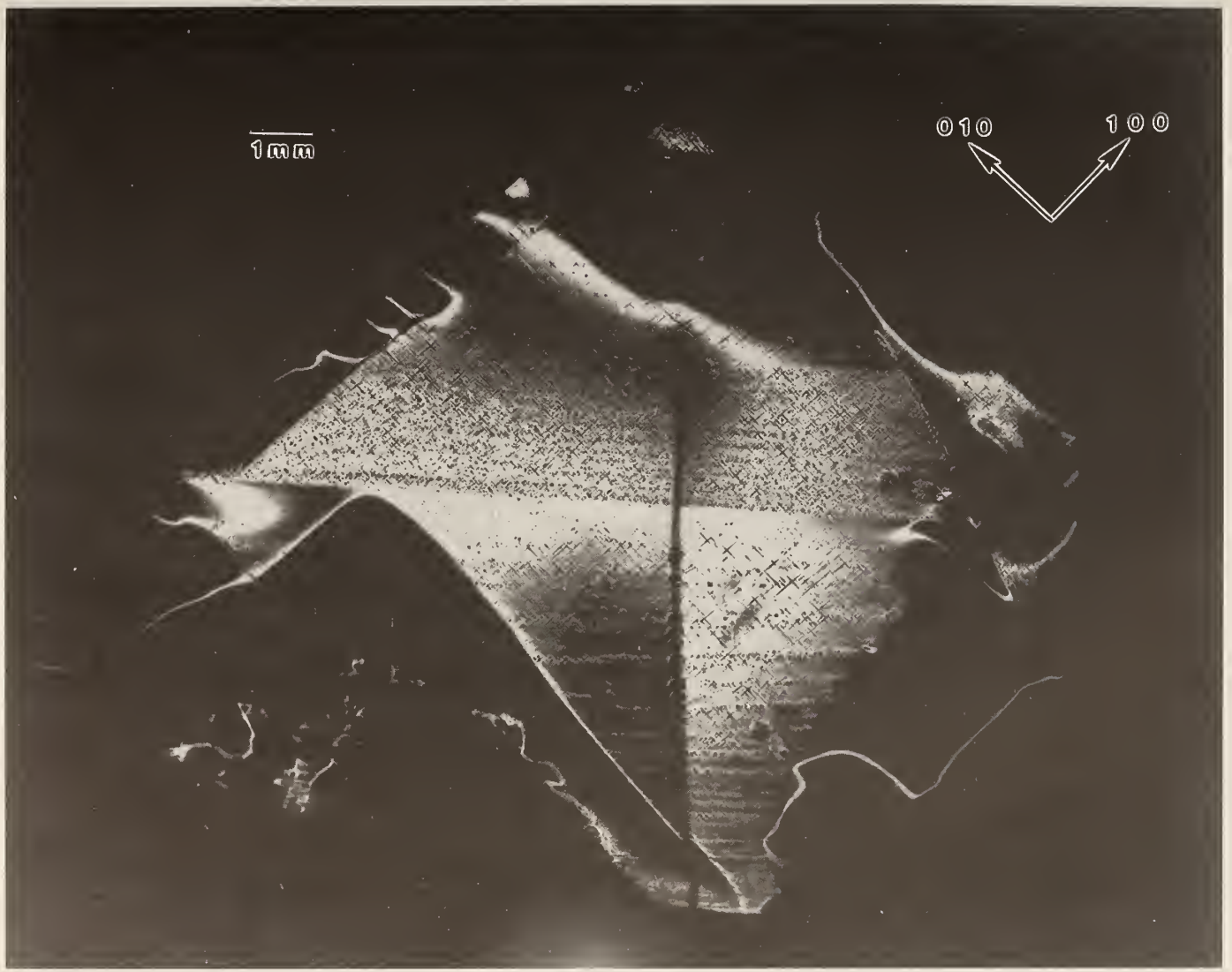

Figure 2. High-resolution (1 1 10) 8 keV diffraction image in Bragg geometry of (001) surface of terrestrial HgI_2 crystal 116, comparable to that grown on Spacelab III. Lighter areas diffract more strongly.

Figure 3. High-resolution (0 1 10) 8 keV diffraction image in Bragg geometry of (001) surface of terrestrial HgI_2 crystal 116, comparable to that grown on Spacelab III. Lighter areas diffract more strongly.

Figure 4. High-resolution (0 1 10) 8 keV diffraction image in Bragg geometry of (001) surface of terrestrial HgI_2 crystal 116, comparable to that grown on Spacelab III. The angle of incidence is 3.6 arc minutes smaller than that for figure 3. Lighter areas diffract more strongly.

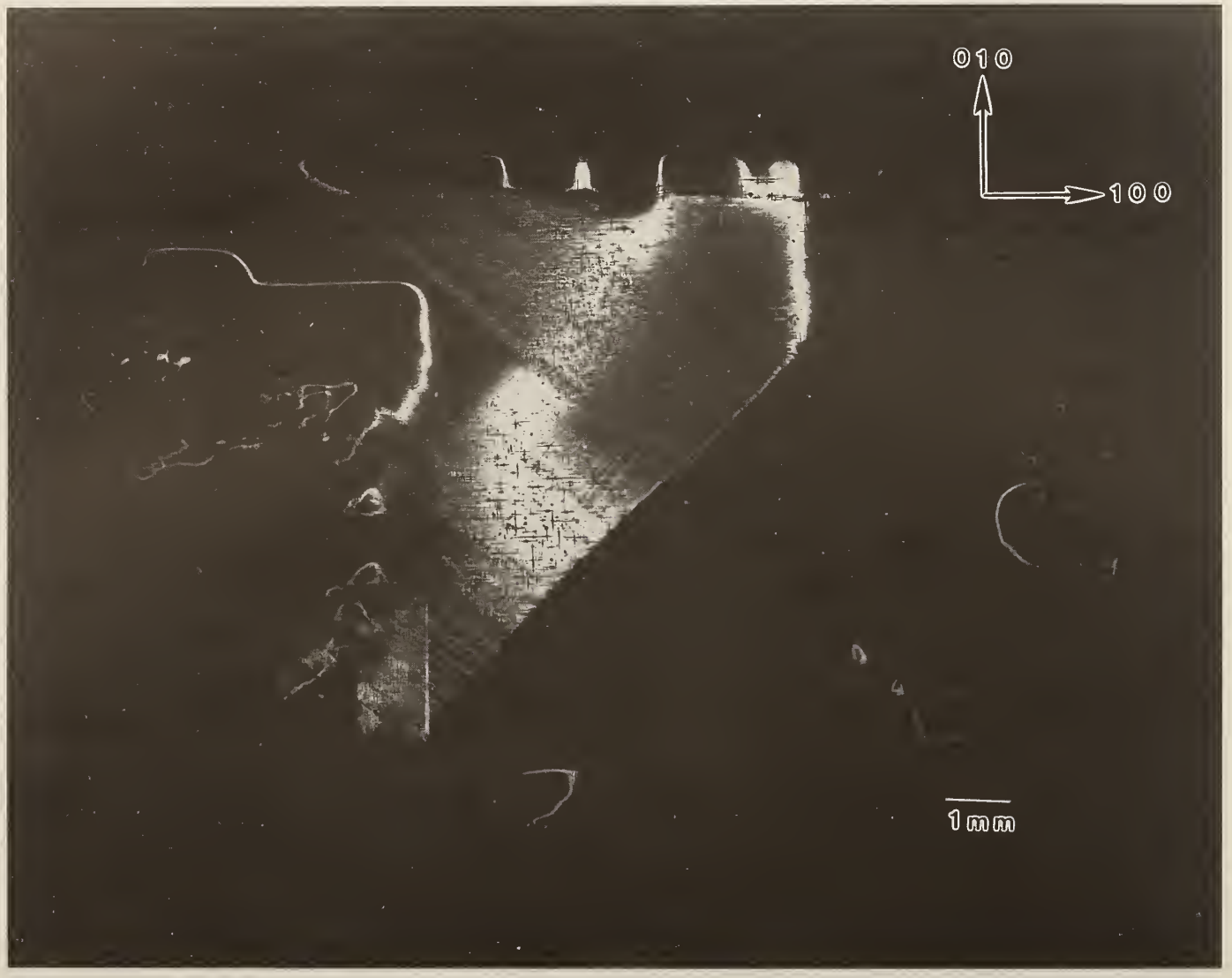

Figure 5. High-resolution (0 1 11) 8 keV diffraction image in Bragg geometry of (001) surface of terrestrial HgI_2 crystal 116, comparable to that grown on Spacelab III. Lighter areas diffract more strongly.

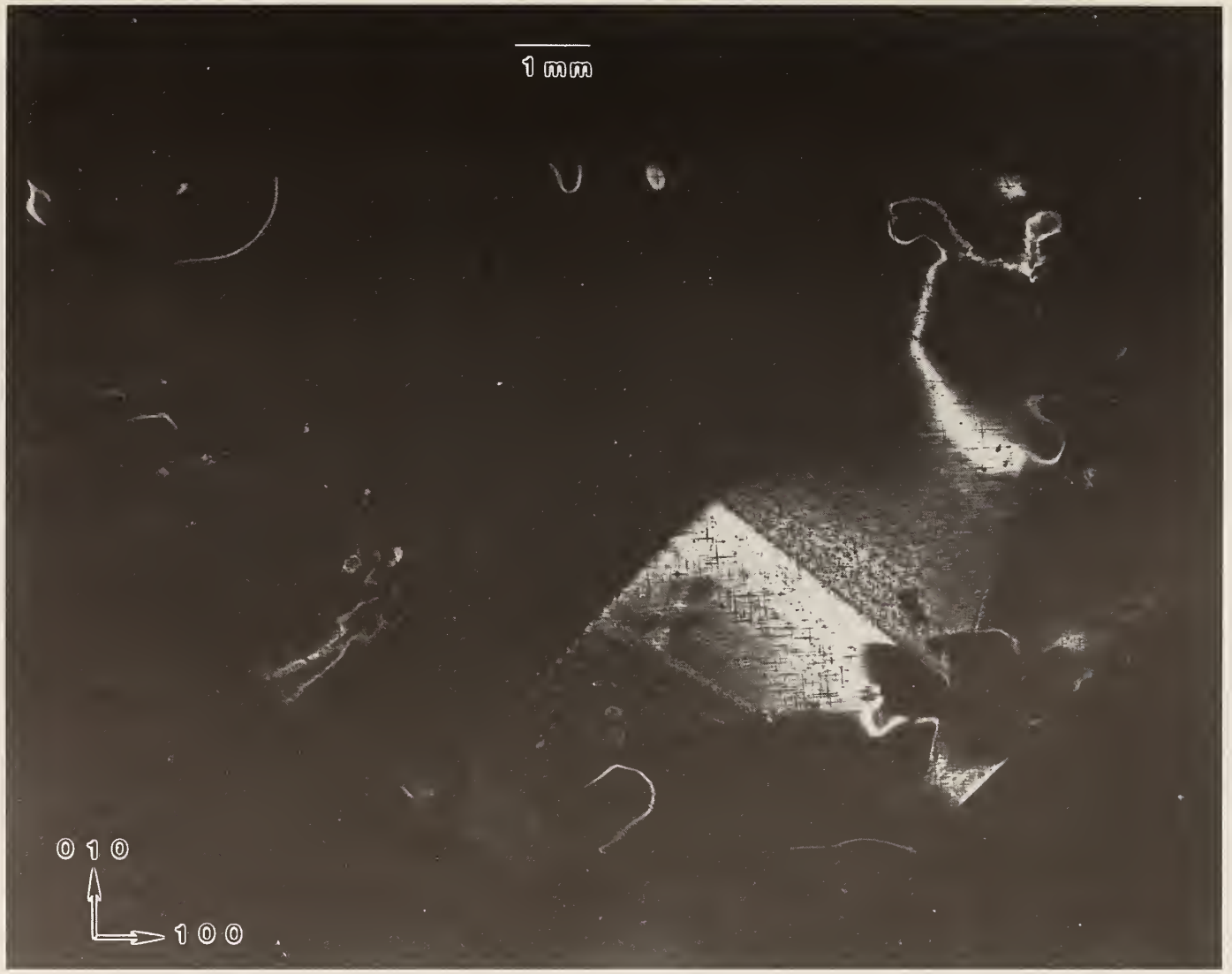

Figure 6. High-resolution (0 1 11) 8 keV diffraction image in Bragg geometry of (001) surface of terrestrial HgI_2 crystal 116, comparable to that grown on Spacelab III. The angle of incidence is 7.8 arc minutes smaller than that for figure 5. Lighter areas diffract more strongly.

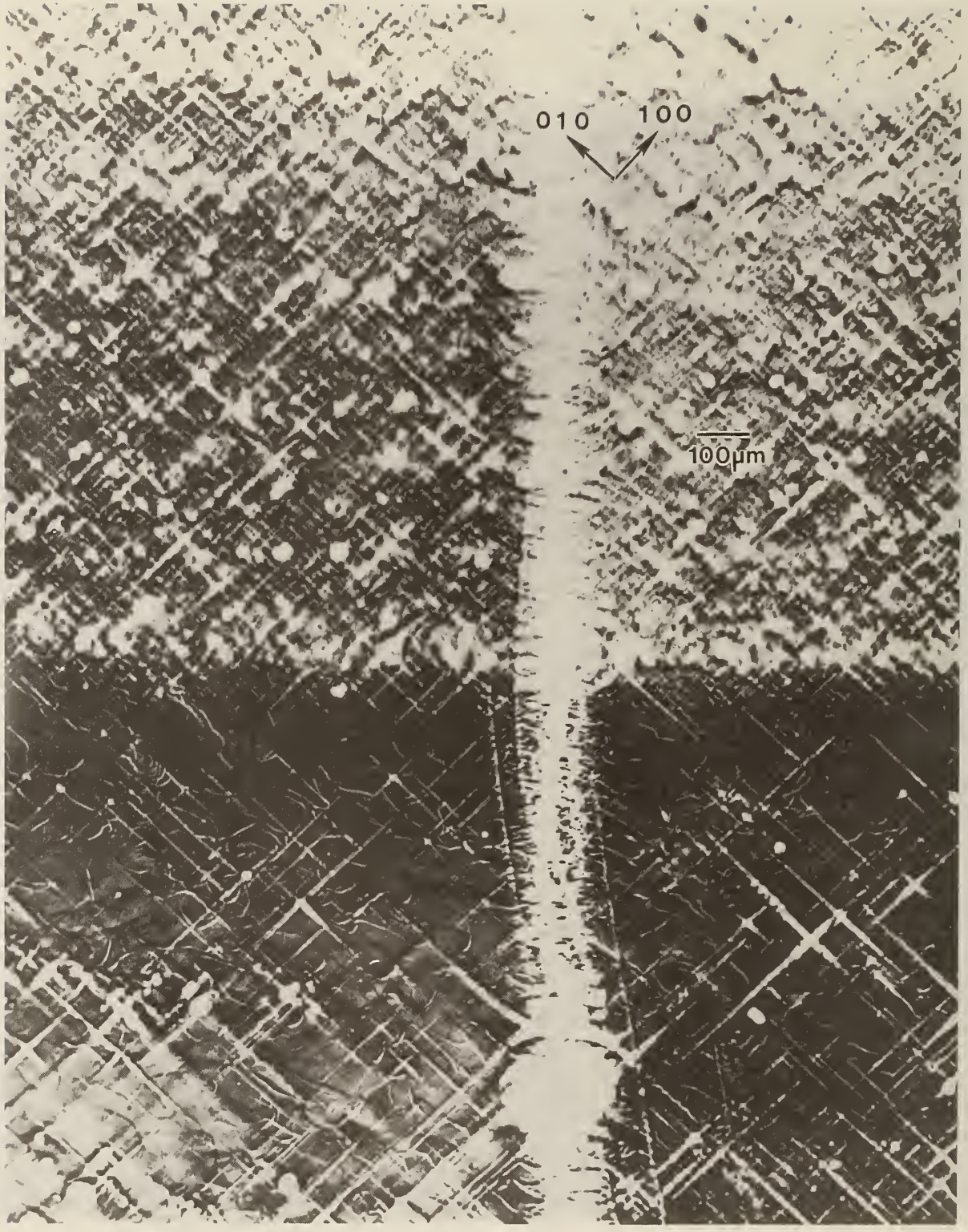

Figure 7. Enlargement of central portion of figure 1, (1 1 12) diffraction. Darker areas diffract more strongly.

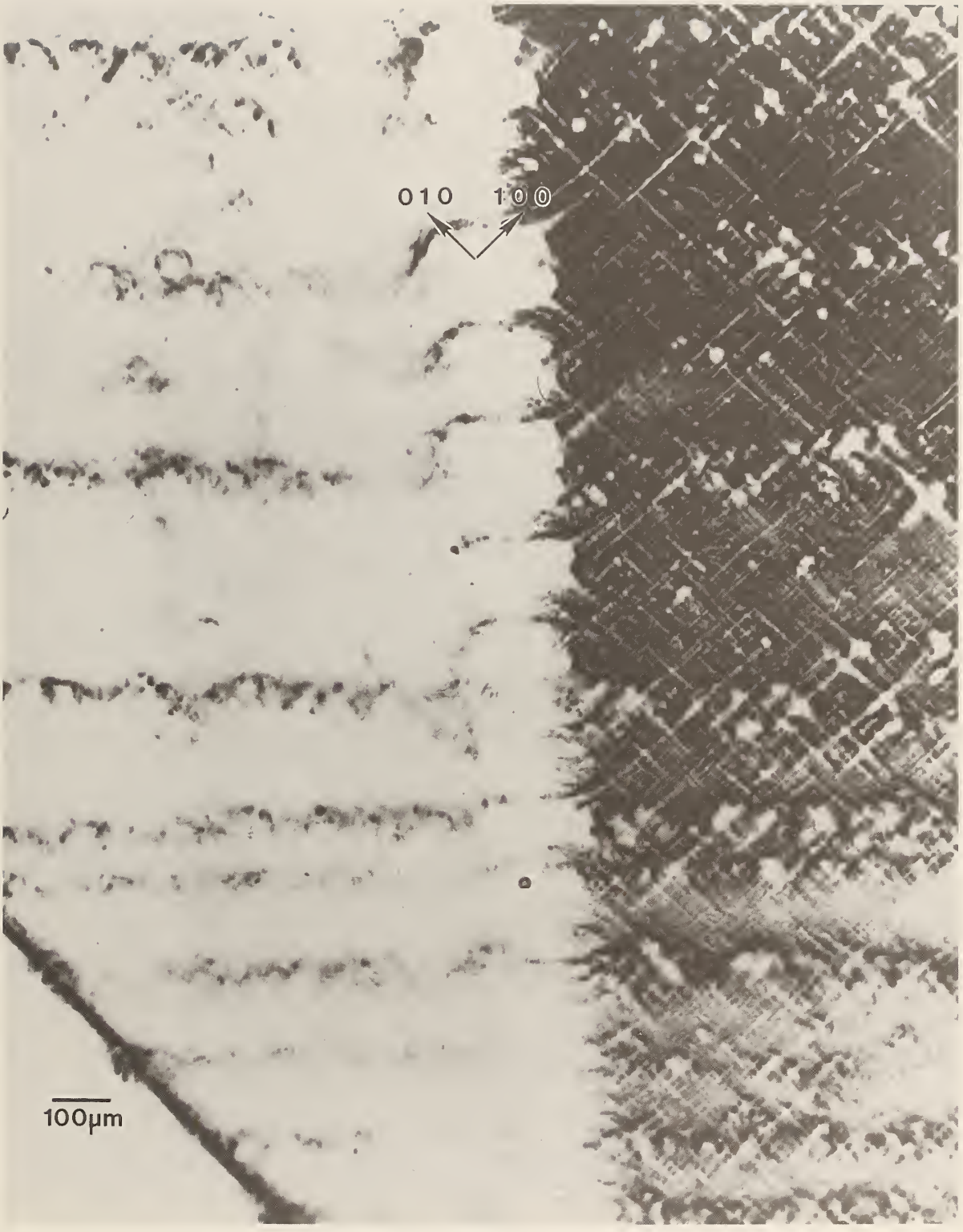

Figure 8. Enlargement of lower central portion of figure 1, (1 1 12) diffraction. Darker areas diffract more strongly.

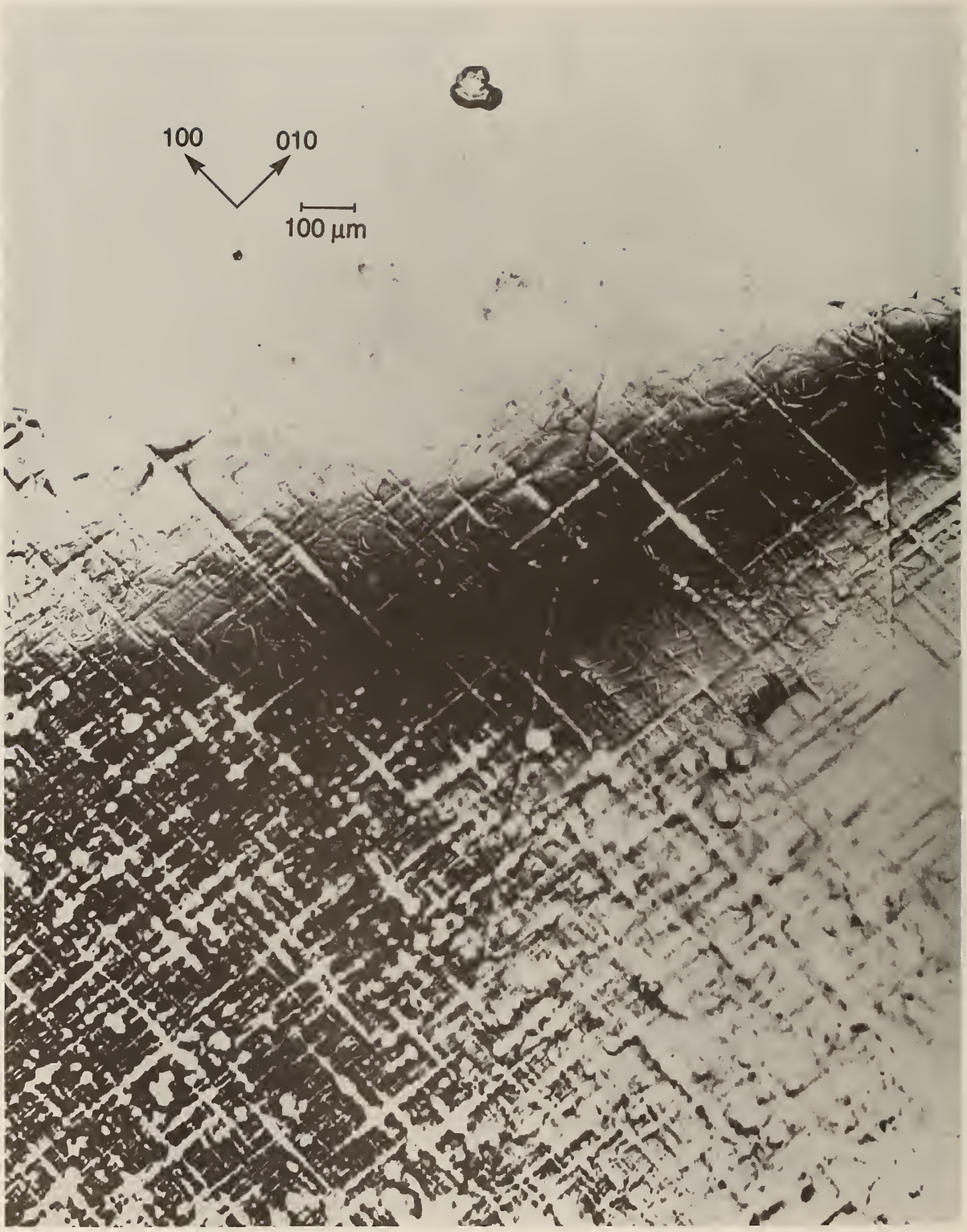

Figure 9. Enlargement of upper central portion of figure 1, (1 1 12) diffraction. Darker areas diffract more strongly.

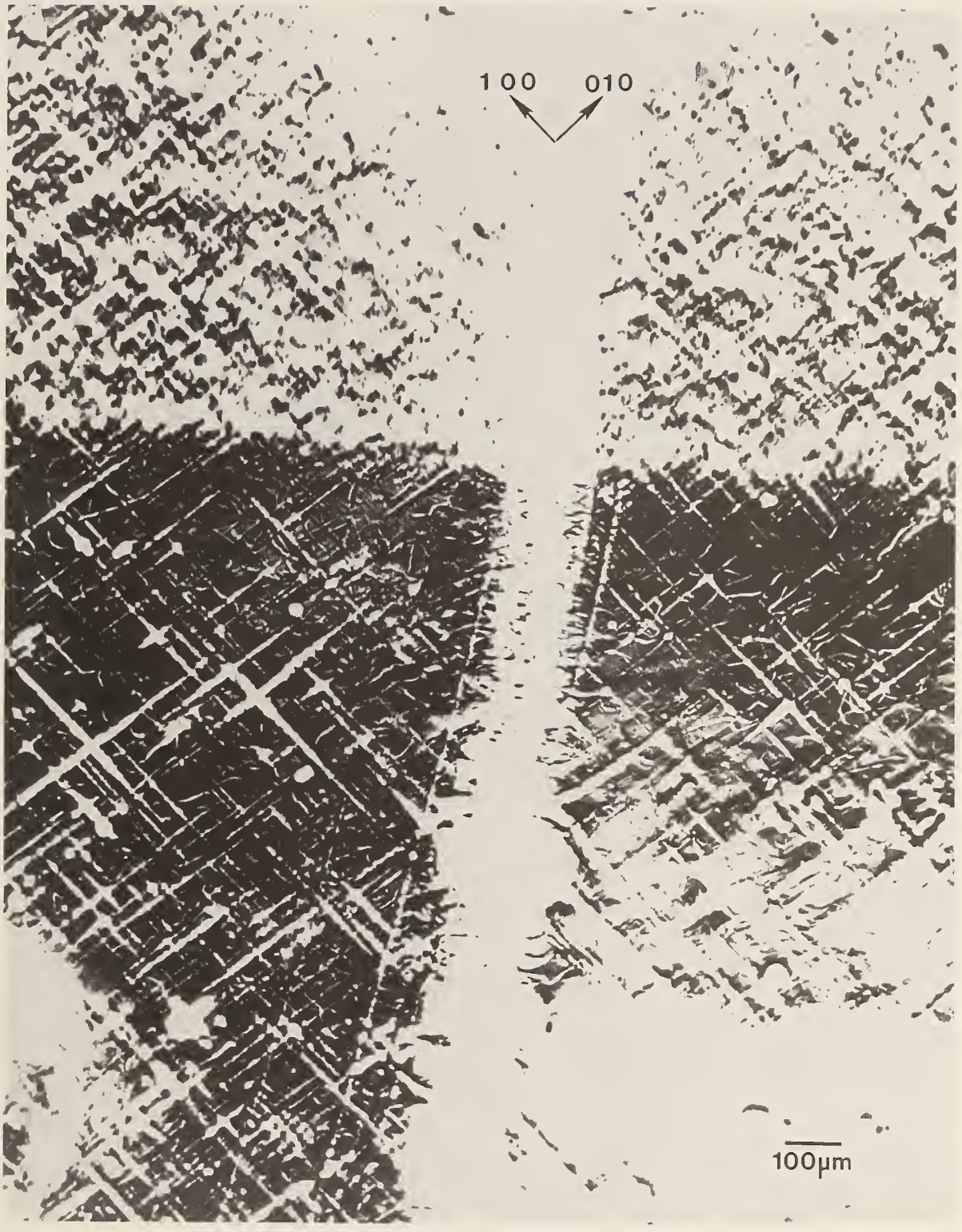

Figure 10. Enlargement of central portion of figure 2, (1 1 10) diffraction. This image is to be compared with the same crystal region imaged in (1 1 12) diffraction, figure 7. Darker areas diffract more strongly.

Figure 11. Enlargement of lower central portion of figure 2, (1 1 10) diffraction. This image is to be compared with the same crystal region imaged in (1 1 12) diffraction, figure 8. Darker areas diffract more strongly.

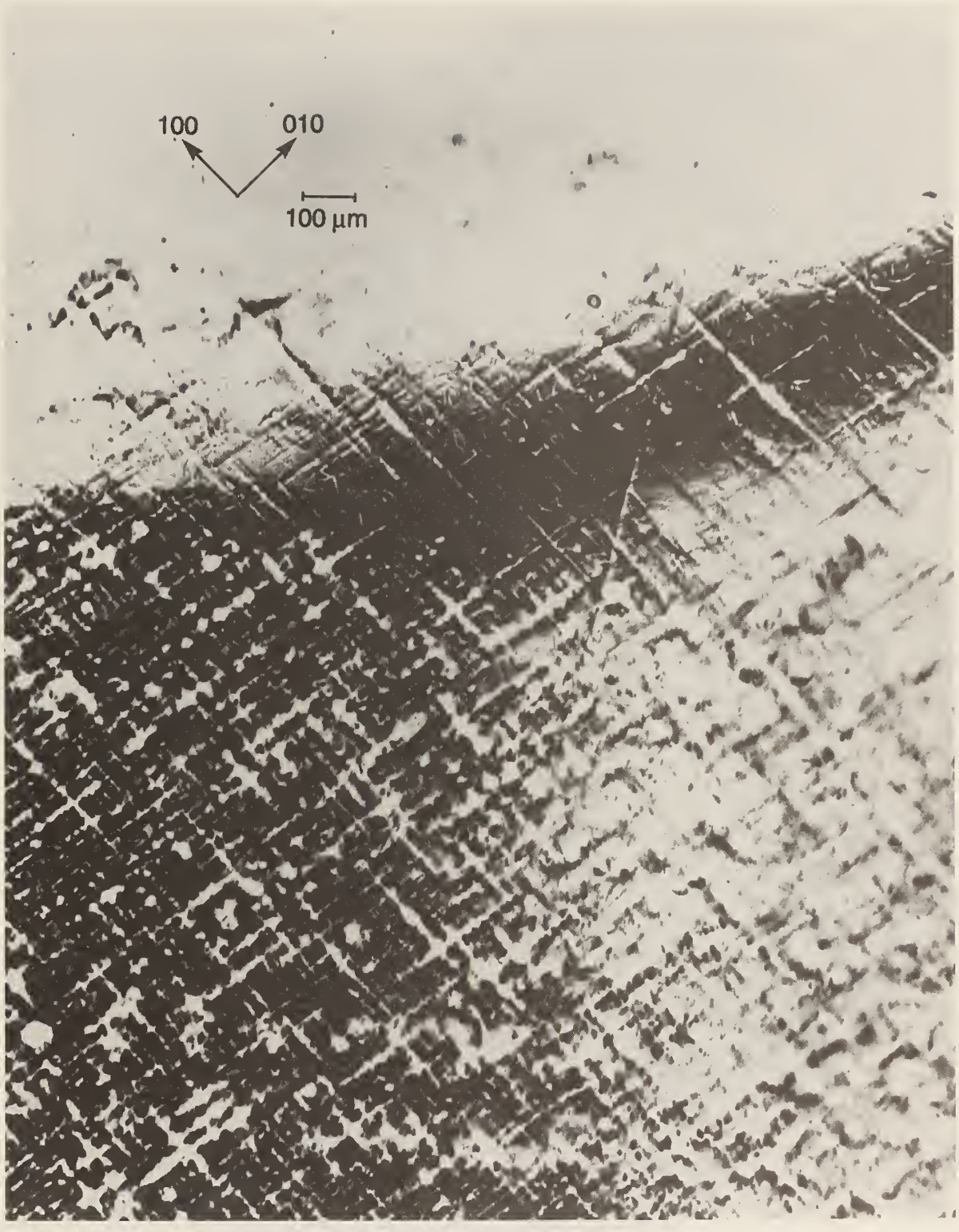

Figure 12. Enlargement of upper central portion of figure 2, (1 1 10) diffraction. This image is to be compared with the same crustal region imaged in (1 1 12) diffraction, figure 9. Darker areas diffract more strongly.

Figure 13. Enlargement of lower left-hand corner of figure 3, (0 1 10) diffraction. This image is to be compared with an overlapping crystal region imaged in (1 1 12) diffraction, figure 8, and in (1 1 10) diffraction, figure 11. Darker areas diffract more strongly.

Figure 14. Enlargement of upper left-hand corner of figure 3, (0 1 10) diffraction. Darker areas diffract more strongly.

Figure 15. Enlargement of the central portion of figure 3, (0 1 10) diffraction. This image is to be compared with the same crystal region imaged in (1 1 12) diffraction, figure 7, and in (1 1 10) diffraction, figure 10. Darker areas diffract more strongly.

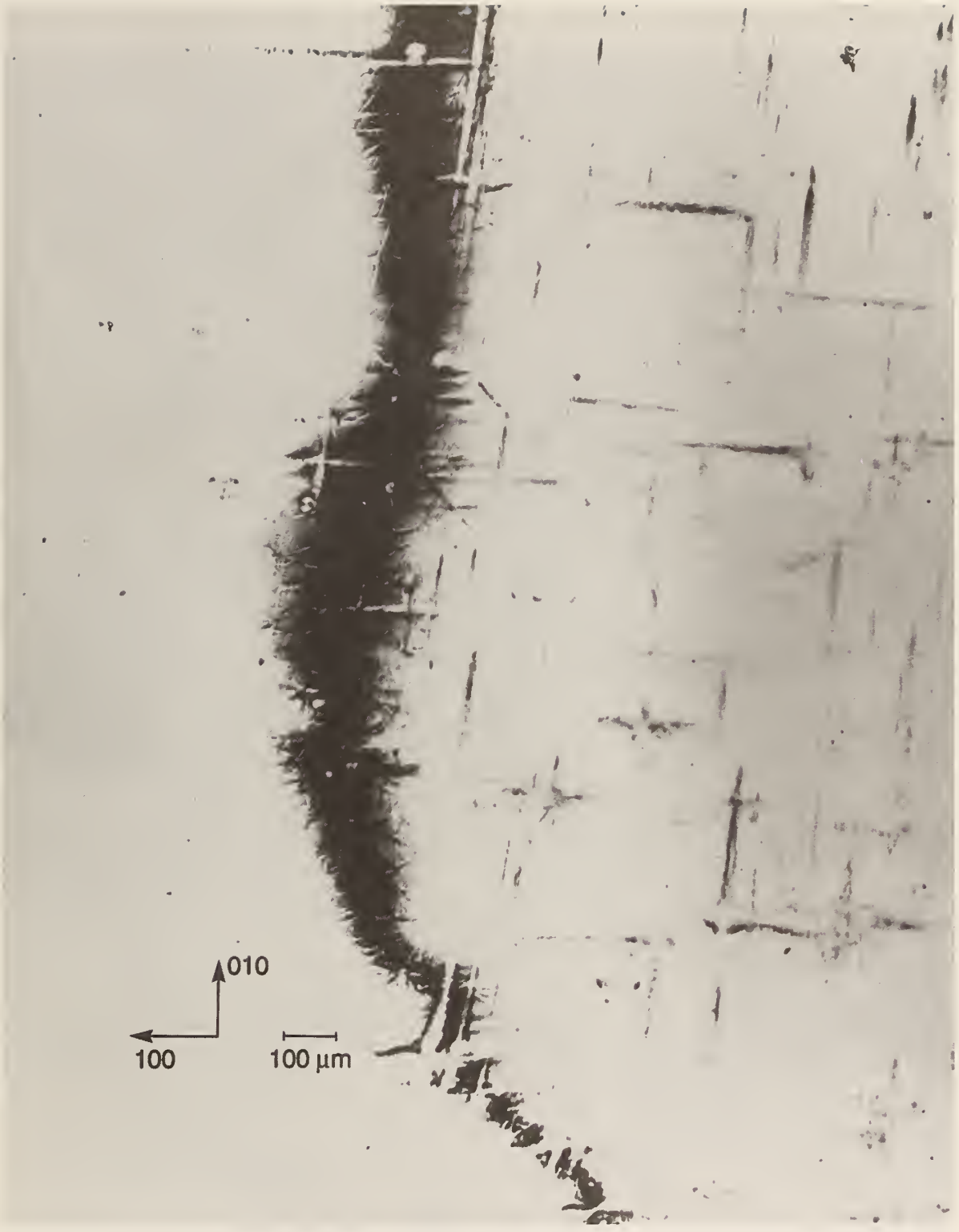

Figure 16. Enlargement of upper central portion of figure 3, (0 1 10) diffraction. The crystal region in this image is contiguous to the region imaged in (1 1 12) diffraction, figure 9, and in (1 1 10) diffraction, figure 12. Darker areas diffract more strongly.

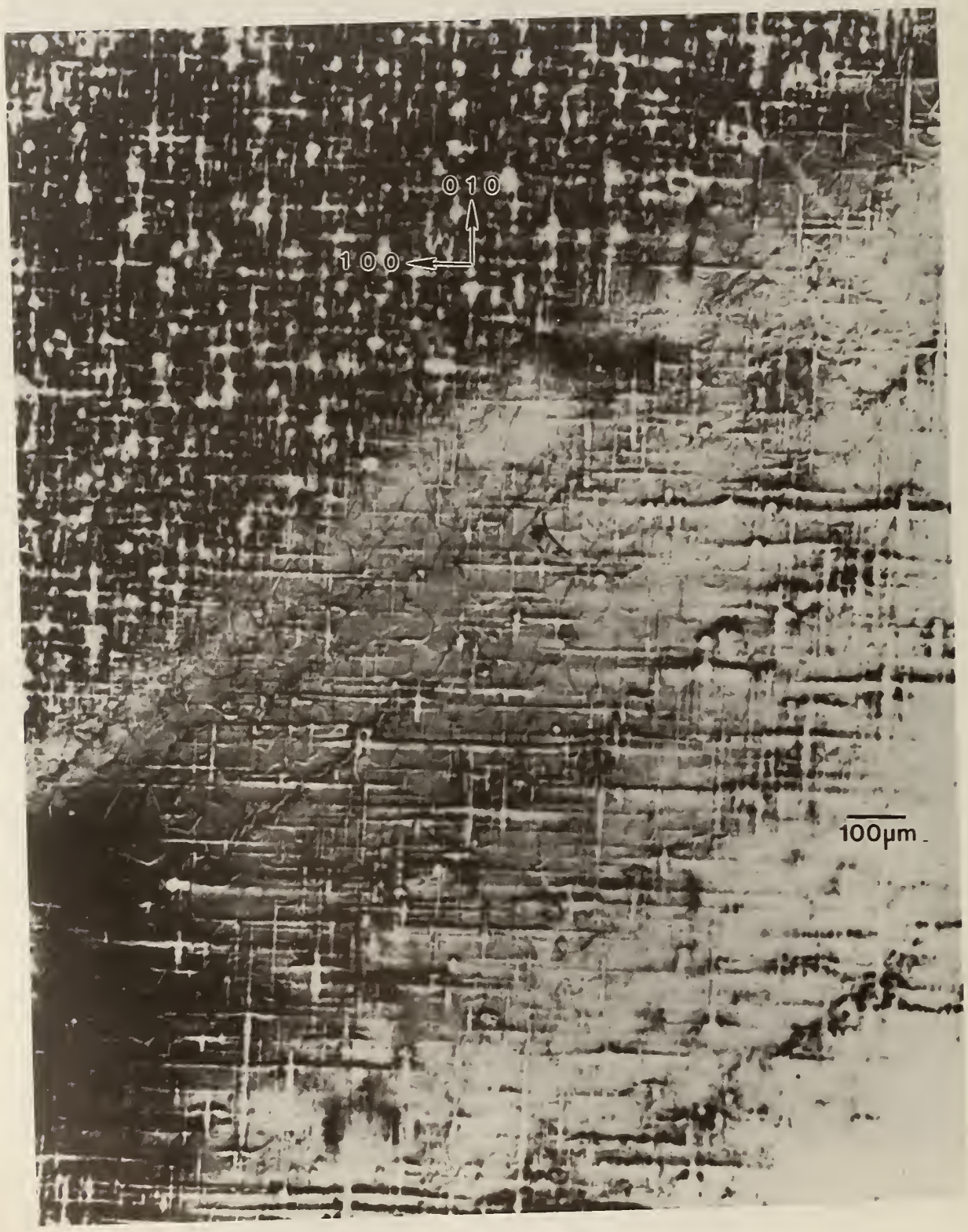

Figure 17. Enlargement of central portion of figure 4, (0 1 10) diffraction. Darker areas diffract more strongly.

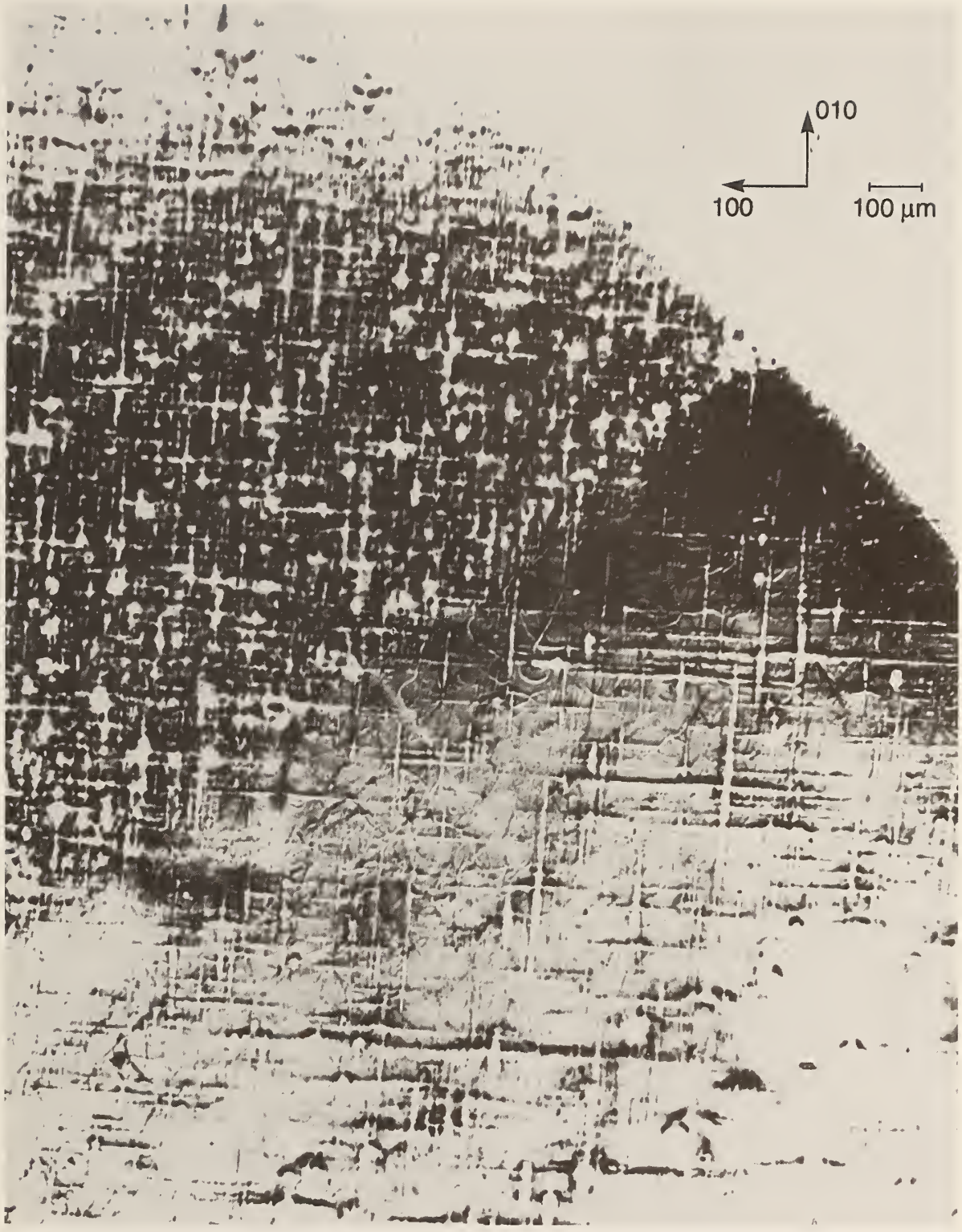

Figure 18. Enlargement of central portion of figure 4, (0 1 10) diffraction, overlapping the region shown in figure 17. The image here is to be compared with the same crystal region imaged in (1 1 12) diffraction, figure 7, and in (1 1 10) diffraction, figure 10. Darker areas diffract more strongly.

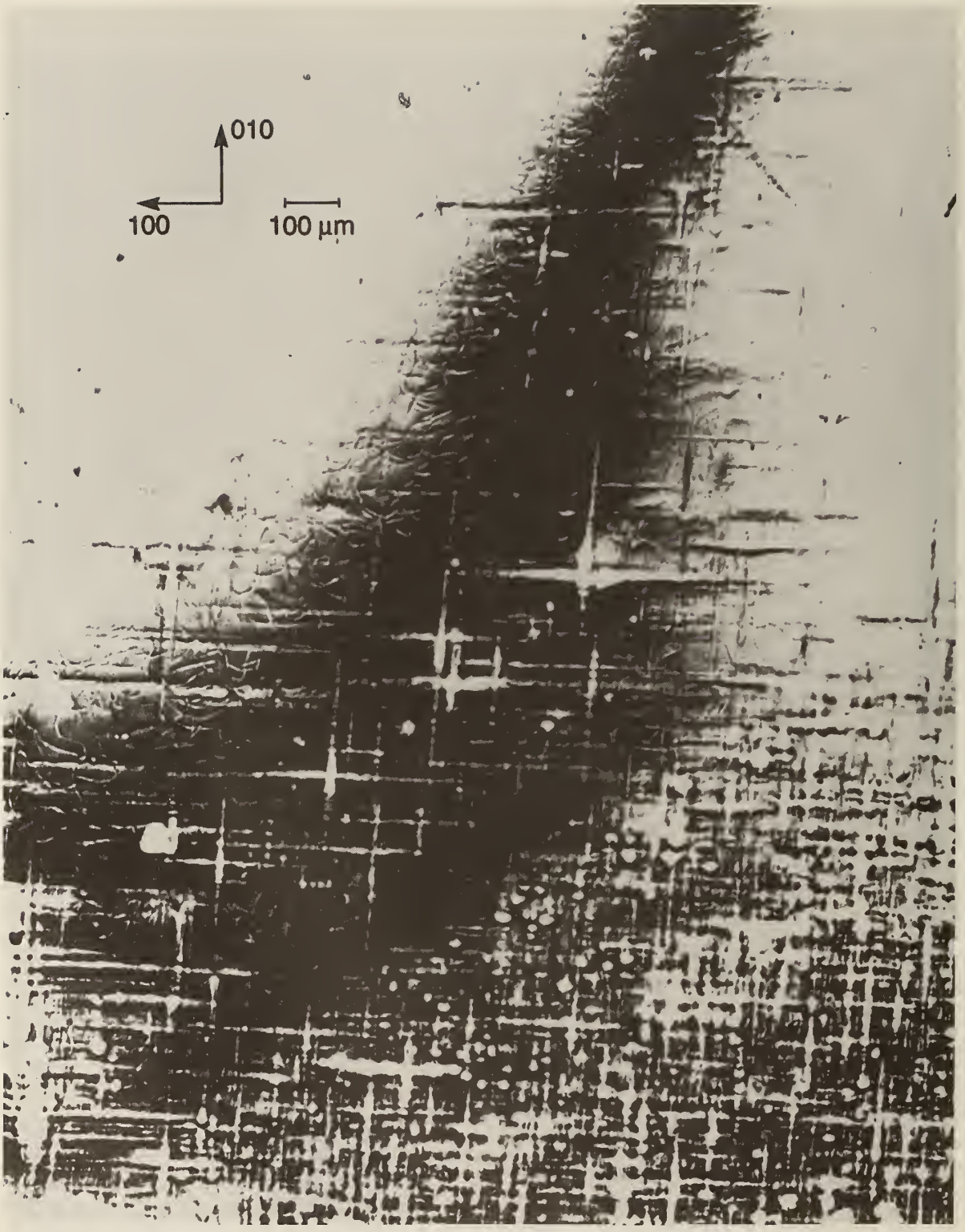

Figure 19. Enlargement of central right hand portion of figure 4, (0 1 10) diffraction. This crystal region overlaps that shown in (1 1 12) diffraction, figure 9, and in (1 1 10) diffraction, figure 12. Darker areas diffract more strongly.

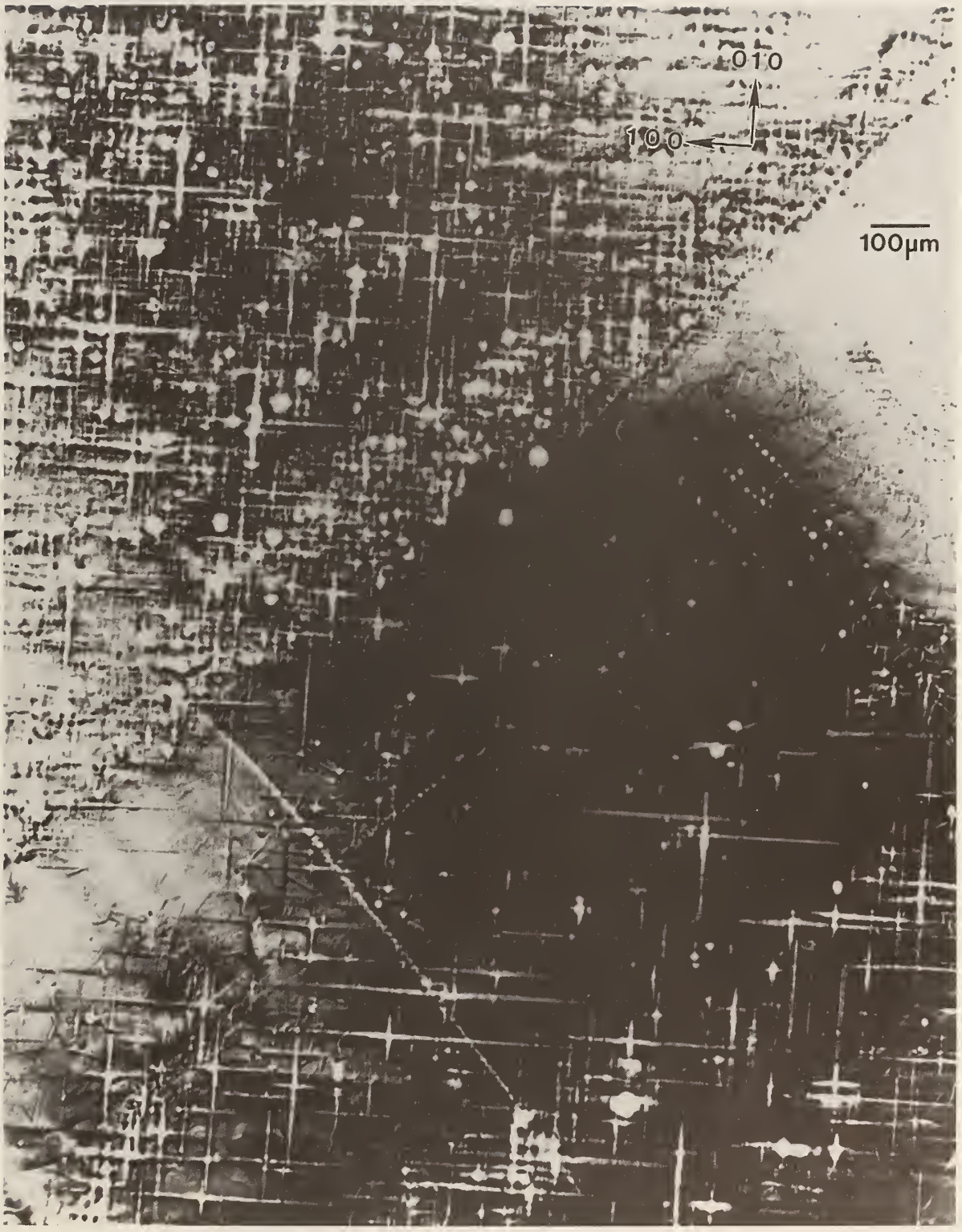

Figure 20. Enlargement of central portion of figure 5, (0 1 11) diffraction. Darker areas diffract more strongly.

Figure 21. Enlargement of central portion of figure 5, (0 1 11) diffraction, which overlaps the region imaged in figure 20 and in (1 1 12) diffraction, figure 7, and in (1 1 10) diffraction, figure 10. Darker areas diffract more strongly.

Figure 22. Enlargement of upper right central portion of figure 5, (0 1 11) diffraction. This image is to be compared with the same crystal region imaged in (0 1 10) diffraction, figure 16, and contiguous to the region imaged in (1 1 12) diffraction, figure 9, and in (1 1 10) diffraction, figure 12. Darker areas diffract more strongly.

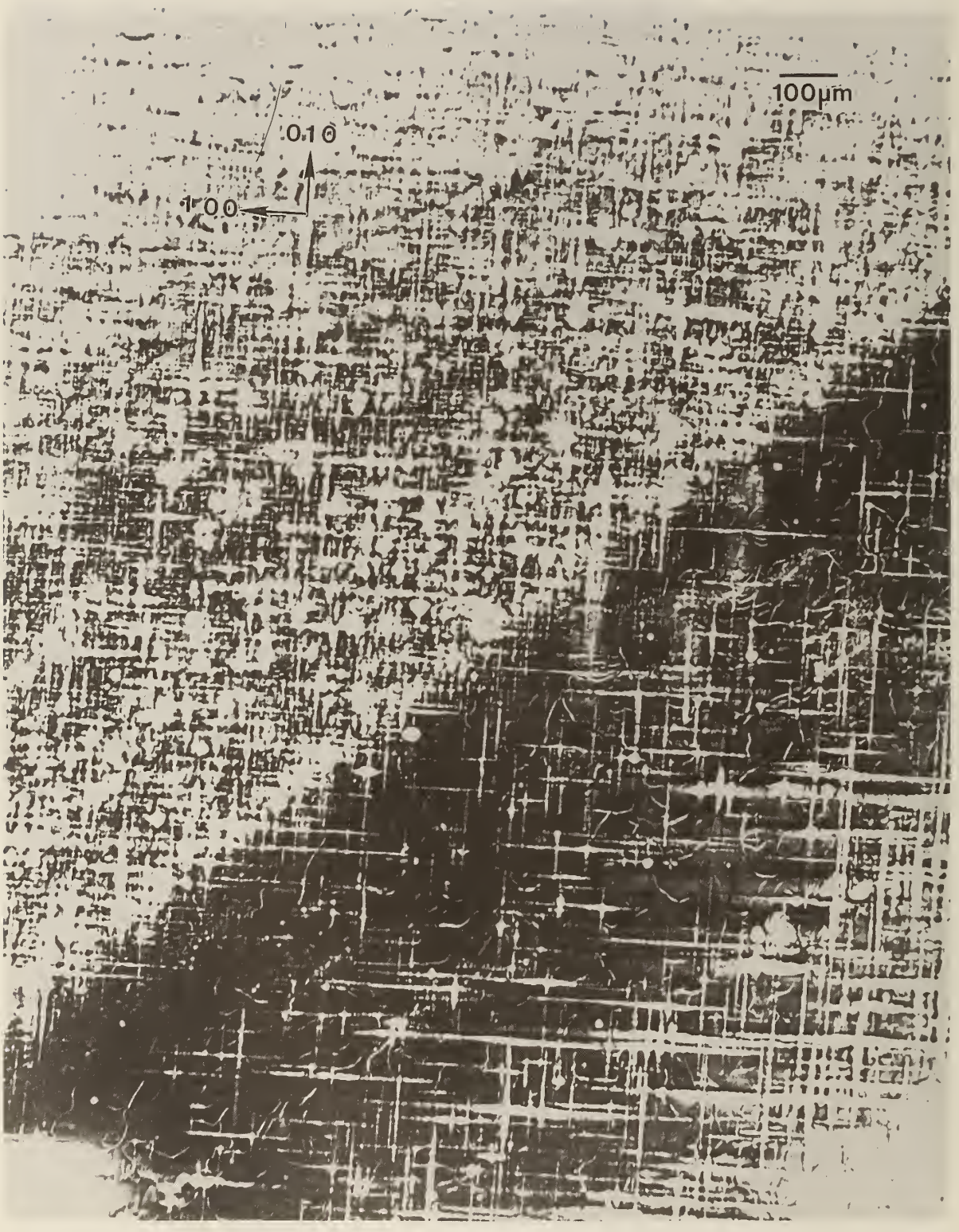

Figure 23. Enlargement of central portion of figure 6, (0 1 11) diffraction. This image is to be compared with the same crystal region shown in (0 1 10) diffraction, figure 17. Darker areas diffract more strongly.

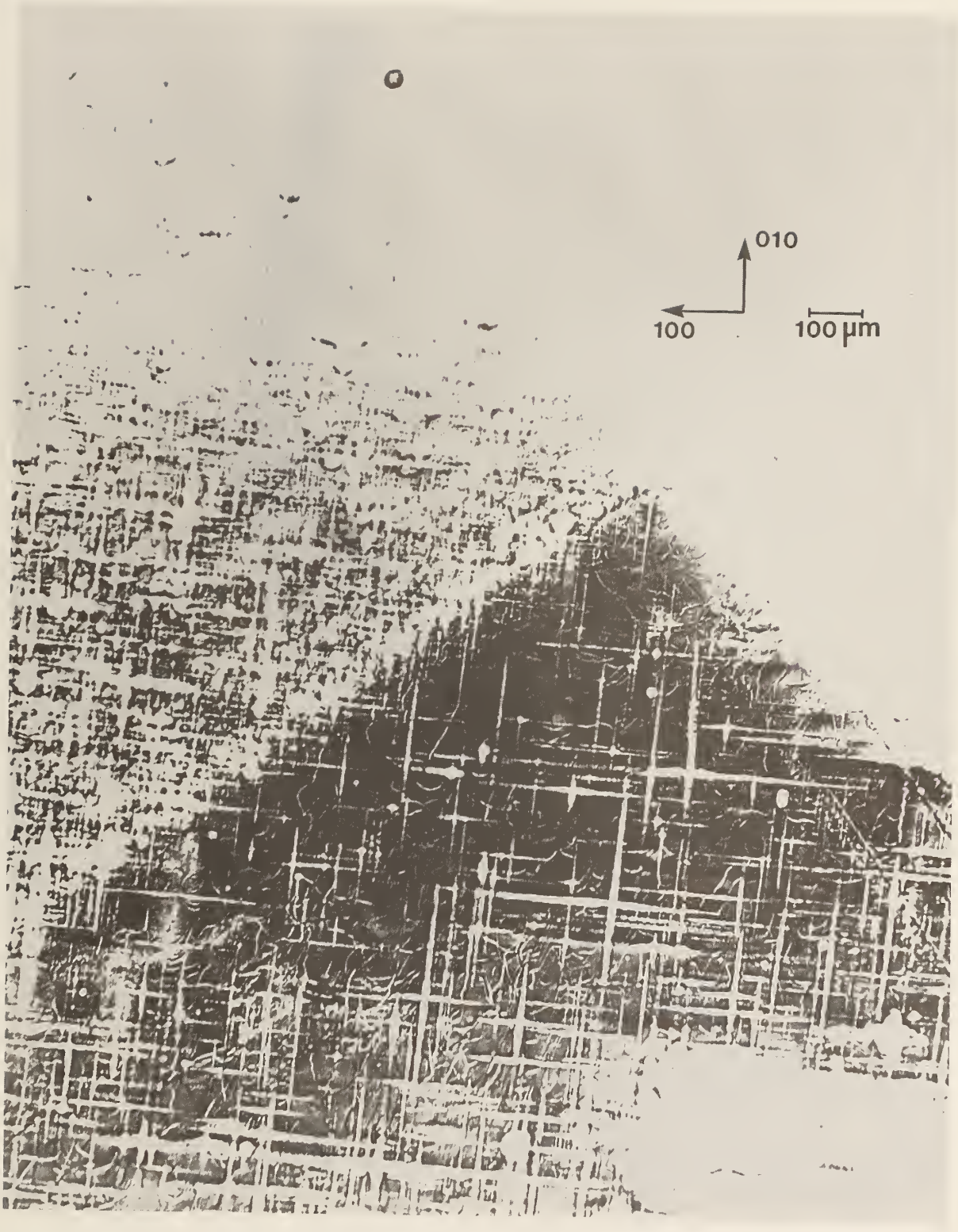

Figure 24. Enlargement of the subgrain junction in the central portion of figure 6, (0 1 11) diffraction. This image overlaps the region imaged in figure 23 and is to be compared with the same crystal region imaged in (1 1 12) diffraction, figure 7, and in (1 1 10) diffraction, figure 10.

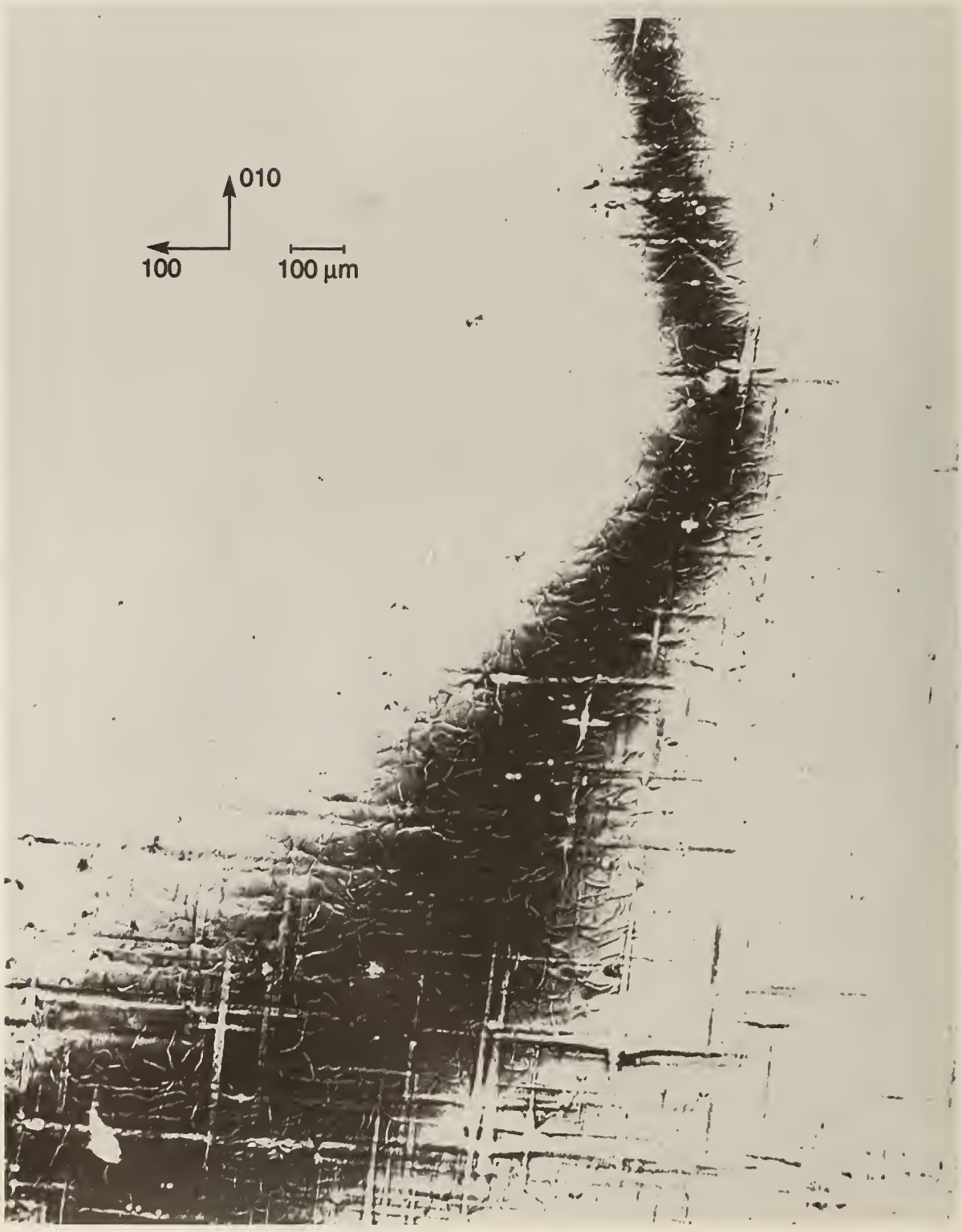

Figure 25. Enlargement of central right hand region of figure 6, (1 1 11) diffraction. This image is to be compared with the same crystal region imaged in (1 1 12) diffraction, figure 9, in (1 1 10) diffraction, figure 12, and in (0 1 10) diffraction, figure 19. Darker regions diffract more strongly.

In those regions characterized by a high density of discrete features, diffraction appear to be restricted to small (≈5 μm) cells of the type observed in scanning cathodoluminescence microscopy [13].

The other areas of the crystal contain similar features typically out of diffraction, but with a much lower density. In addition, however, these regions contain thin, curved features marked by varying sections of higher diffraction, lower diffraction, or alternating regions of higher and lower diffraction in tandem. The inability to observe diffraction in Laue geometry in the current series of experiments, because of the sample thickness, precludes firm identification now of these features as dislocations.

The nature and arrangement of these various features in this sample appear to make this crystal into a Rosetta stone in understanding the evolution of irregularity in mercuric iodide. Perhaps the initial question that arises is associated with the origin of the lattice twist. Does it arise during growth or only later during subsequently handling of this very soft crystal?

Six distinct observations all indicate that this lattice twist occurred during growth. The first two are that the twist axis does not extend across the entire crystal, and that once started, the magnitude of the apparent separation of the two parts of the images does not increase. It is difficult to conceive of such a partial lattice twist, one lying precisely in the (001) plane, developing through inadvertent mishandling. The third observation is that this twist axis is normal to the [$1\bar{1}0$] layered texture formed by a high density of additional phase features. These layers appear to be broad striations formed during growth; the [110] lattice twist axis thus appears to be aligned with the crystal growth direction. Fourth, the gradually curved nature of some of the linear multiple phase configurations in the vicinity of the lattice rotation is more consistent with growth than with post-growth bending. Fifth, the onset of the lattice twist immediately precedes a major textural change that appears to be growth-related. The final observation is the bending that has been noted in the lattice twist axis, bending that differs in the two resulting subgrains.

Additional examination of the interfaces between the widest stratum of high-density features and the adjacent low feature density strata, Figures 9, 12, 19, and 7, 10, 15, 17, 18, 20, 21, 23, 24, respectively, confirm the growth orientation and the origin of the lattice twist. The linear additional phase features in the low-density layer immediately adjacent to the high-density region near the center of the crystal appear correlated closely with individual features in the high-density region. Growth thus took place in this part of the crystal from the high-density stratum to the low-density stratum, i.e., in a direction projecting onto the (001) crystal surface in the [$1\bar{1}0$] direction. Moreover, as just

noted, the sharp lattice twist appears to begin immediately preceding the onset of the broad textural stratum of high density of (precipitate) features, where it joins the preceding low feature density textural stratum.

All of these observations are consistent with a growth model in which growth begins in the extreme [110] corner of this crystal (in figure 1, for example, this is the top corner) and proceeds relatively uneventfully in the [110] direction (downward in figure 1, for example), or at least in a direction projected onto this direction in the images, until just before the onset of the wide swath of a high density of additional phase features, one of which initiated the sharp lattice twist visible in figures 9, 12, 16, 19, 22, 25. This twist then propagated for the remainder of the growth. During this subsequent growth, briefer periods of relatively high additional phase density alternate with periods of relatively low additional phase density.

Several closely related questions now arise. What is the nature of the additional phase(s)? What causes the additional phase(s) to form? Why does one form appear oriented crystallographically in {100} directions of the matrix? What restricts diffraction to small regions in some areas? And, finally, are the features that are out of diffraction responsible for the much higher degree of long range lattice perfection in lattice orientation (within a few seconds of arc over several millimeters), with which they appear to be associated?

An important observation is made in the evaporation of such crystals. As material is removed, small specks of foreign material similar in size to the additional phase features observed in this study accumulate on the surface, at an irregular rate. Chemical analysis indicates these specks are neither mercury nor iodine precipitates but rather consist of metal organic impurities with a carbon content of the order of 70% and a wide variety of metals. It is tempting to associate these observed impurity formations with the additional phase(s) observed in diffraction and therefore to conclude that these impurities reside in such crystals in discrete form.

The morphology of the diffraction images permits us to develop two alternative growth models, which tie together all of these observations. Growth over a region of a few micrometers forms a crystal with a relatively high degree of purity and crystal perfection, creating small regions that diffract strongly. Impurities are rejected from the crystal during this stage of the growth process, in a manner similar to constitutional supercooling, and accumulate near the growth surface.

In one model, the level of impurities after growth of a few micrometers accumulates to such an extent that they precipitate out, marking the local growth surface in {100} directions. At

reentrant corners of such {100} growth surfaces a globular precipitate possibly forms. In a second model, the rejection of impurity stimulates dendritic growth, which leaves the linear features observed in {100} directions. In this case, the globular form of the precipitate may form in the reentrant dendritic locations. Alternatively, the features that appear to be globular may simply represent the cross section of dendrites normal to the image surface. None of our observations to date permit us to distinguish absolutely between these two models.

Either model must be modulated by an as yet unidentified process that controls the general impurity level and produces as a result textural stripes or striations delineated by the density of precipitates. The resulting composite formed in either model resists deformation. It consists of relatively pure and thus relatively strain-free components.

2. Spacelab III Crystal

The crystal grown in Spacelab III diffracts over a wider angular range, about one and one half degrees. Full high-resolution diffraction images appear in figures 26-28, with enlarged regions of these in figures 29-31. It is clear from the appearance of the full images as well as from the one and one half degree acceptance angle for diffraction that the lattice orientation or parameter of the space crystal in its entirety is less uniform than the comparable terrestrial crystal shown in figures 1-6: that is, less of the space crystal appears in diffraction at a given angle of incidence than does the comparable terrestrial crystal, indicating gradual variation either in lattice parameter or lattice orientation, or both.

Perhaps closely related, but potentially far more important, is absence in the enlargements of the images of the Spacelab III crystal of arrays of features that are out of diffraction, the textural arrays characteristic of the comparable terrestrial crystal. A few irregular regions of the order of 50 μm across that are out of diffraction are observed, but they are much less pervasive and sharply delineated than are those in the terrestrial crystal. None of the crystallographically oriented regular regions that are typically out of diffraction in the images of the comparable terrestrial crystal are observed in the Spacelab III crystal. The formation of regions of additional phase(s) thus appears to be almost completely suppressed in the crystal grown in microgravity.

One set of features visible in the enlarged images of the Spacelab III crystal is not observed in the images of its terrestrial counterpart: small (10-30 μm) highly diffracting spots in the vicinity of the main highly diffracting regions. These features suggest cells oriented in a direction differing from the direction

Figure 26. High-resolution (008) 8 keV diffraction image in Bragg geometry of (001) surface of Spacelab III HgI_2 crystal 118. Lighter areas diffract more strongly.

Figure 27. High-resolution (1 1 10) 8 keV diffraction image in Bragg geometry of (001) surface of Spacelab III HgI_2 crystal 118. Lighter areas diffract more strongly.

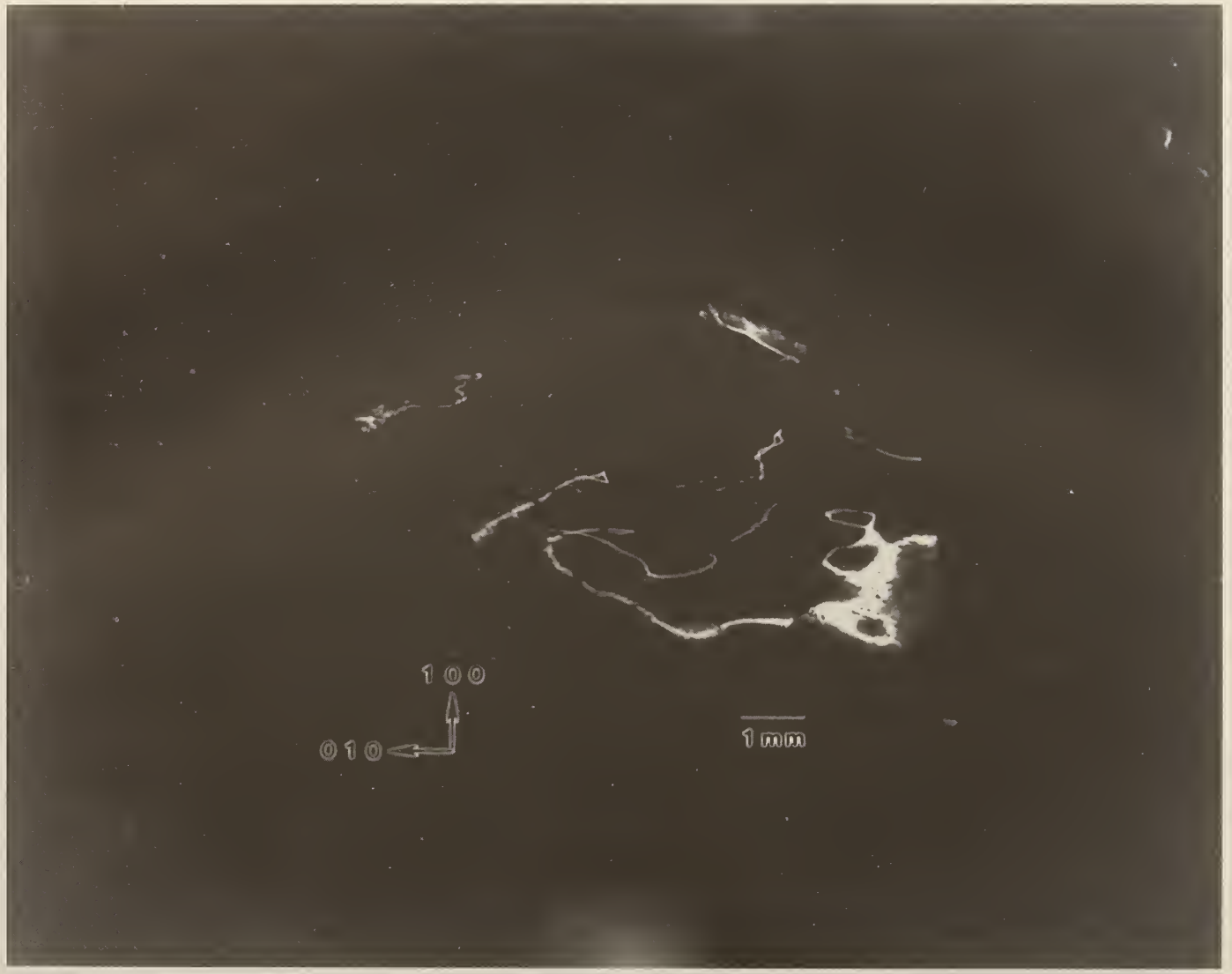

Figure 28. High-resolution (1 0 10) keV diffraction image in Bragg geometry of (001) surface of Spacelab III HgI_2 crystal 118. Lighter areas diffract more strongly.

Figure 29. Enlargement of main region of figure 26, (008) diffraction. Darker areas diffract more strongly.

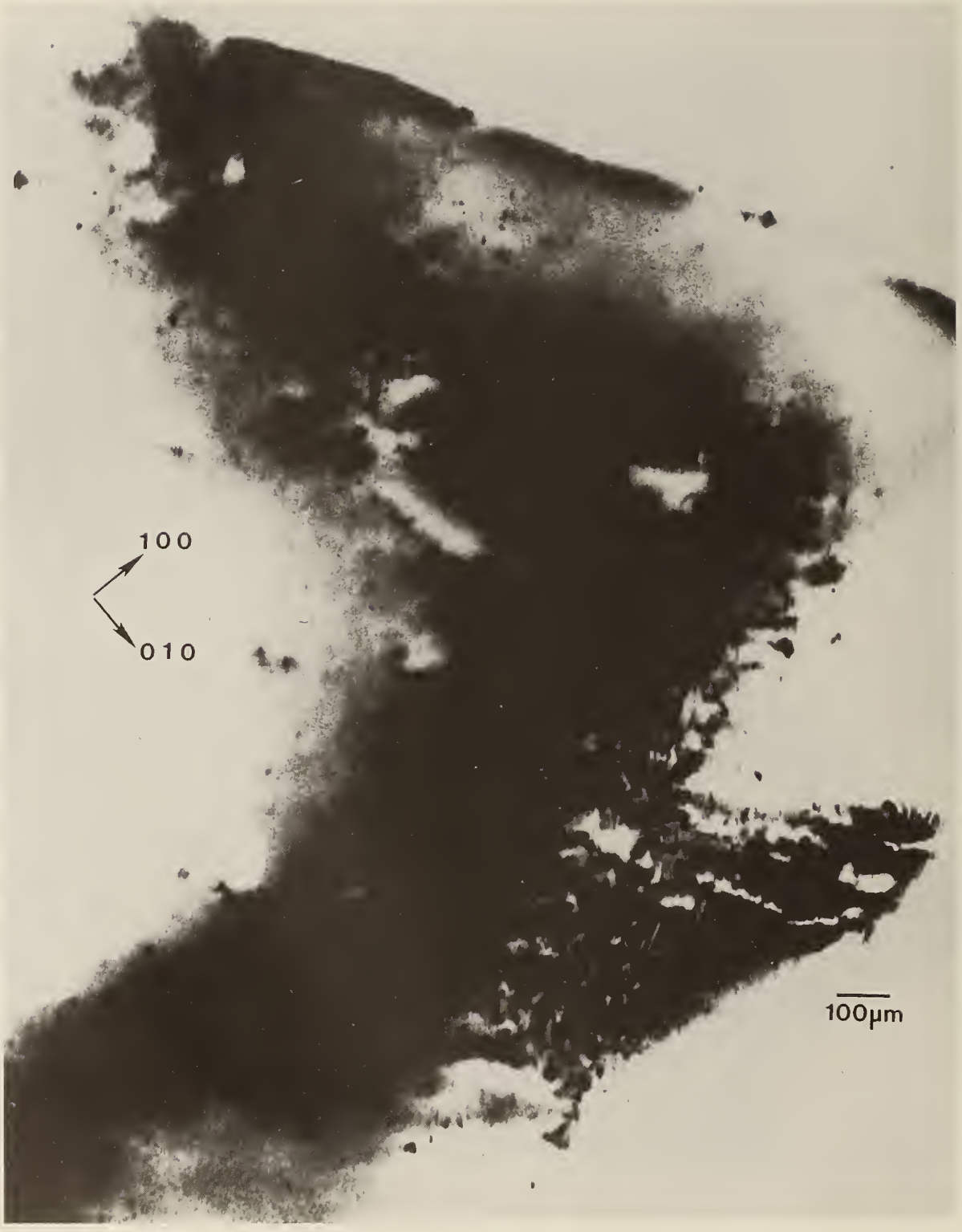

Figure 30. Enlargement of main region of figure 27, (1 1 10) diffraction. Darker areas diffract more strongly.

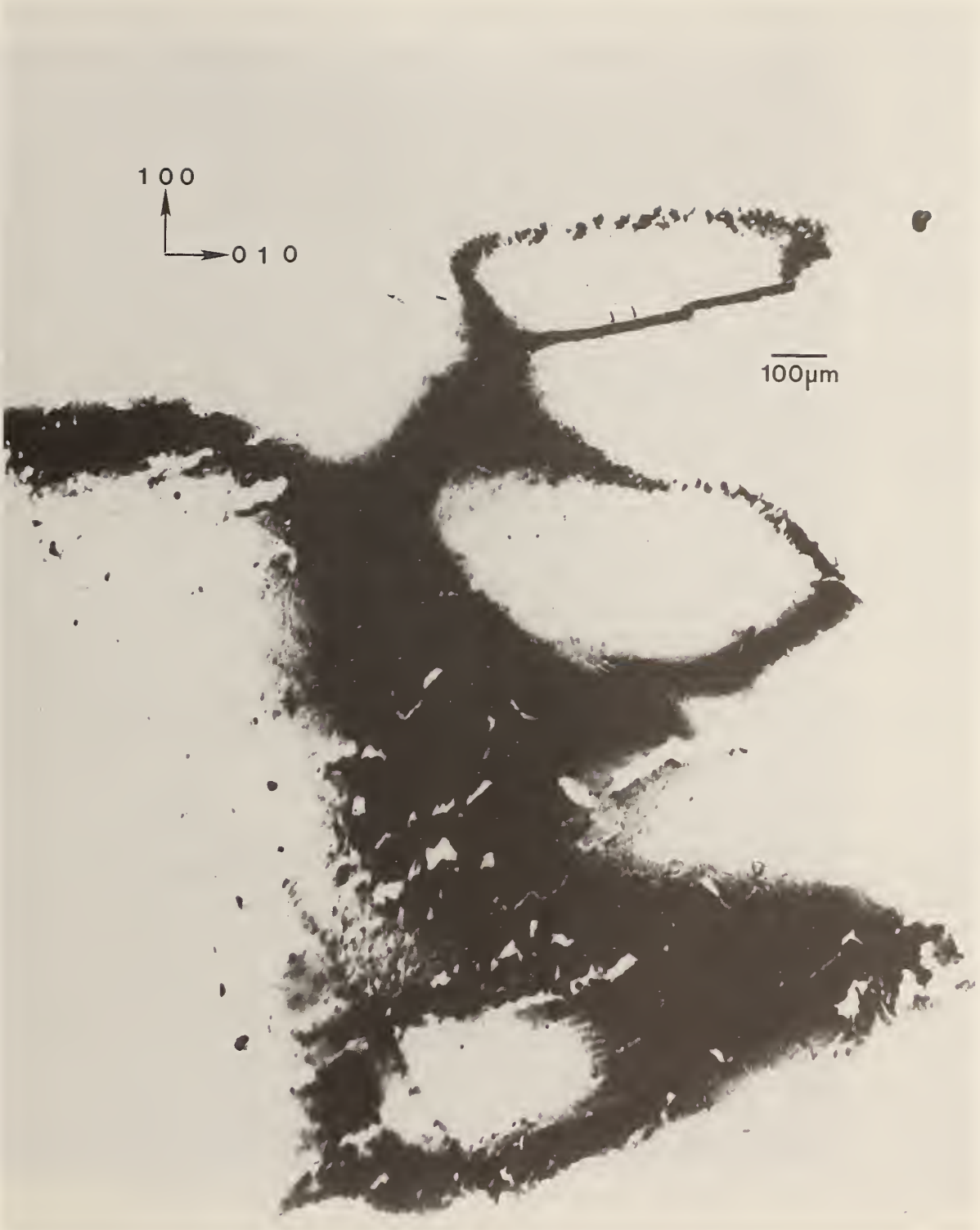

Figure 31. Enlargement of main region of figure 28, (1 0 10) diffraction. Darker areas diffract more strongly.

of the surrounding matrix by perhaps a few tens of arc seconds. Such regions may also be present in the terrestrial crystal, but if so they are obscured by the heavy incidence of additional phase(s).

The Spacelab III sample differed from the terrestrial sample not only by its growth in microgravity, but also by the superposition of graphite electrodes; so that its performance as a neutron and x-ray detector could be measured. Since graphite is relatively transparent to x-rays, these electrodes were not expected to interfere with the imaging process itself. While they could in principle have affected the surface strain, we found no evidence for this.

However, this crystal was not encapsulated. With the passage of the 5 years that this crystal has been in the laboratory, some deterioration in electronic performance of the device made from it actually has been observed, as is characteristic also of unencapsulated devices made in terrestrial environments.

The role of microgravity in the drastic reduction in the formation of the additional phase(s) observed in the comparable terrestrial crystal is not yet understood. The observed gradual variation in lattice is consistent with varying retention within the lattice of some foreign material. This analysis leads to increased interest in the results of the growth of a mercuric iodide from the much purer material scheduled for a future flight.

3. Terrestrial Crystal to Be Compared to a Future Flight Crystal

The third mercuric iodide crystal, grown from higher purity material similar to that to be used on a future flight, diffracts over a full two degrees. Complete high-resolution diffraction images appear in figures 32-33, with enlarged regions of these in figures 34-35. The extent and character of the diffraction in these images, reflecting the general lattice uniformity, resembles much more the diffraction from the Spacelab III crystal than that from its terrestrially-grown counterpart. Moreover, the absence of an array of small features that are out of diffraction also gives these images much more the character of those from the Spacelab III crystal than those from the terrestrial crystal grown about the same time from similar material. The complete absence of evidence for additional phases in this high purity crystal is consistent with the thesis that the features that are out of diffraction in images of the earlier crystals are impurities, but this thesis certainly is not proved conclusively by this correlation.

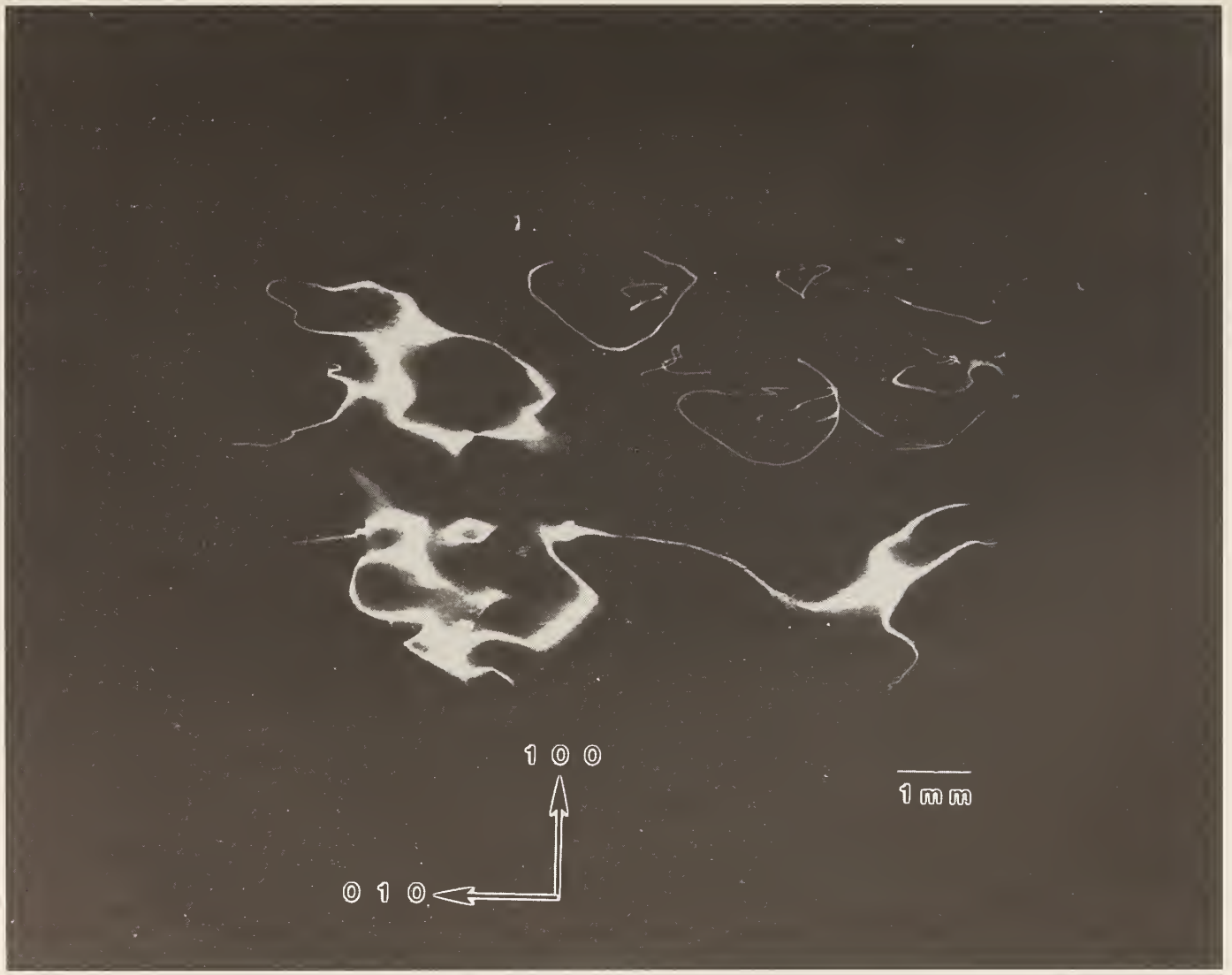

Figure 32. High-resolution (1 0 10) 8 keV diffraction image in Bragg geometry of (001) surface of terrestrial HgI_2 crystal 113, comparable to crystal to be grown on IML 1. Lighter areas diffract more strongly.

Figure 33. High-resolution (1 1 10) 8 keV diffraction image in Bragg geometry of (001) surface of terrestrial HgI_2 crystal 113, comparable to crystal to be grown on IML 1. Lighter areas diffract more strongly.

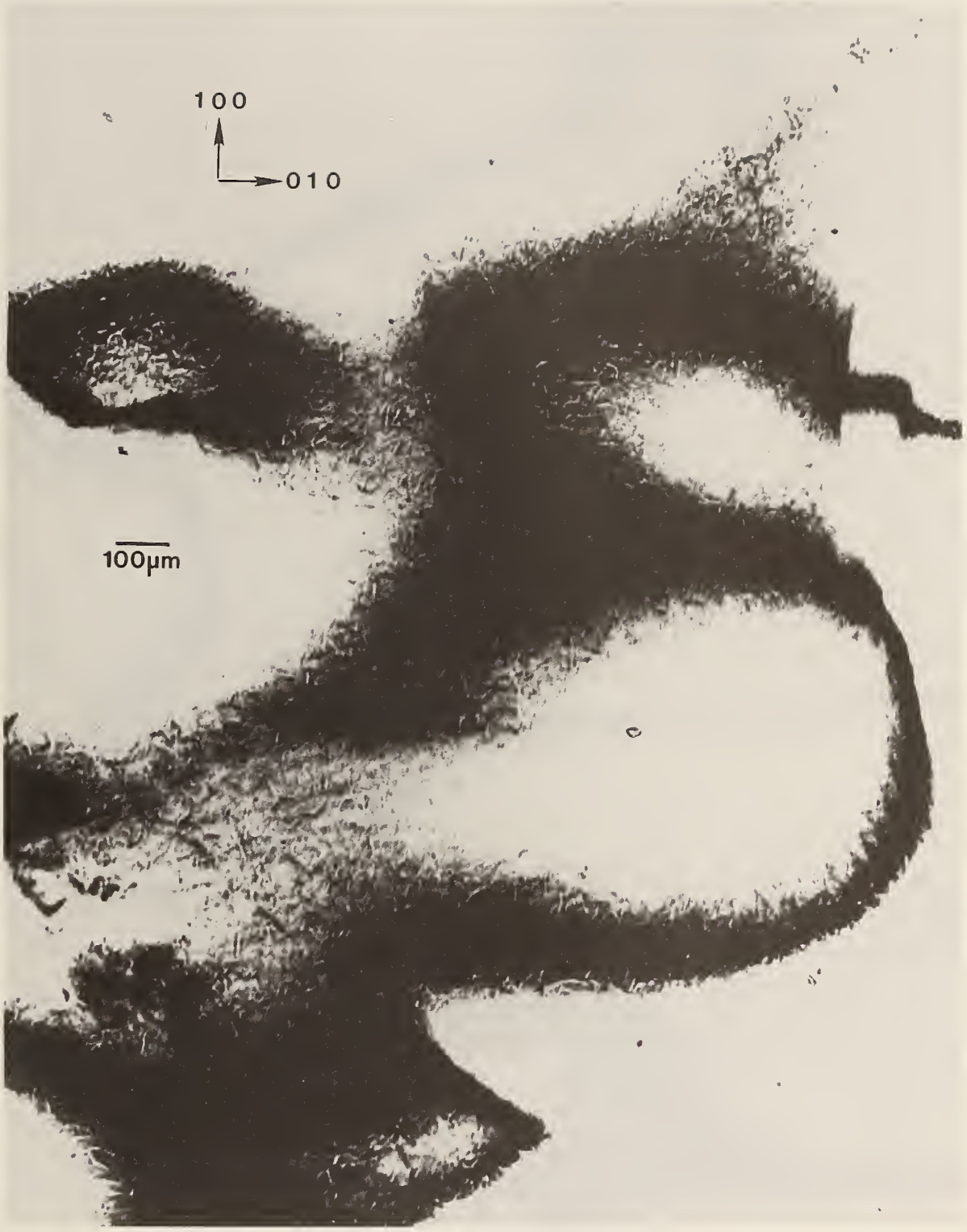

Figure 34. Enlargement of lower left portion on figure 32, (1 0 10) diffraction. Darker areas diffract more strongly.

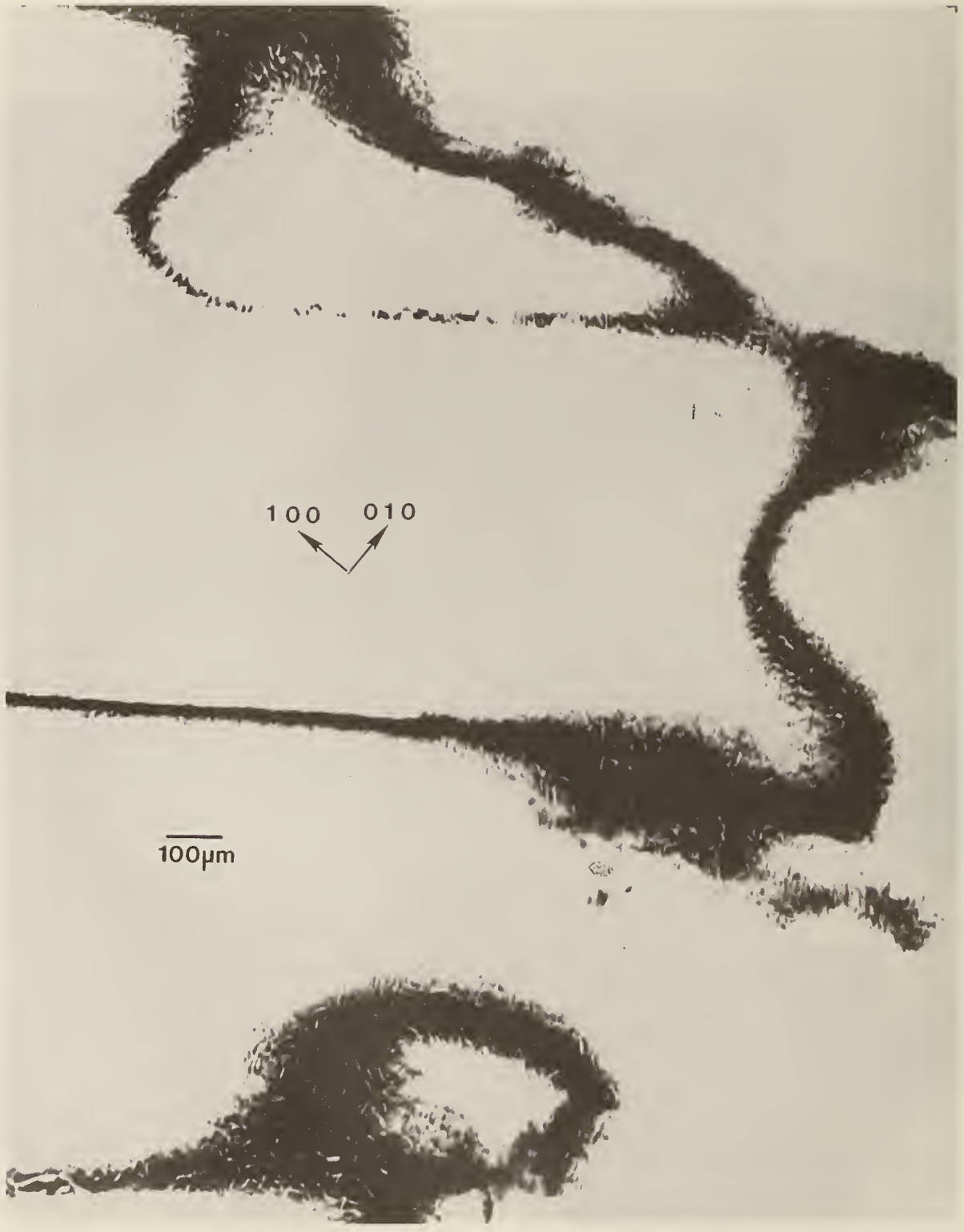

Figure 35. Enlargement of lower central portion of figure 33, (1 1 10) diffraction. Darker areas diffract more strongly.

We turn now to the extremely important comparison of detectors made from the Spacelab III crystal and from terrestrial crystals resembling those of this study. The performance of devices made from the new high purity material approaches the original performance of the device made from the Spacelab III crystal. The improved performance of the Spacelab III crystal is traceable to the higher mobility of its charge carriers. Recent improvements in terrestrial crystal growth represented by the crystal examined here have led to improved carrier lifetime. Although the electronic improvements are quite distinct in these two cases, in neither of them do we find the additional phase features that we have observed in the first terrestrial crystal. Thus absence of a additional phase precipitates appears to be much more important to device performance than the generally higher level of lattice uniformity that we observe in the first terrestrial crystal. The stiffening provided by additional phase precipitates apparently comes at too high a price in terms of charge carrier trapping.

Future space growth of this high purity material now assumes particular interest. Will incorporation of residual impurities in the final crystal even below their currently low level in the charge material be achieved in space growth? And, if so, will these lower impurity levels lead to greater general lattice uniformity? And finally, will this new level of regularity result in still further improvement in device performance?

B. Lead Tin Telluride

1. Terrestrial Crystal Comparable to STS 61A Crystal

Various regions of the terrestrially grown sample of lead tin telluride, similar to one grown on STS 61 A, diffract as the crystal is rocked over a full two degrees. Full high-resolution diffraction images are shown in figures 36-43. Growth was in the [001] direction, which is oriented "down" in all figures.

The sample was a regular half cylinder. The sharply delineated irregular outlines of the images in figures 36 and 38 thus indicate immediately that several grains are present: the curvature of the [110] (right hand) edge indicates that a subsidiary grain started to grow almost simultaneously with the main grain. Then, after 1 centimeter of growth, a third grain started to grow between the center of the boule and the opposite edge of the main grain. It grew laterally more rapidly than the nucleating grain, however, displacing and, after another 2 centimeters, completely overtaking the growth of the nucleating grain. The new grain is brought into diffraction in figures 37 and 39 simply by rotation of the sample about the boule (growth) axis.

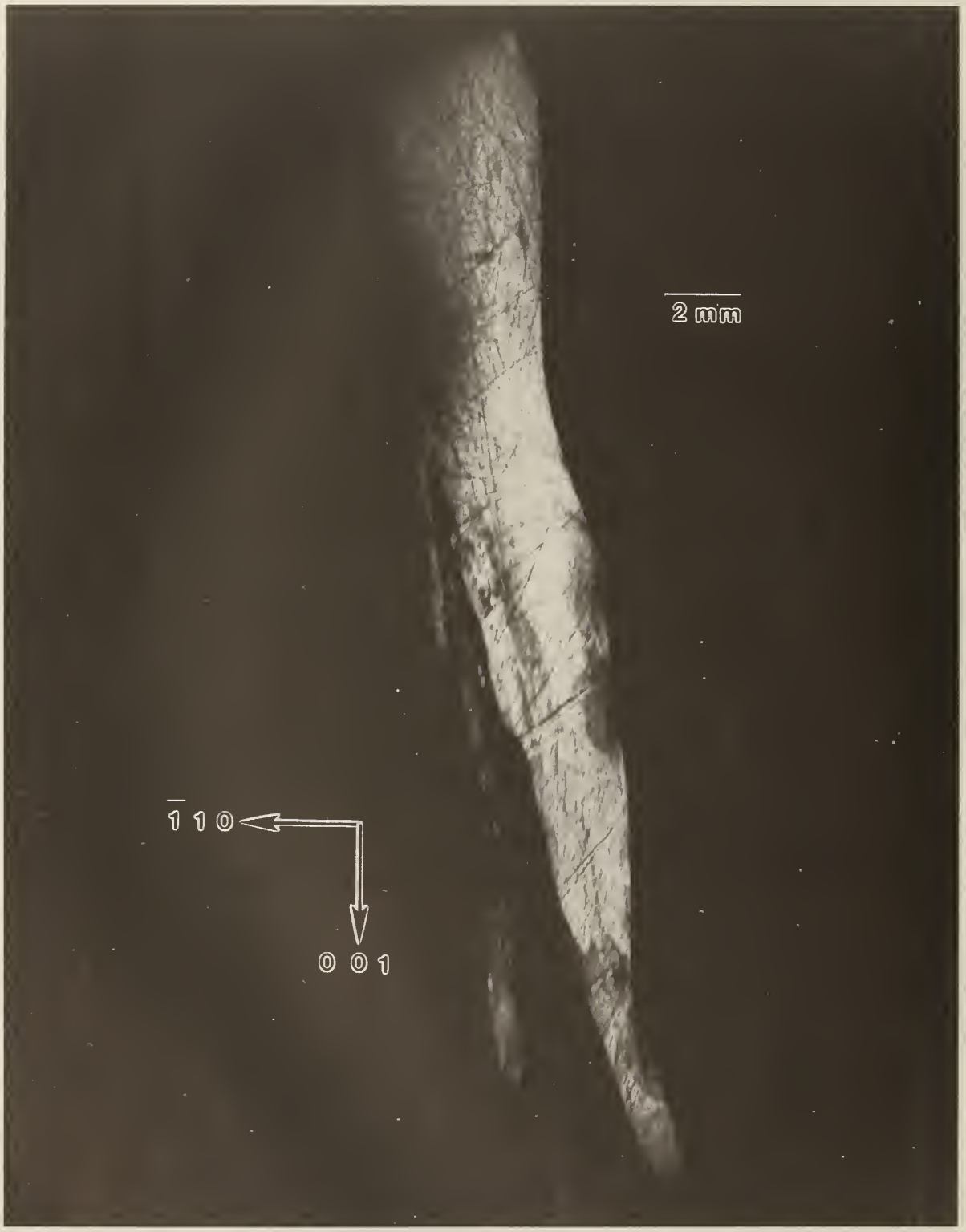

Figure 36. High-resolution (220) 8 keV diffraction image in Bragg geometry of approximately (220) surface of terrestrial PbSnTe crystal 108. The growth direction is [001]. Lighter areas diffract more strongly.

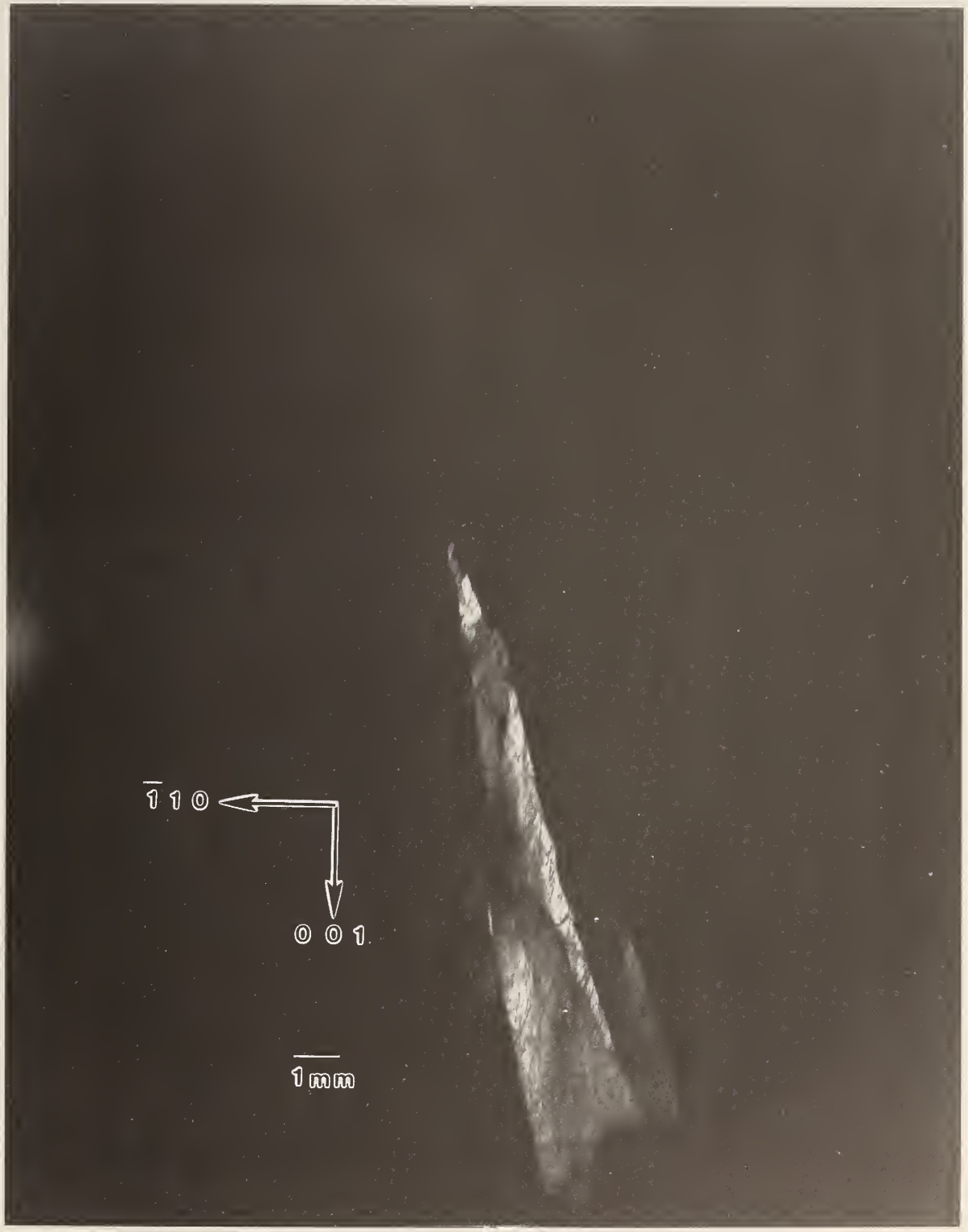

Figure 37. High-resolution (220) 8 keV diffraction image in Bragg geometry of approximately (220) surface of terrestrial PbSnTe crystal 108. The angle of incidence is 33 arc minutes larger than that for figure 36; the growth direction is [001]. Lighter areas diffract more strongly.

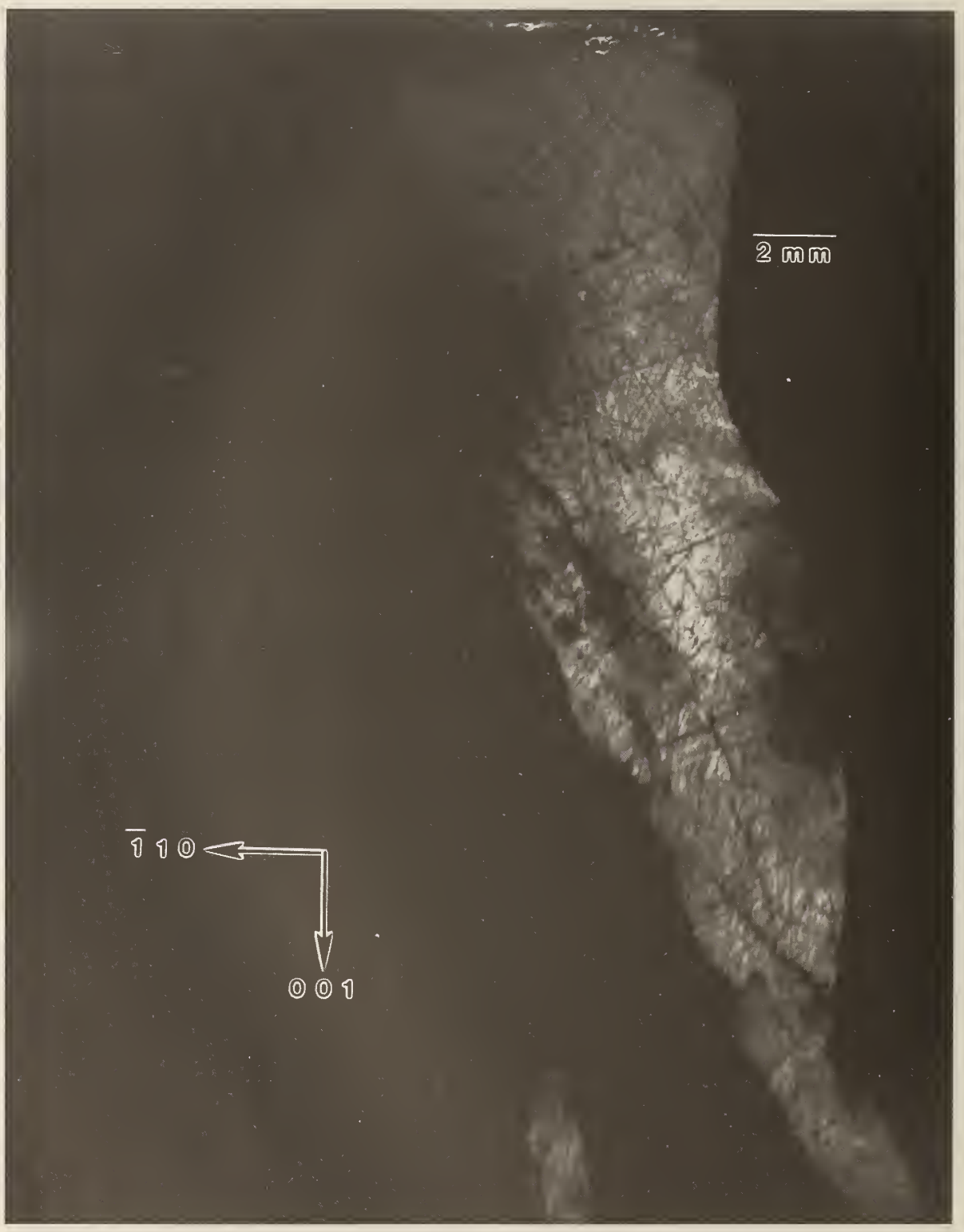

Figure 38. High-resolution (620) 8 keV diffraction image in Bragg geometry of approximately (220) surface of terrestrial PbSnTe crystal 108. The growth direction is [001]. Lighter areas diffract more strongly.

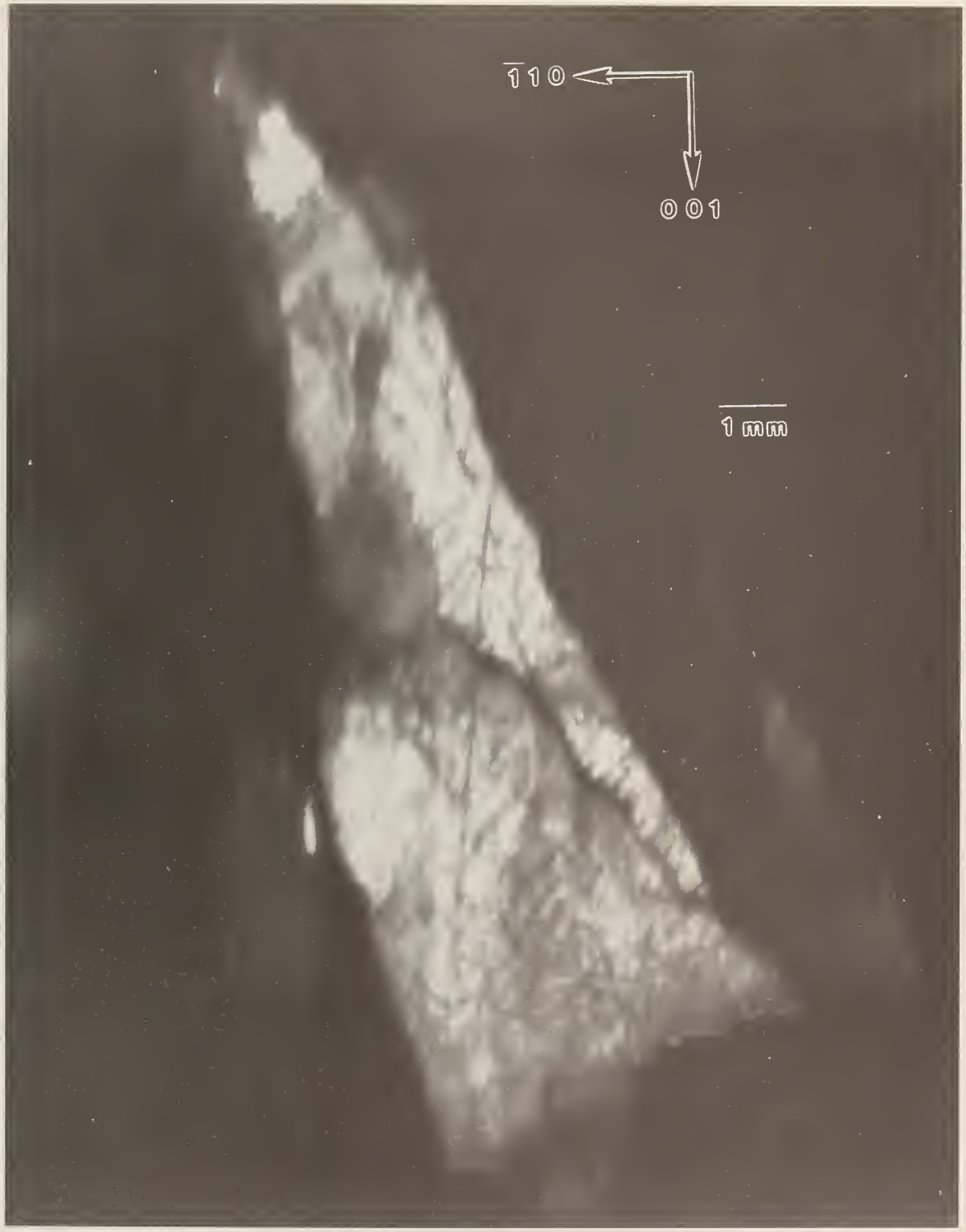

Figure 39. High-resolution (620) 8 keV diffraction image in Bragg geometry of approximately (220) surface of terrestrial PbSnTe crystal 108. The angle of incidence is 36 arc minutes smaller than that for figure 38; the growth direction is [001]. Lighter areas diffract more strongly.

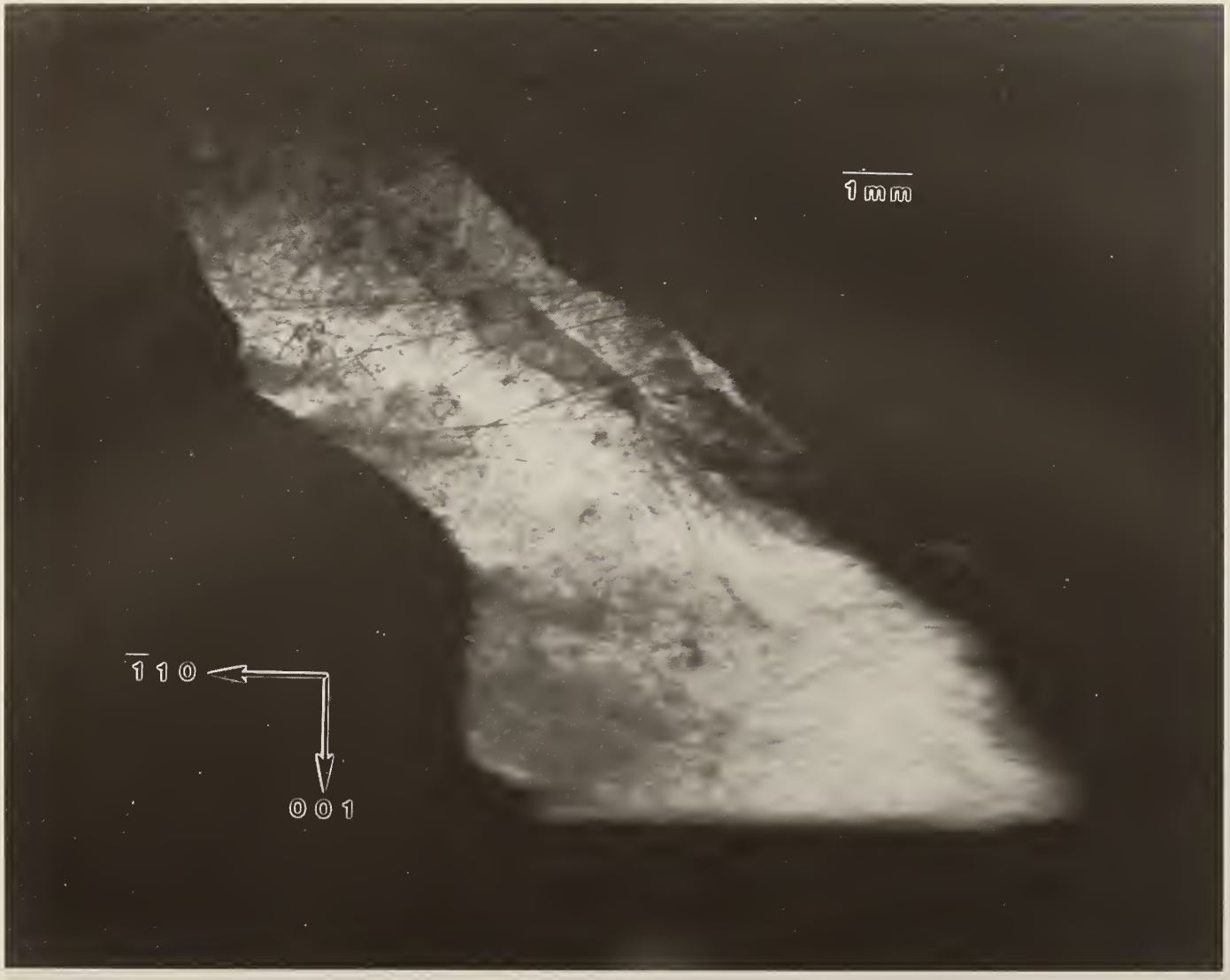

Figure 40. High-resolution (220) 8 keV diffraction image in Bragg geometry of approximately (220) surface of terrestrial PbSnTe crystal 108. The sample here was observed at 90° to its orientation for figures 36 and 37. The growth direction is [001]. Lighter areas diffract more strongly.

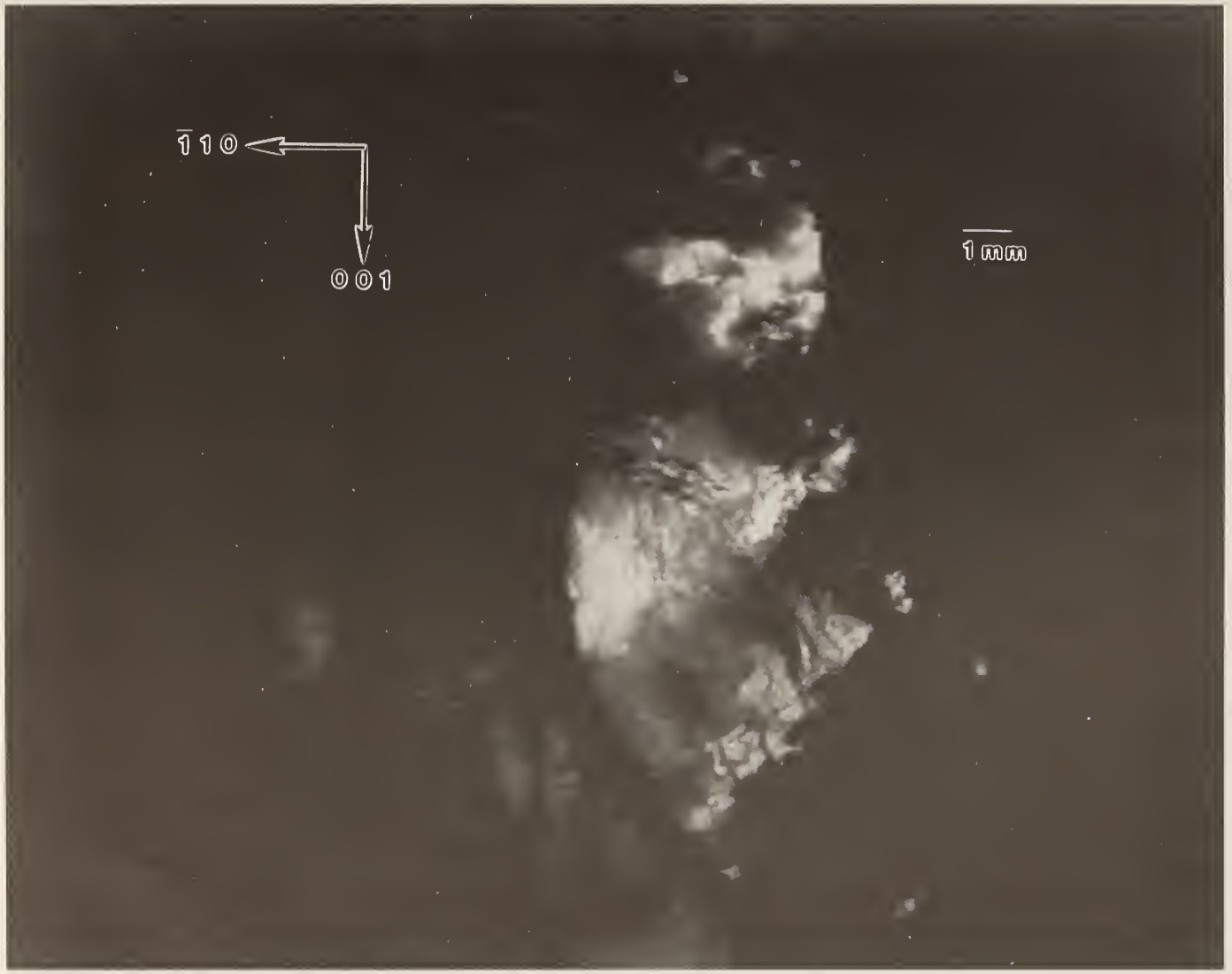

Figure 41. High-resolution (444) 8 keV diffraction image in Bragg geometry of approximately (220) surface of terrestrial PbSnTe crystal 108. The growth direction is [001]. Lighter areas diffract more strongly.

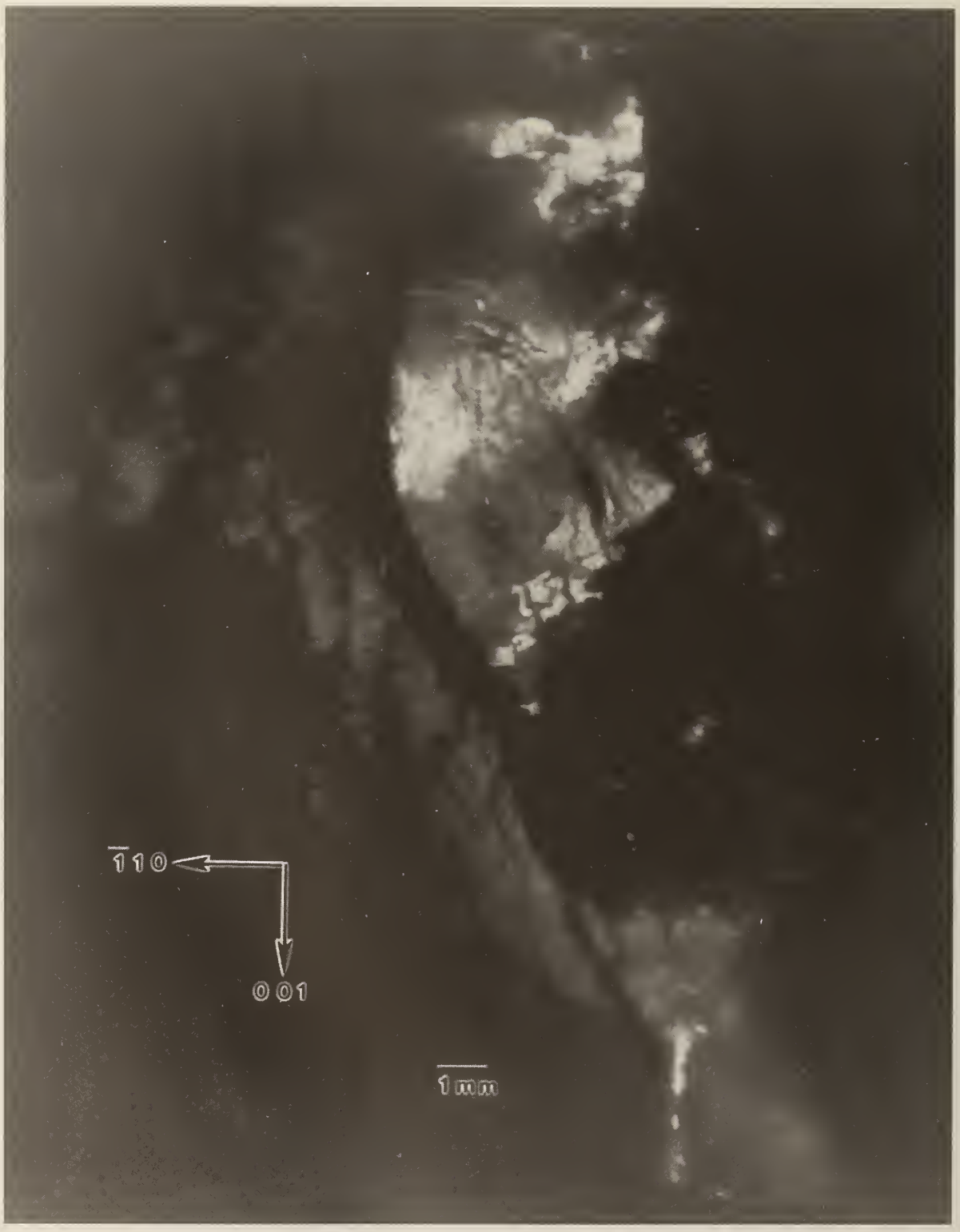

Figure 42. Second high-resolution (444) 8 keV diffraction image in Bragg geometry of approximately (220) surface of terrestrial PbSnTe crystal 108. The growth direction is [001]. Lighter areas diffract more strongly.

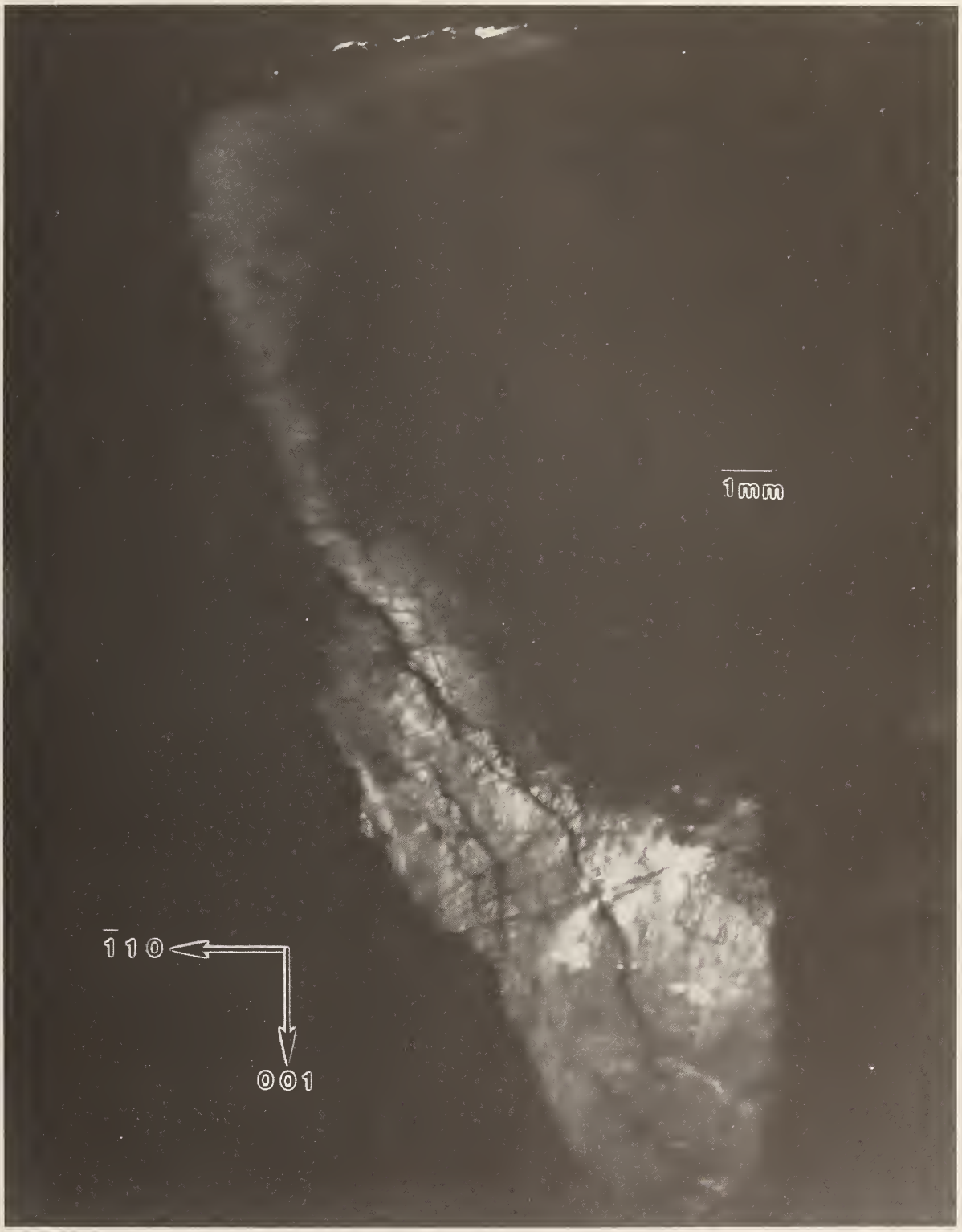

Figure 43. Third high-resolution (444) 8 keV diffraction image in Bragg geometry of approximately (220) surface of terrestrial PbSnTe crystal 108. The angle of incidence is 30 arc minutes smaller than that for figure 42; the growth direction is [001]. Lighter areas diffract more strongly.

Subgrains within each of the main grains are clearly visible through terraced variation in contrast. The generally strong diffraction from a 1.5 cm length of each of the two principal grains observed is notable, however, in light of the increase in tin level from 14% to 18% during the first 3 centimeters of growth visible in these images [27]. The fractional change in lattice constant over the 1.5 cm length of the grains is 4×10^{-4}, which changes the Bragg angle by 90 arc seconds. Nevertheless, diffraction is observed in a single image of one of the grains through broadening by kinematic scattering, which is difficult to quantify, as well as by local compositional variation. Because of the mixture of these two broadening mechanisms, unfortunately we can not use the broadening to evaluate the degree of local compositional variation.

Nevertheless, other aspects of this variation are evident in the enlargements in figures 44-55. Cellular regions of high diffraction varying in size from 10 to several hundred micrometers are observed. They are separated by lines of reduced diffraction that are 10-50 μm wide.

Many of these lines at first glance appear to be scratches because of their curvature and random orientation. However, three characteristics typical of surface scratches, such as those visible for example in the gallium arsenide images to which we turn later, are not observed in these linear features. First, the lines vary in width, both from line to line, and even over the length of a given line. In reality these lines separate cellular regions of high diffraction. Second, the boundaries of the lines are very indistinct. And third, contrast reversal is never observed in them. They are invariably out of diffraction over their entire length and even as the crystal is rotated while it is observed by video camera. Thus, while we cannot rule out scratches, their images differ markedly in several respects from those of typical scratches in other materials. Moreover, they are not observed in the image of the space-grown sample, whose images follow.

We are thus left with the postulate that the highly diffracting cells are separated by material of other phase(s). The indistinctness of the boundaries between these regions of differing phase strongly suggest gradual change in chemical composition on a scale of 1-10 μm or so, in contrast to the sharp delineation between diffracting and non diffracting features in the images of mercuric iodide discussed above. The intrusion of material of different phase(s) is clearly important. The pseudobinary phase diagram along the lead-tin axis predicts complete miscibility [30]. However, the observation of similar structure following electrolytic etching led twenty years ago to a series of experiments on the metal/tellurium ratio, which delineated its importance in the growth of this material. This earlier work provides a satisfactory model for the current observations as well [31][30].

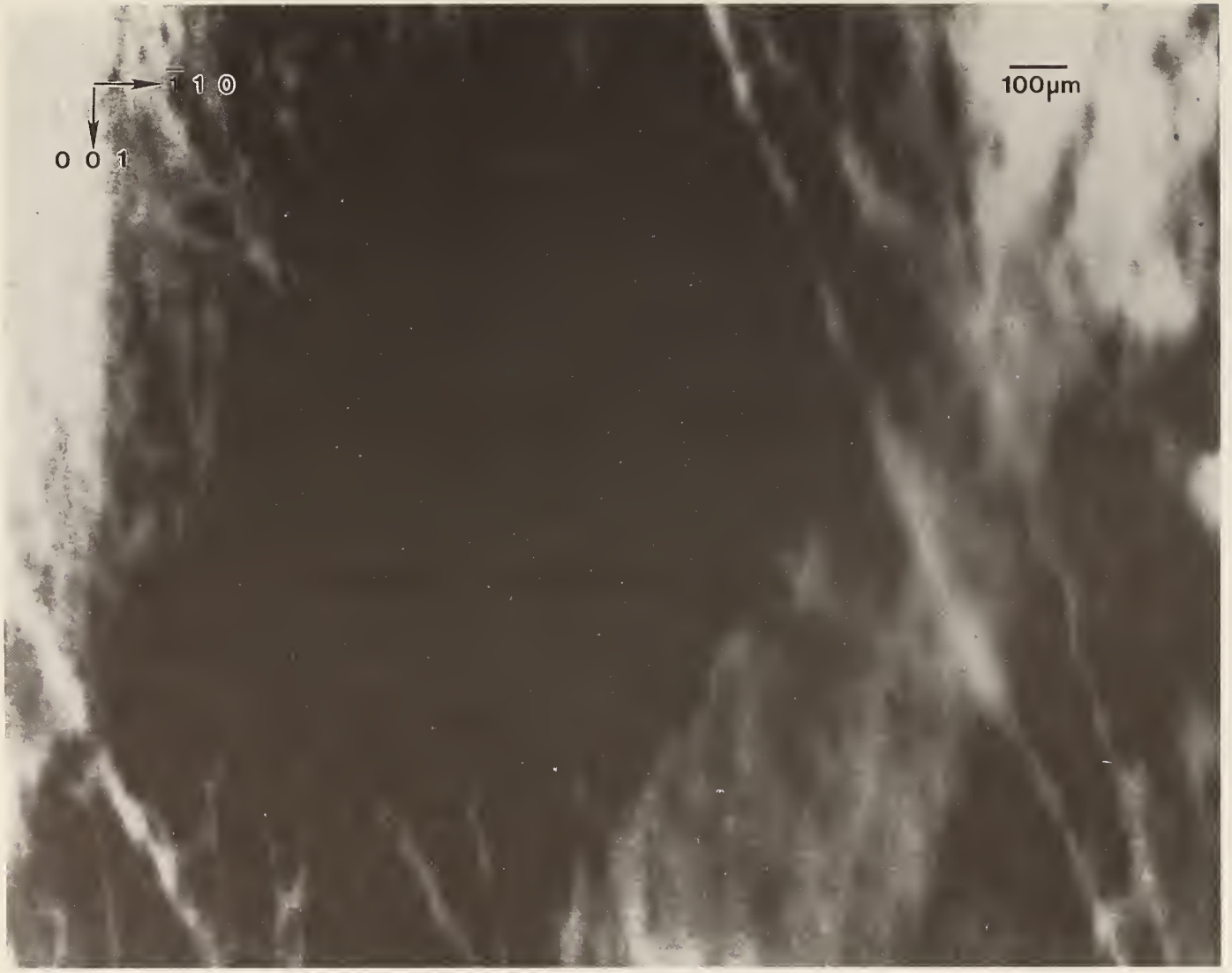

Figure 44. Enlargement of central portion of figure 36, (220) diffraction. Darker areas diffract more strongly.

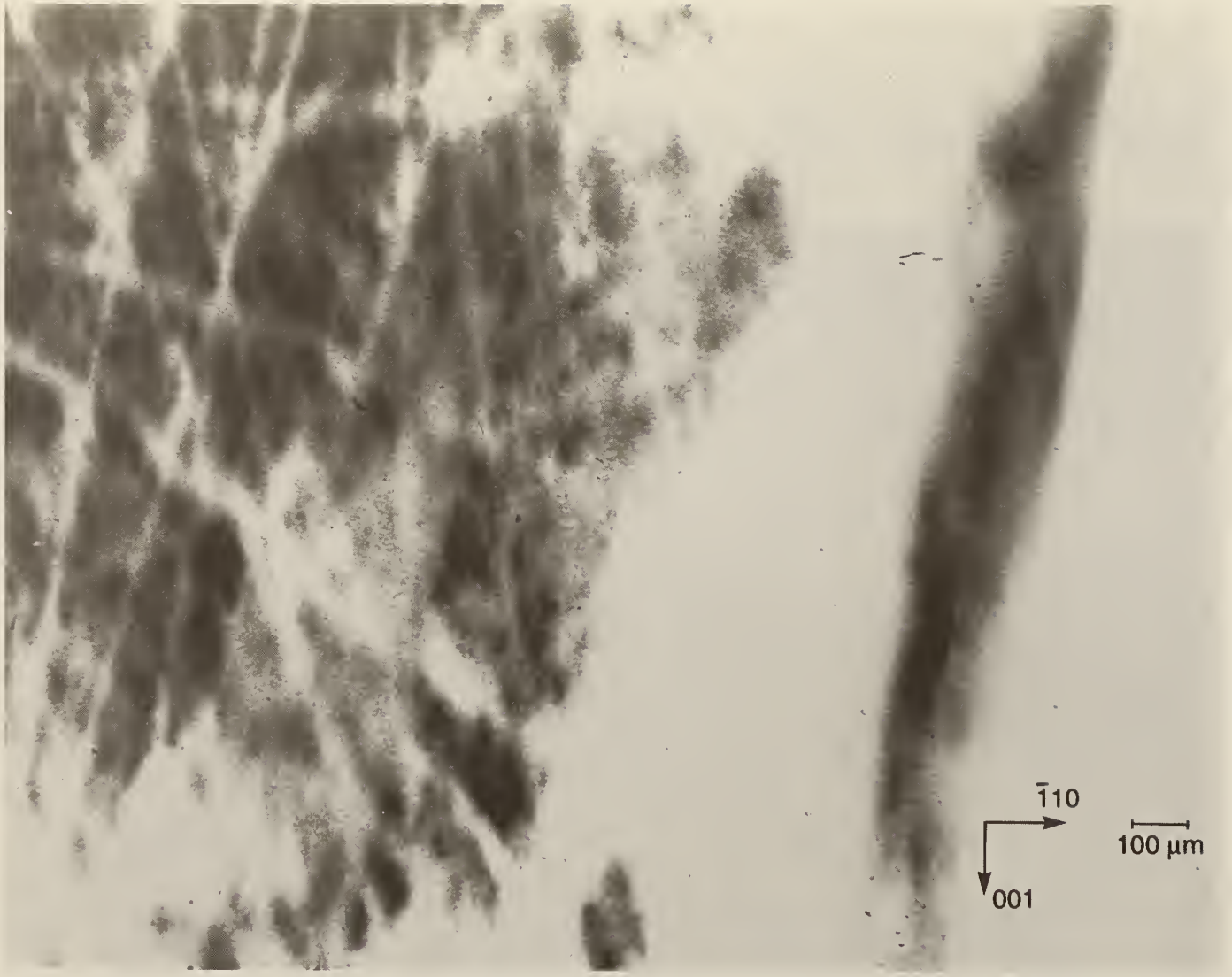

Figure 45. Enlargement of the onset of the new grain in the middle of figure 36, (220) diffraction. This image is to be compared with the same crystal region in figure 47 and imaged in (620) diffraction in figures 49 and 51. Darker areas diffract more strongly.

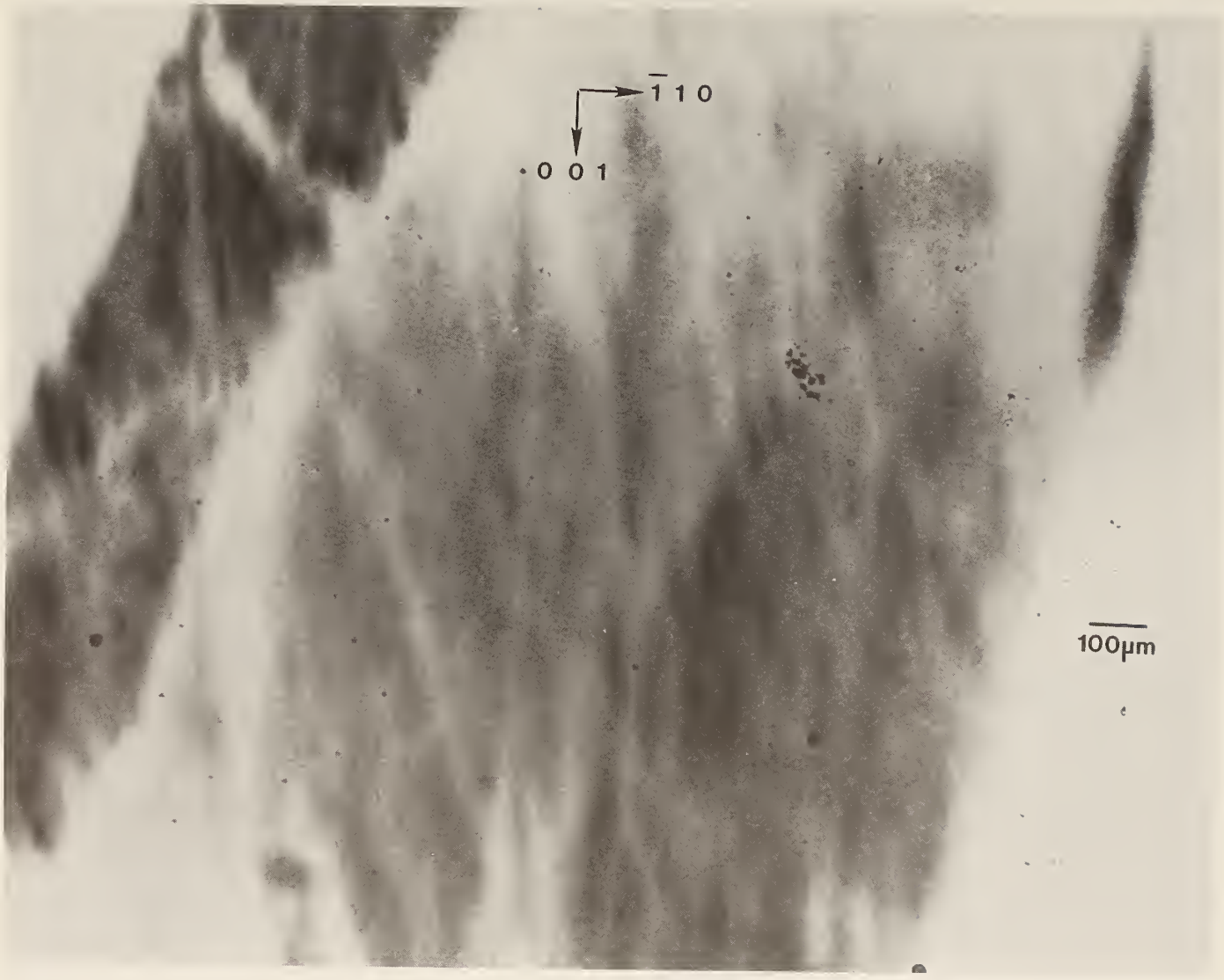

Figure 46. Enlargement of central portion of figure 37, (220) diffraction. Darker areas diffract more strongly.

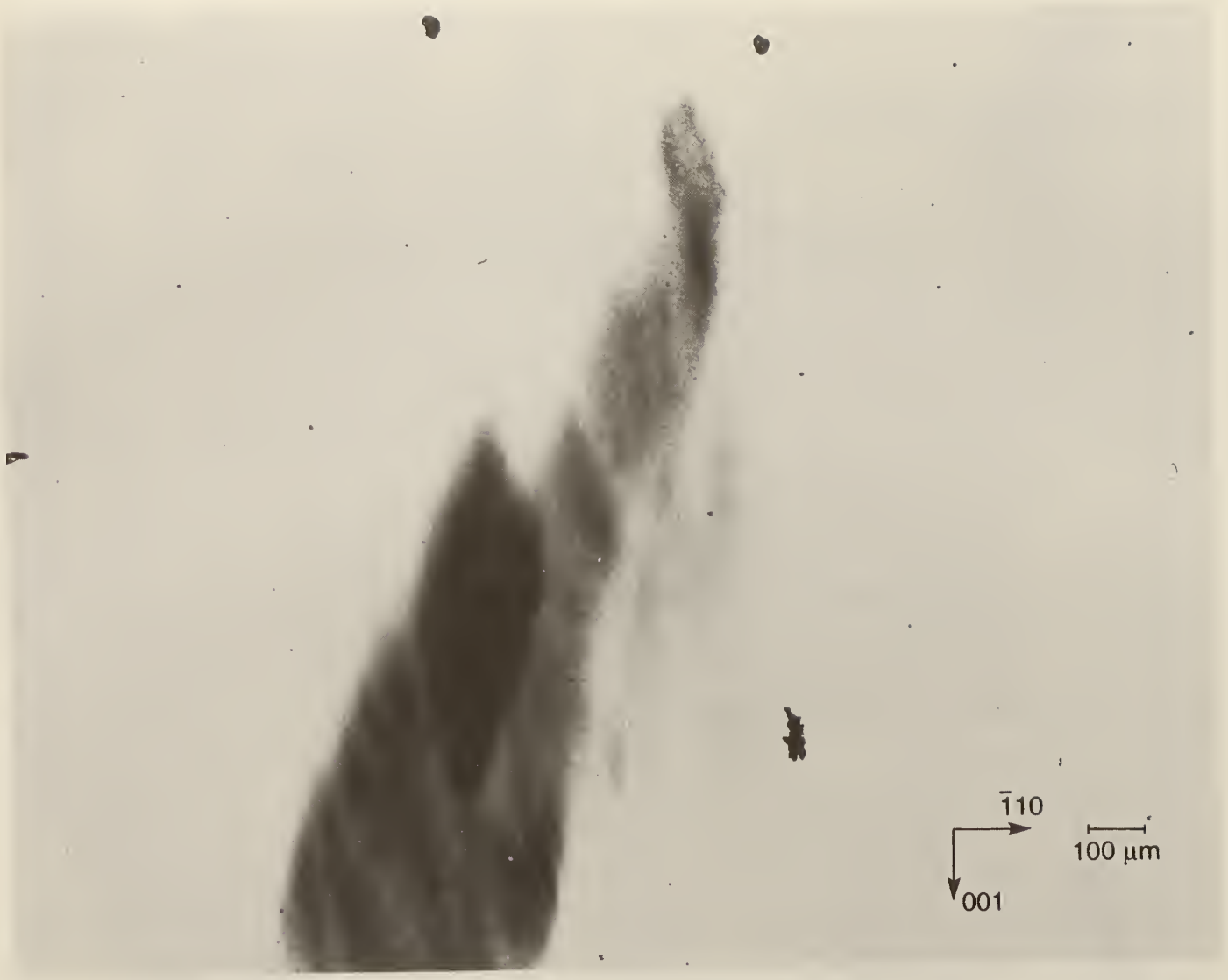

Figure 47. Enlargement of the onset of the new grain at the top of figure 37, (220) diffraction. This image is to be compared with the same crystal region in figure 45 and imaged in (620) diffraction in figures 49 and 51. Darker areas diffract more strongly.

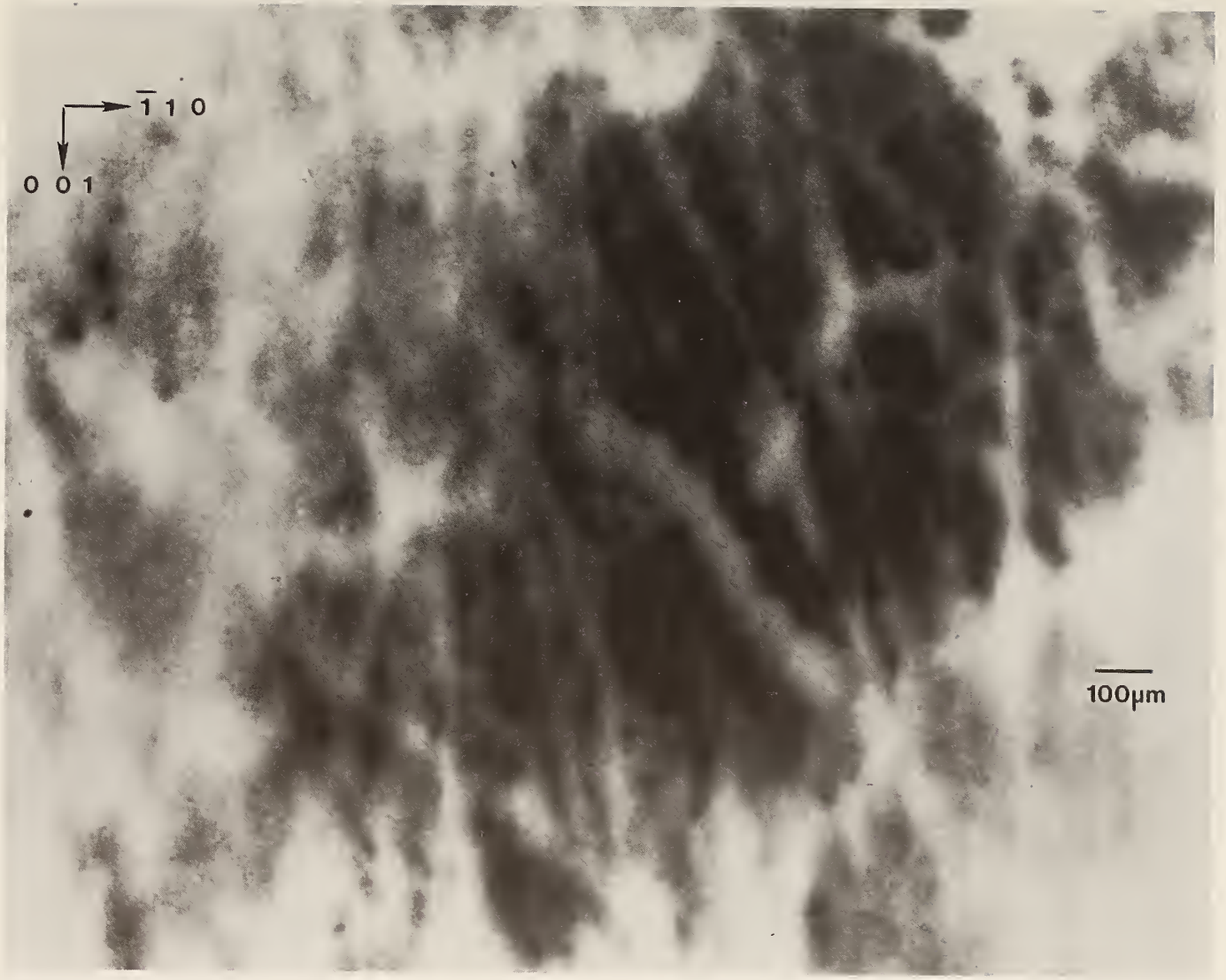

Figure 48. Enlargement of central portion of figure 38, (620) diffraction. Darker areas diffract more strongly.

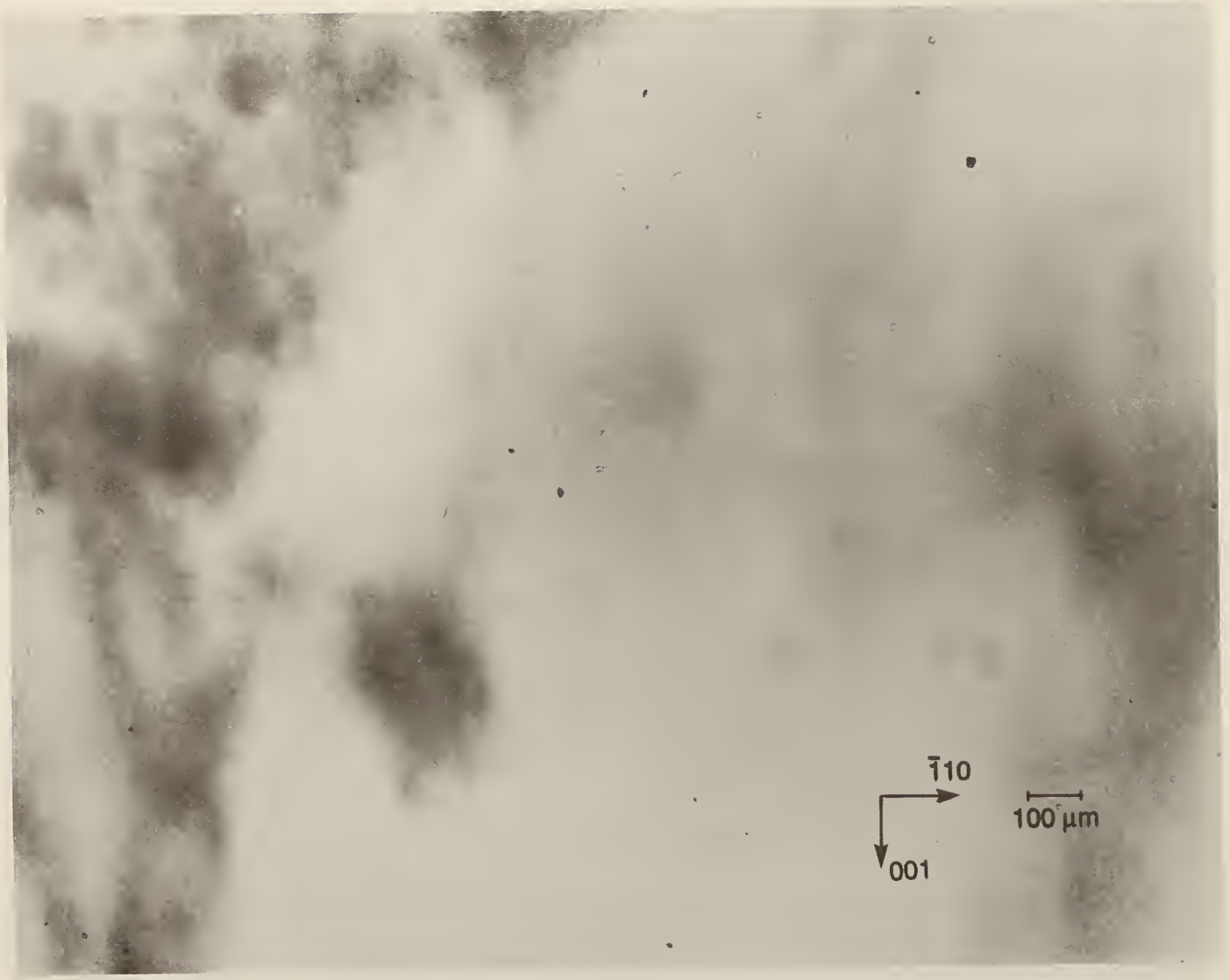

Figure 49. Enlargement of the onset of the new grain in the middle of figure 38, (620) diffraction. This image is to be compared with the same crystal region in figure 51 and imaged in (220) diffraction in figures 45 and 47. Darker areas diffract more strongly.

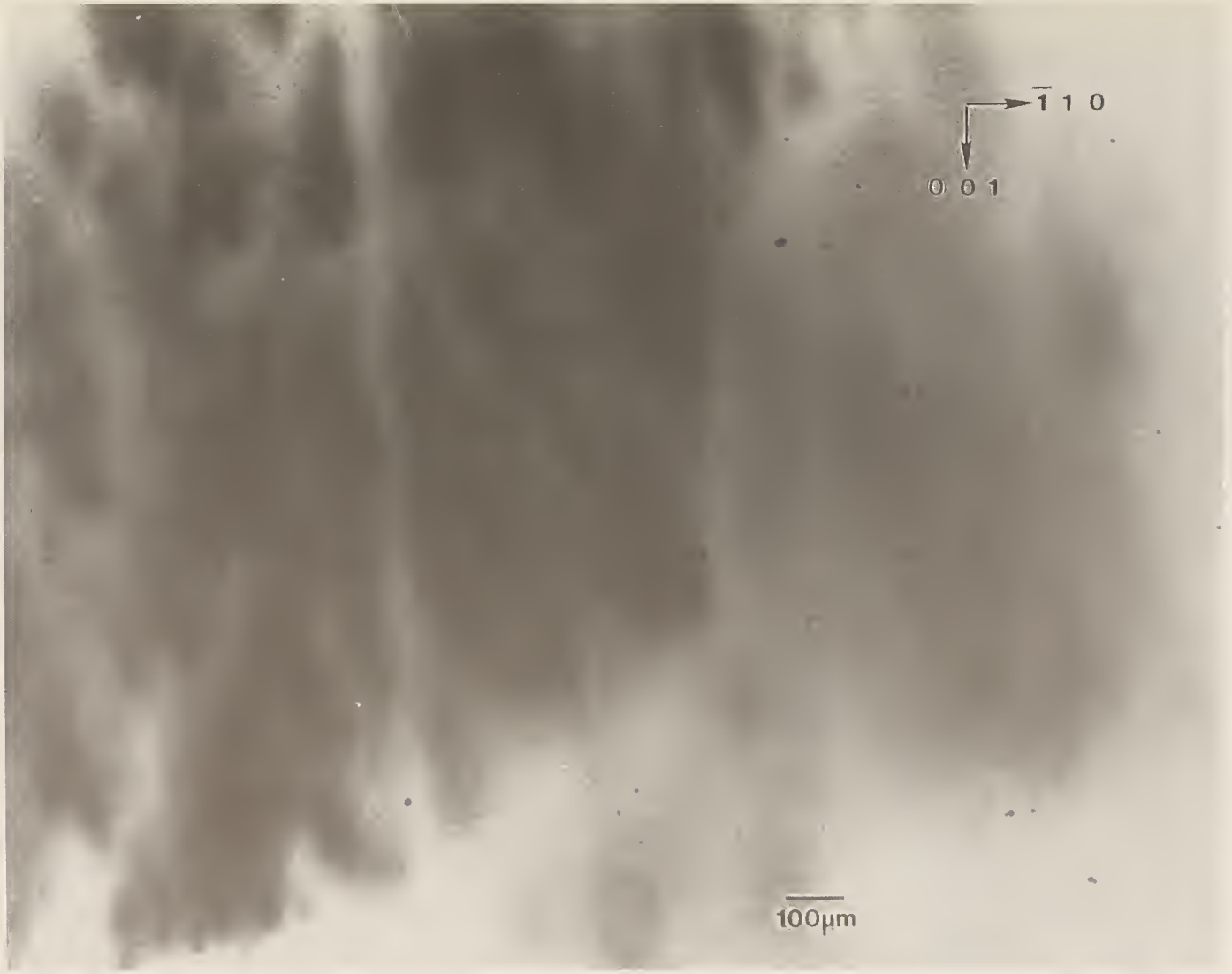

Figure 50. Enlargement of central portion of figure 39, (620) diffraction. Darker areas diffract more strongly.

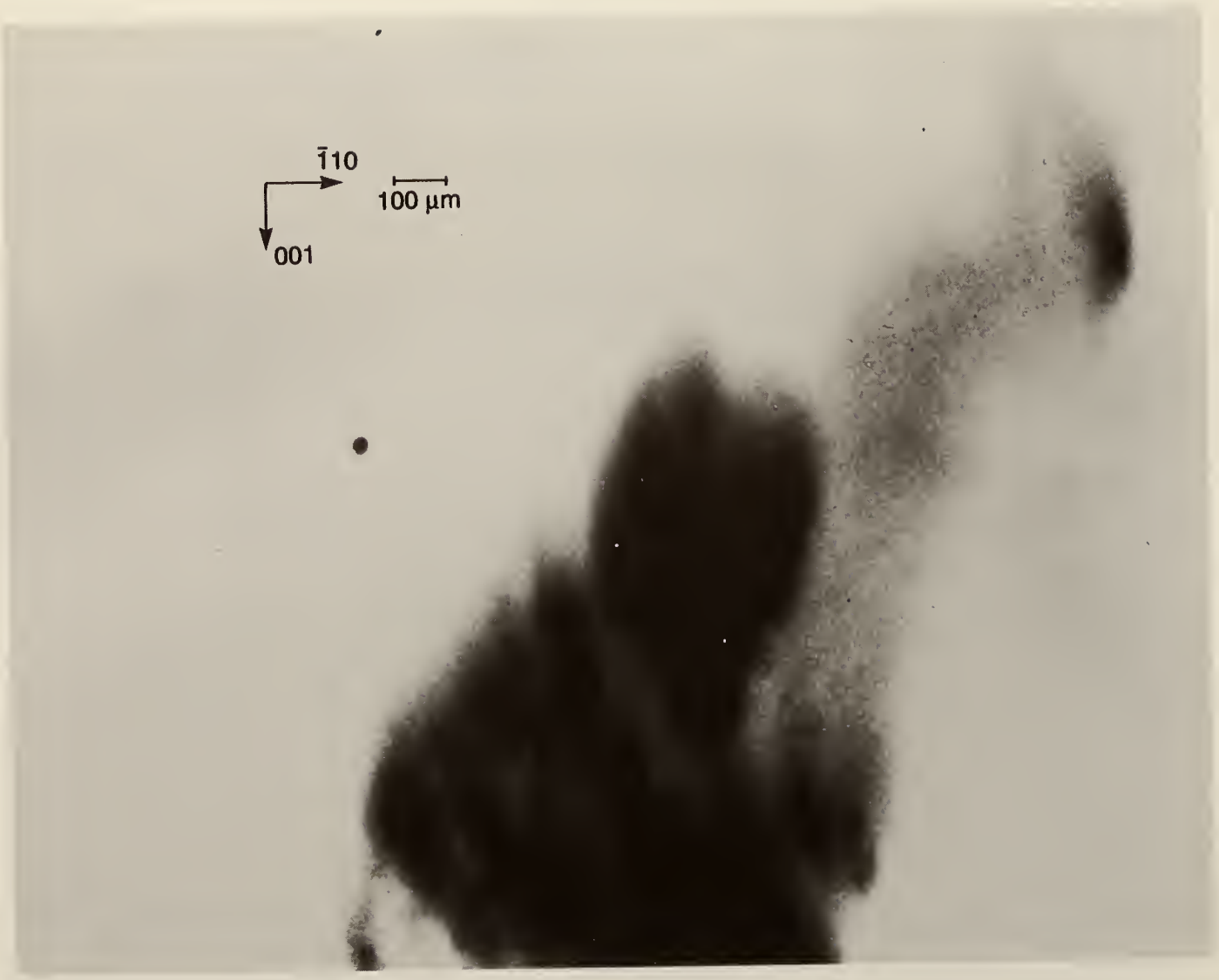

Figure 51. Enlargement of the onset of the new grain at the top of figure 39, (620) diffraction. This image is to be compared with the same crystal region imaged in figure 49 and in (220) diffraction in figures 45 and 47. Darker areas diffract more strongly.

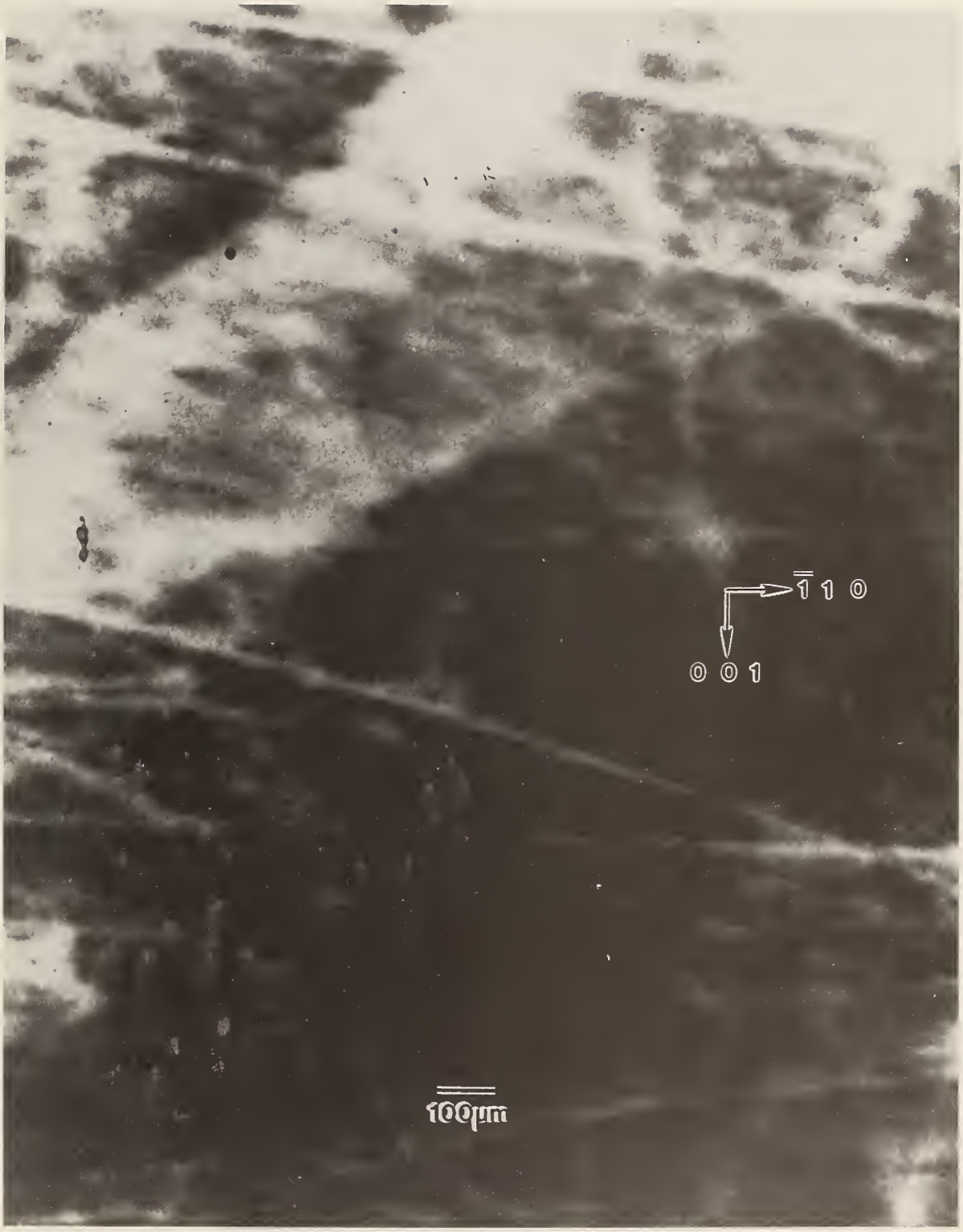

Figure 52. Enlargement of upper right portion of figure 40, (220) diffraction. Darker areas diffract more strongly.

Figure 53. Enlargement of left central portion of figure 41, (444) diffraction. Darker areas diffract more strongly.

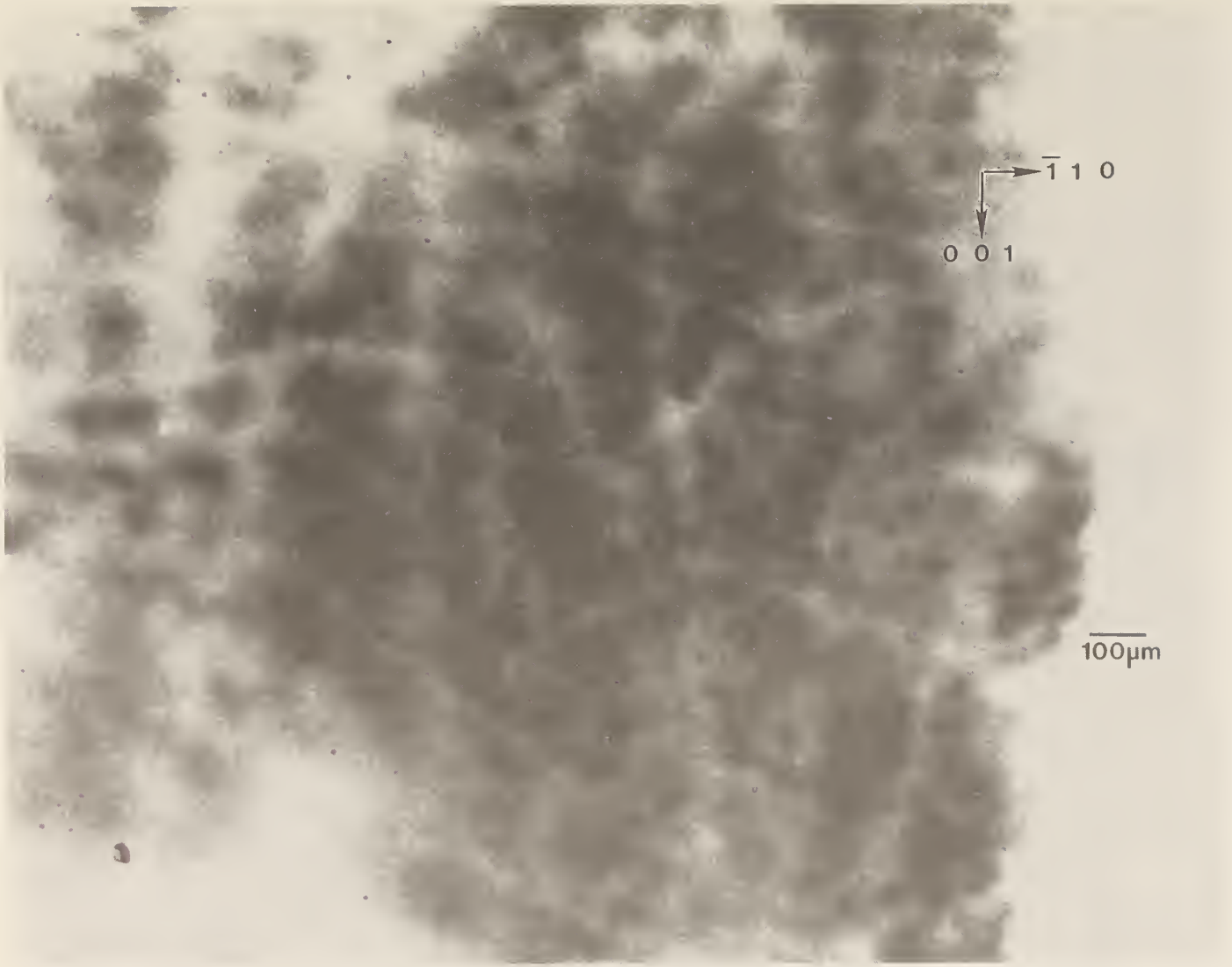

Figure 54. Enlargement of left central portion of figure 42, (444) diffraction. Darker areas diffract more strongly.

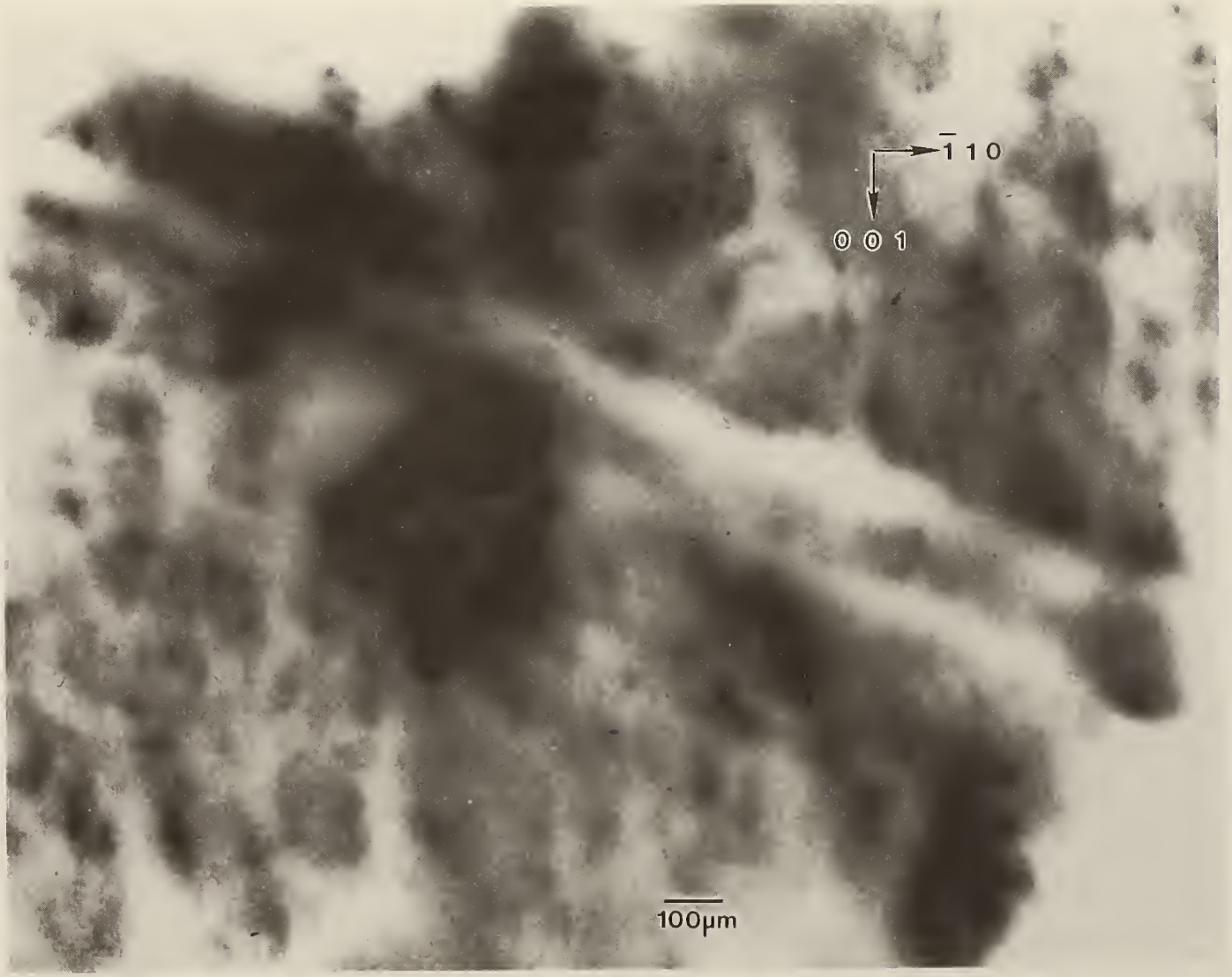

Figure 55. Enlargement of lower portion of figure 43, (444) diffraction. Darker areas diffract more strongly.

While the metal constituents are widely recognized to be interchangeable, a single phase is preserved only with tellurium concentration in excess of 51%. Below this value, two phases are formed, differing in metal/tellurium ratio. Since the tellurium concentration of the current crystals is 50.1%, two phases are actually to be expected. Constitutional supercooling may also play an important role, depending on the the temperature gradients imposed [31].

2. STS 61A Crystal

A full image of the space shuttle STS 61A crystal appears in figure 56 and an enlargement of the central portion of this in figure 57. The multigrain nature of the STS 61A crystal is superficially similar to that of the terrestrial crystal. But, while these images appear qualitatively similar to the full images for the corresponding terrestrial crystal, they differ in important ways.

Each grain is more generally uniform than those of the terrestrial crystal. This uniformity follows a drastic reduction in the incidence of linear features and subgrains. As a result, variation in diffraction on a scale of 10-100 micrometers is greatly reduced. Thus, while the granular structure resembles that for the terrestrial crystal, variation within individual grains from the intrusion of a distinct second phase appears to be greatly suppressed in microgravity. The absence of thermo-solutal instability for this system in microgravity was noted in the preceding section.

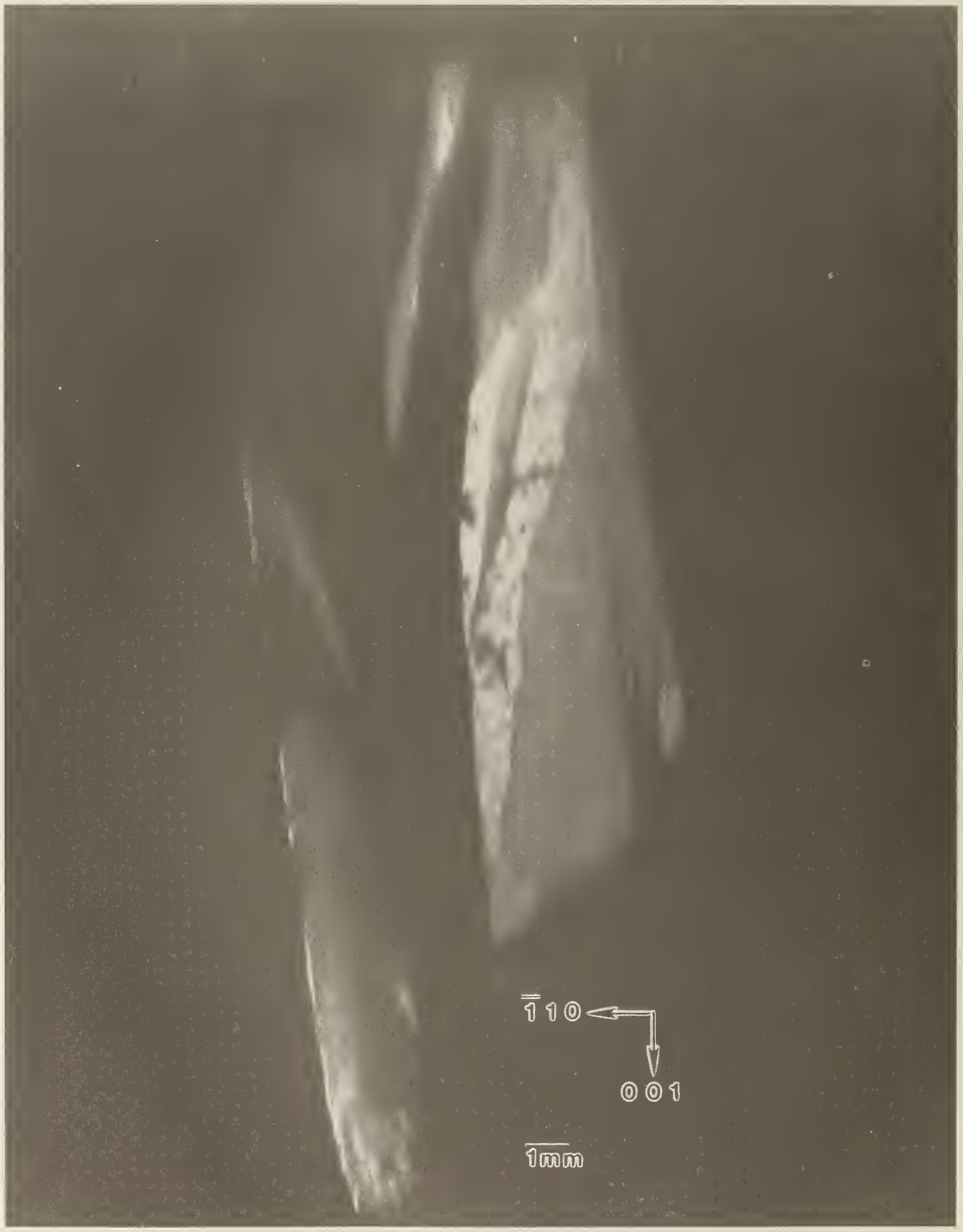

Figure 56. High-resolution (220) 8 keV diffraction image in Bragg geometry from approximately (220) surface of PbSnTe crystal 111, grown on STS 61A. The growth direction is [001]. Lighter areas diffract more strongly.

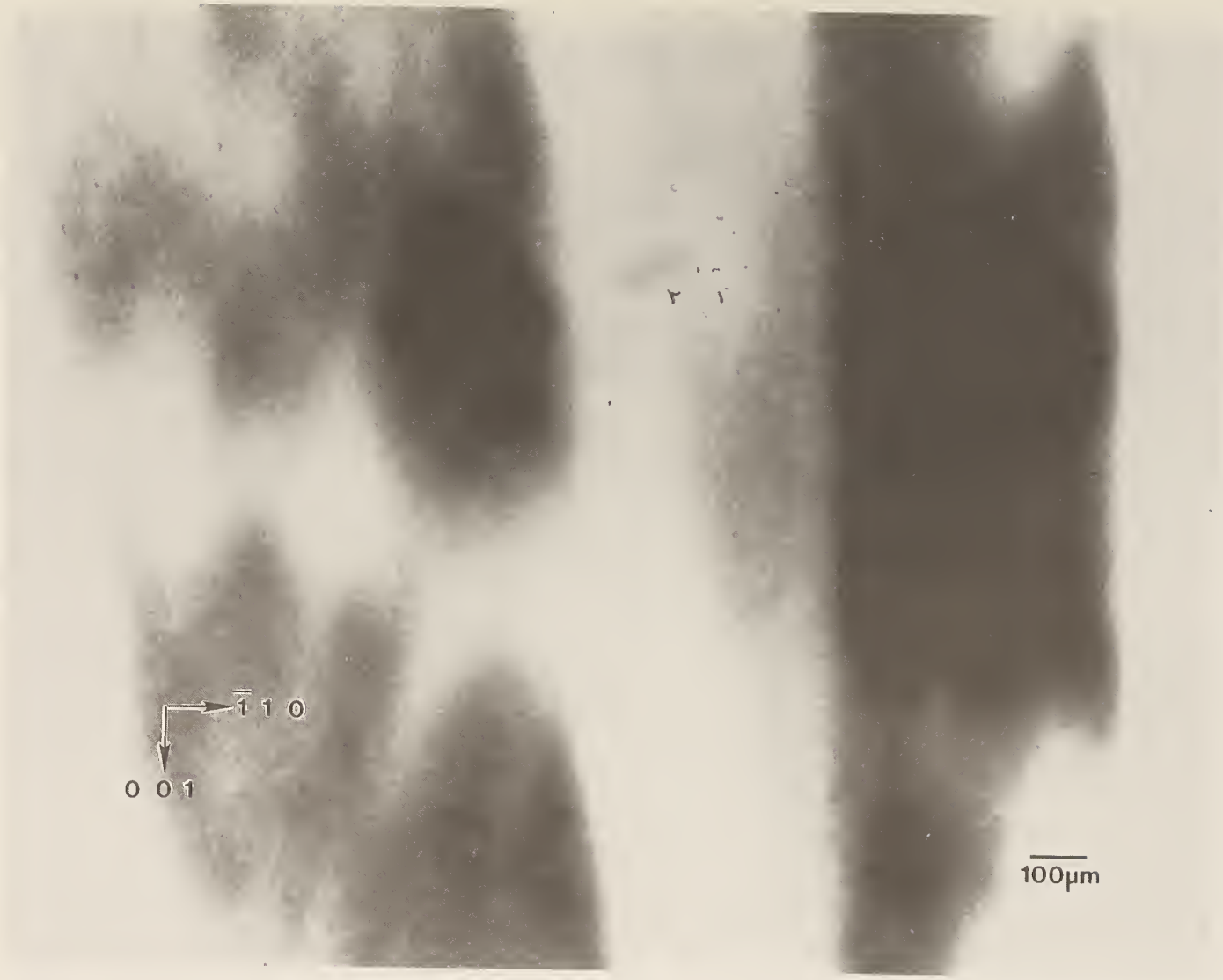

Figure 57. Enlargement of central portion of figure 56, (220) diffraction. Darker areas diffract more strongly.

C. Triglycine Sulfate

A normal slice taken from the terrestrial seed crystal with additional growth achieved on Spacelab III diffracts into images, each of which appears over less than half of an arc minute. Full high-resolution diffraction images appear in figures 58-63, with enlargements in figures 64-71. The character of the diffraction from this crystal is very different from that of the others. This crystal was thin enough and low enough in atomic number to allow diffraction in Laue geometry. Moreover, superimposed images of this crystal taken as it was rotated about its [100] and [001] axes appear in closely spaced groups, each associated with the diffraction directions expected for diffraction from one set of (h00) or (00ℓ) planes, respectively. The various images have similar, but not identical, shapes. Subsequent work, summarized in table 2, indicates that the various members of a given group of images appearing at nearly similar diffraction angles come into diffraction at differing sample orientation.

TABLE 2

Layer	Figure No.	(hkl)	Orientation (°)
C2	58	300	+6.6
B3	59	200	+2.1
B1	60	200	+2.5
A2	62	001	-19.2
A3	63	001	-36.8

The appearance of images in groups indicates that this crystal consists of layered grains whose lattices are similar but rotated with respect to one another by rotation about the [100] and [001] axes. Since each image is ostensibly nearly "complete," the grain boundaries are roughly parallel to the (010) crystal surface. In an optically thick material, transmission through such a layered crystal would be precluded by the misalignment of the successive grains. However, this crystal is optically thin, permitting the observation of symmetrical diffraction from each of the grains in turn. From the occurrence of similar features in pairs of images, which can be ascribed to features shared by adjacent grains at their interface and the degree of clarity, we can assign a tentative order to the various grains as intersected by the x-ray beam. This is the order in which their images are presented in the figures and in table 2. Most of the features thus appear to be

Figure 58. High-resolution (300) 10 keV diffraction image in Laue geometry from (001) surface of grain C2 of TGS crystal 120, from Spacelab III. Lighter areas diffract more strongly.

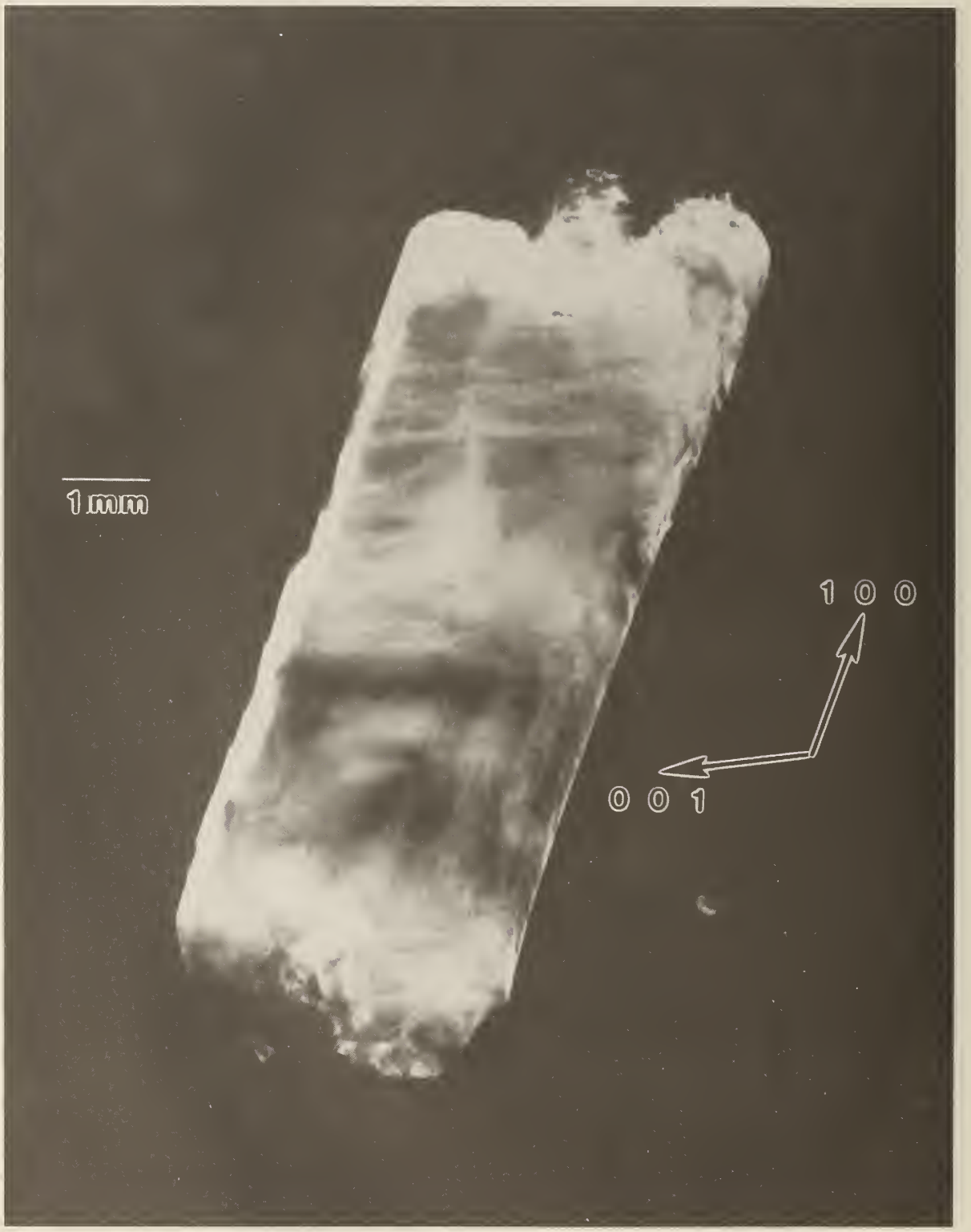

Figure 59. High-resolution (200) 10 kev diffraction image in Laue geometry from (001) surface of grain B3 of TGS crystal 120, from Spacelab III. Lighter areas diffract more strongly.

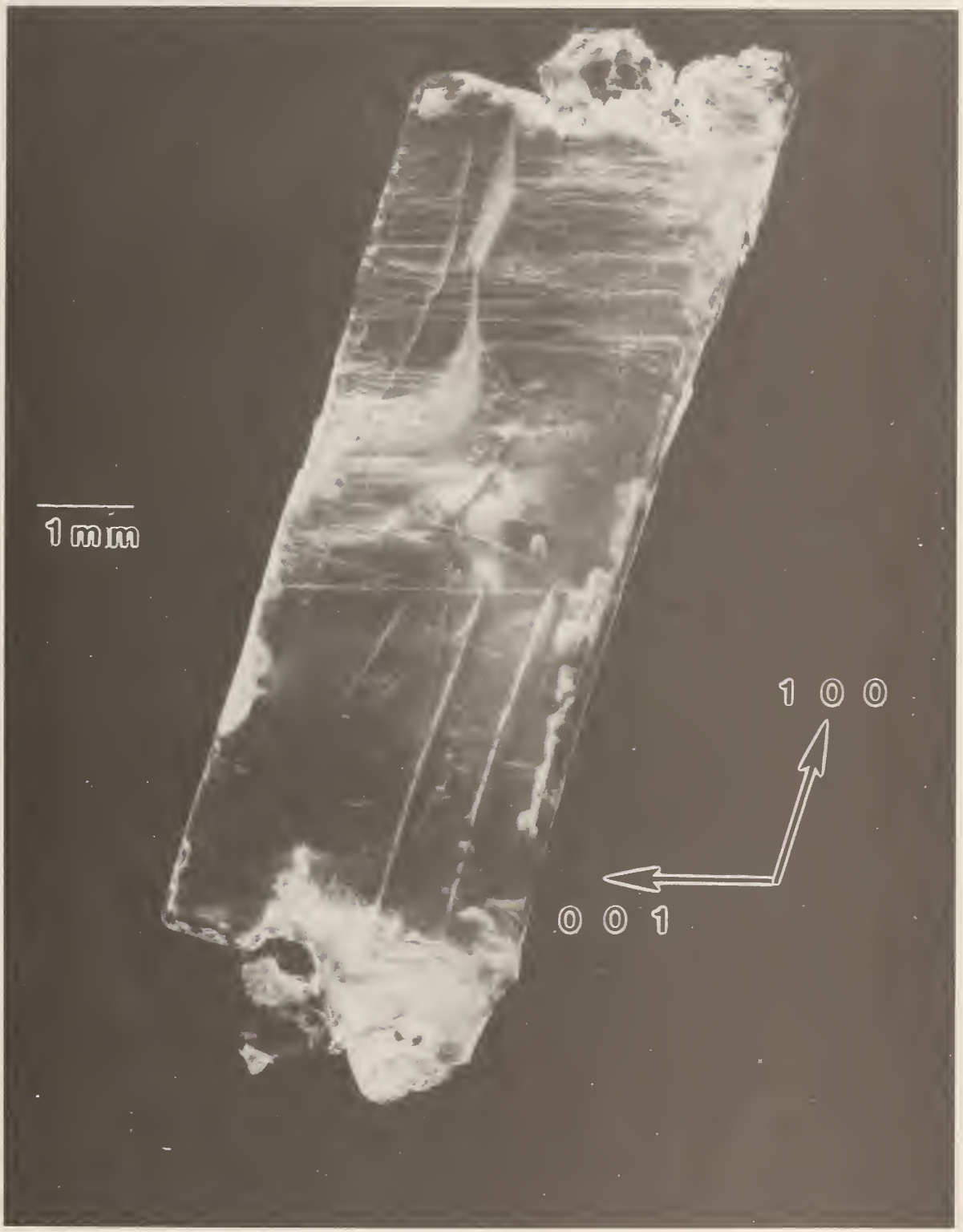

Figure 60. High-resolution (200) 10 keV diffraction image in Laue geometry from grain B1 of TGS crystal 120, from Spacelab III. Lighter areas diffract more strongly.

Figure 61. High-resolution (200) 10 keV diffraction image in Laue geometry from grain B1 of TGS crystal 120, from Spacelab III. Lighter areas diffract more strongly.

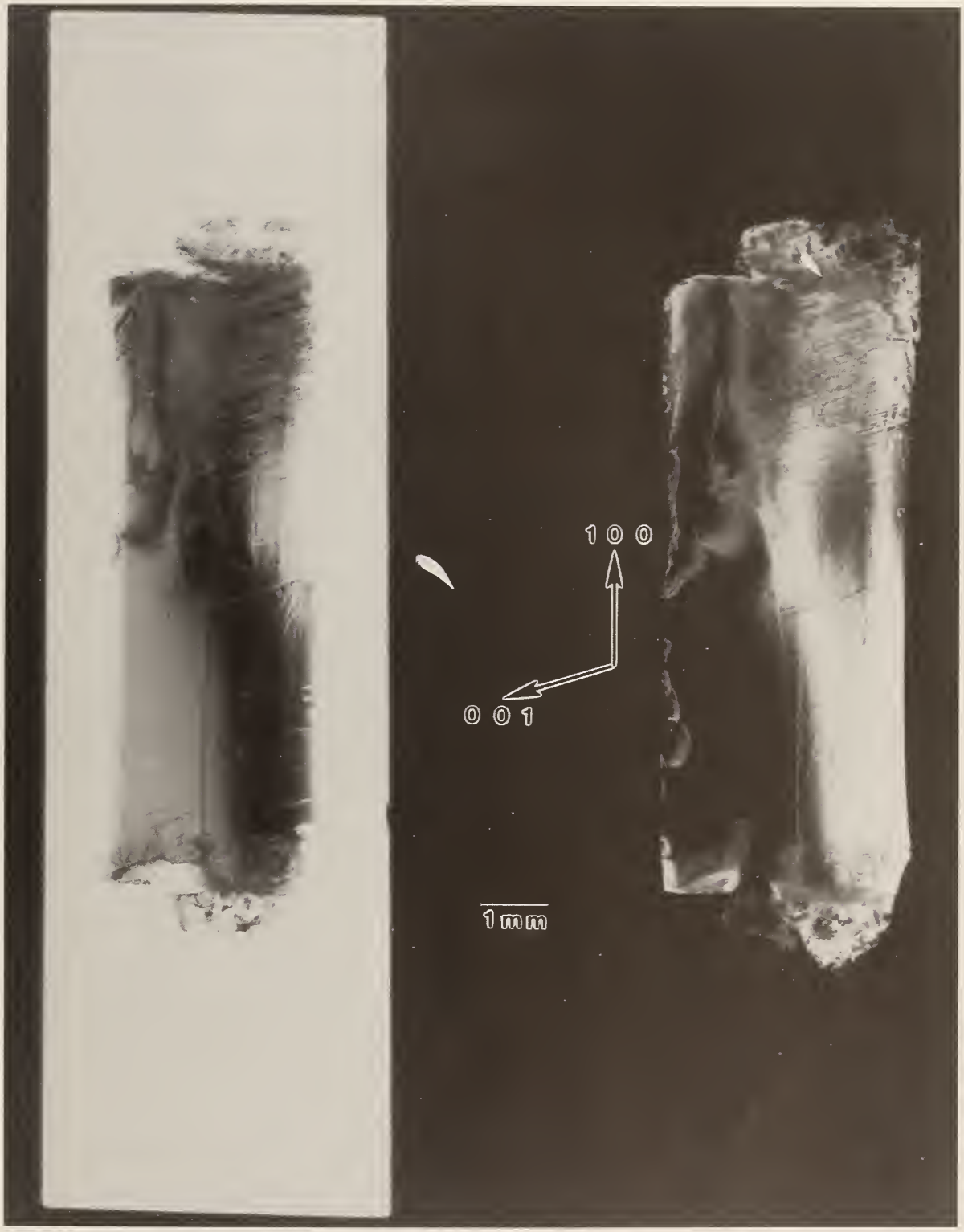

Figure 62. High-resolution (001) 10 keV diffraction image in Laue geometry from grain A2 of TGS crystal 120, from Spacelab III. Lighter areas diffract more strongly.

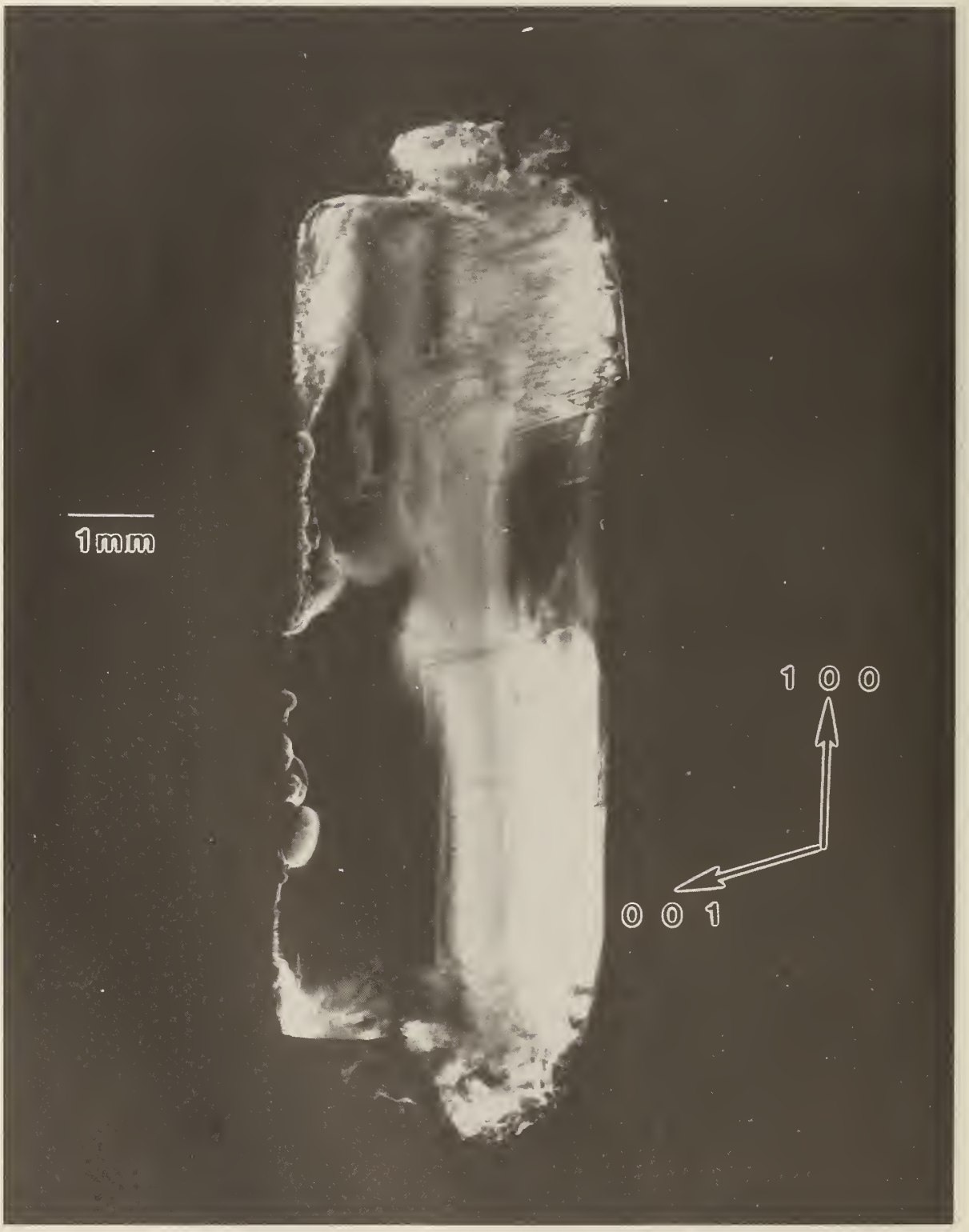

Figure 63. High-resolution (001) diffraction image in Laue geometry from grain A2 of TGS crystal 120, from Spacelab III. Lighter areas diffract more strongly.

Figure 64. Enlargement of middle left-hand edge of figure 58, (300) diffraction. Darker areas diffract more strongly.

Figure 65. Enlargement of central portion of figure 58, (300) diffraction. Darker areas diffract more strongly.

Figure 66. Enlargement of lower left-hand edge of figure 59, (200) diffraction. Darker areas diffract more strongly.

Figure 67. Enlargement of lower right-hand edge of figure 59, (200) diffraction. Darker areas diffract more strongly.

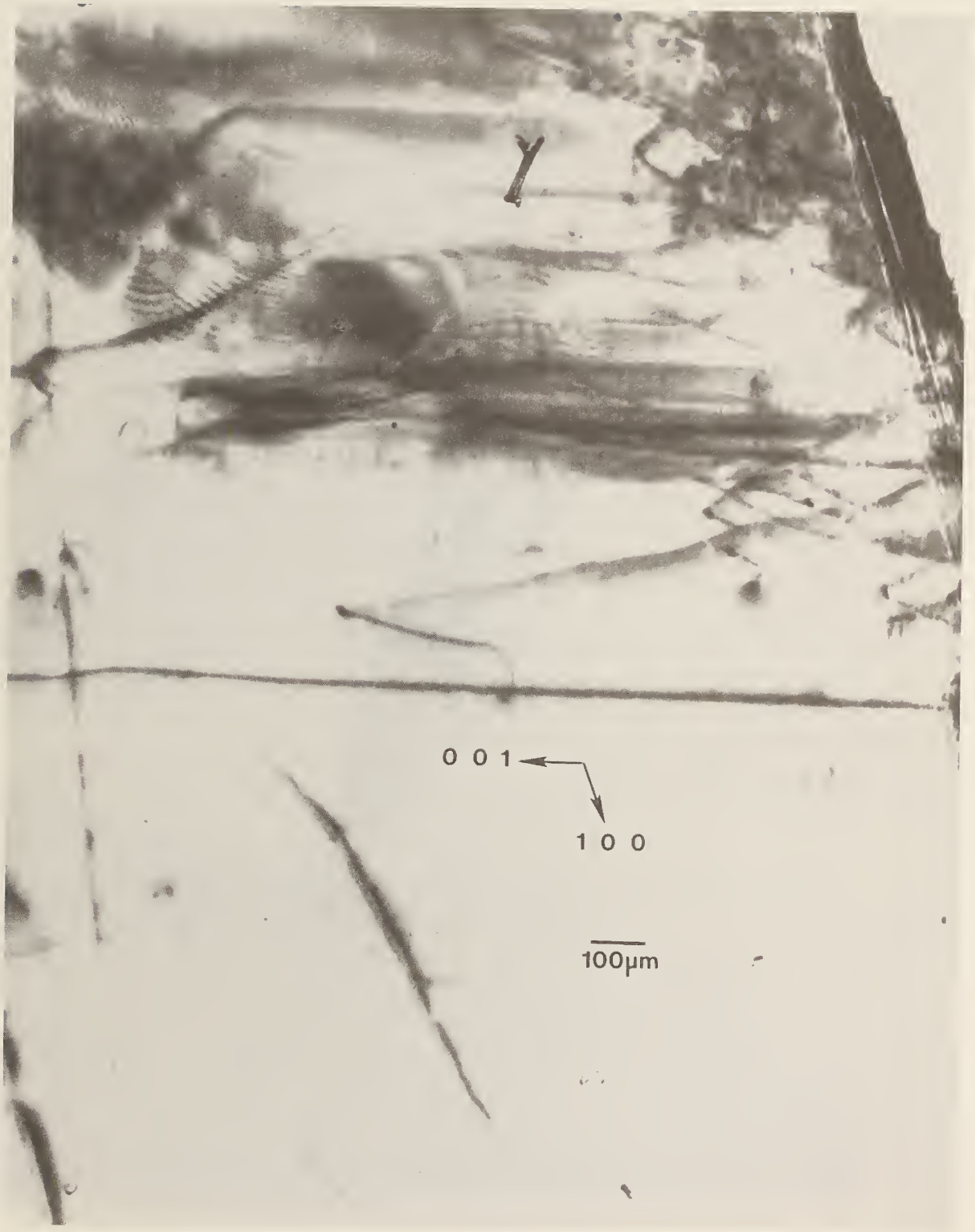

Figure 68. Enlargement of middle left-hand edge of figure 60, (200) diffraction. Darker areas diffract more strongly.

Figure 69. Enlargement of lower left-hand edge of figure 61, (200) diffraction. Darker areas diffract more strongly.

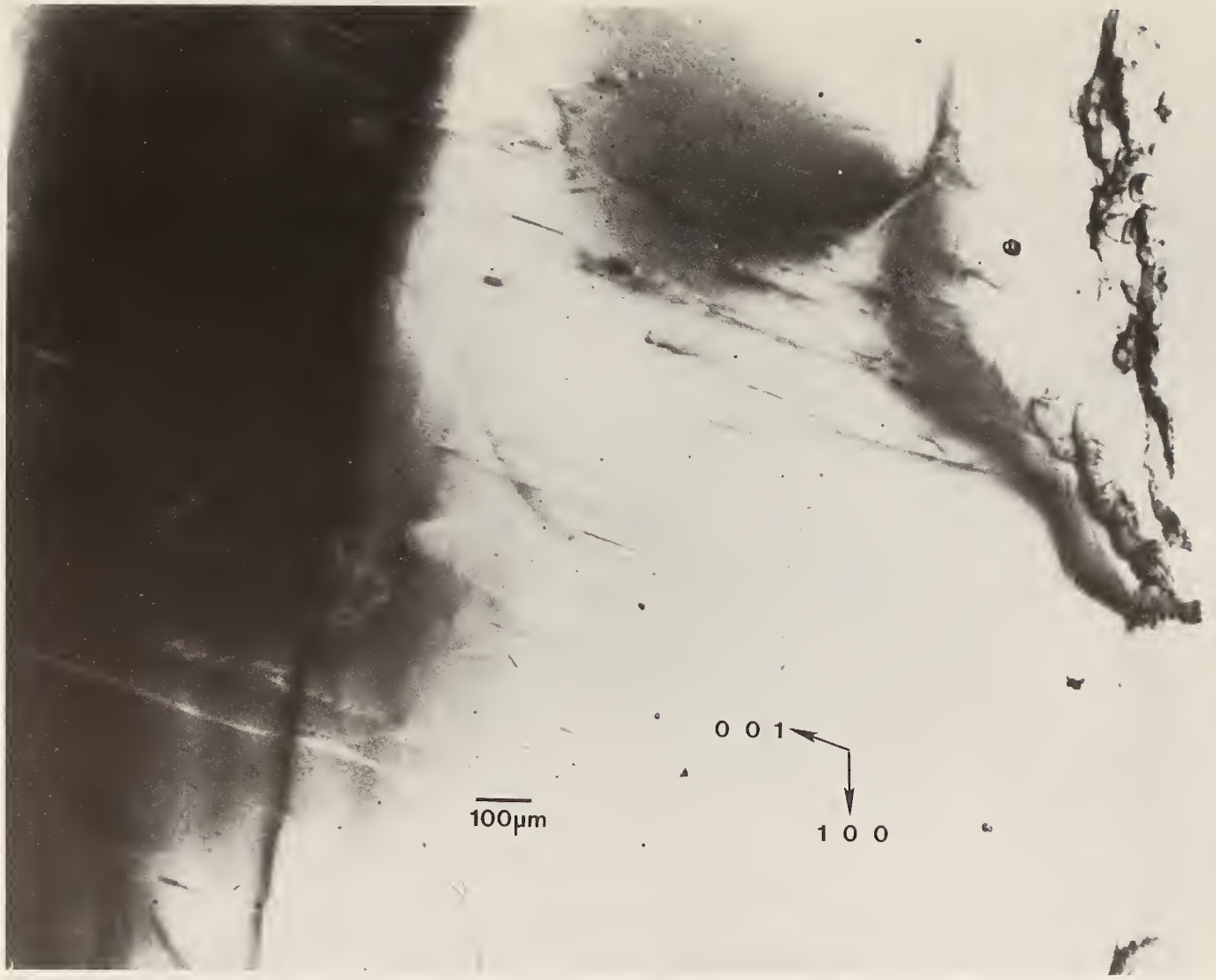

Figure 70. Enlargement of middle left-hand edge of figure 62, (001) diffraction. Darker areas diffract more strongly.

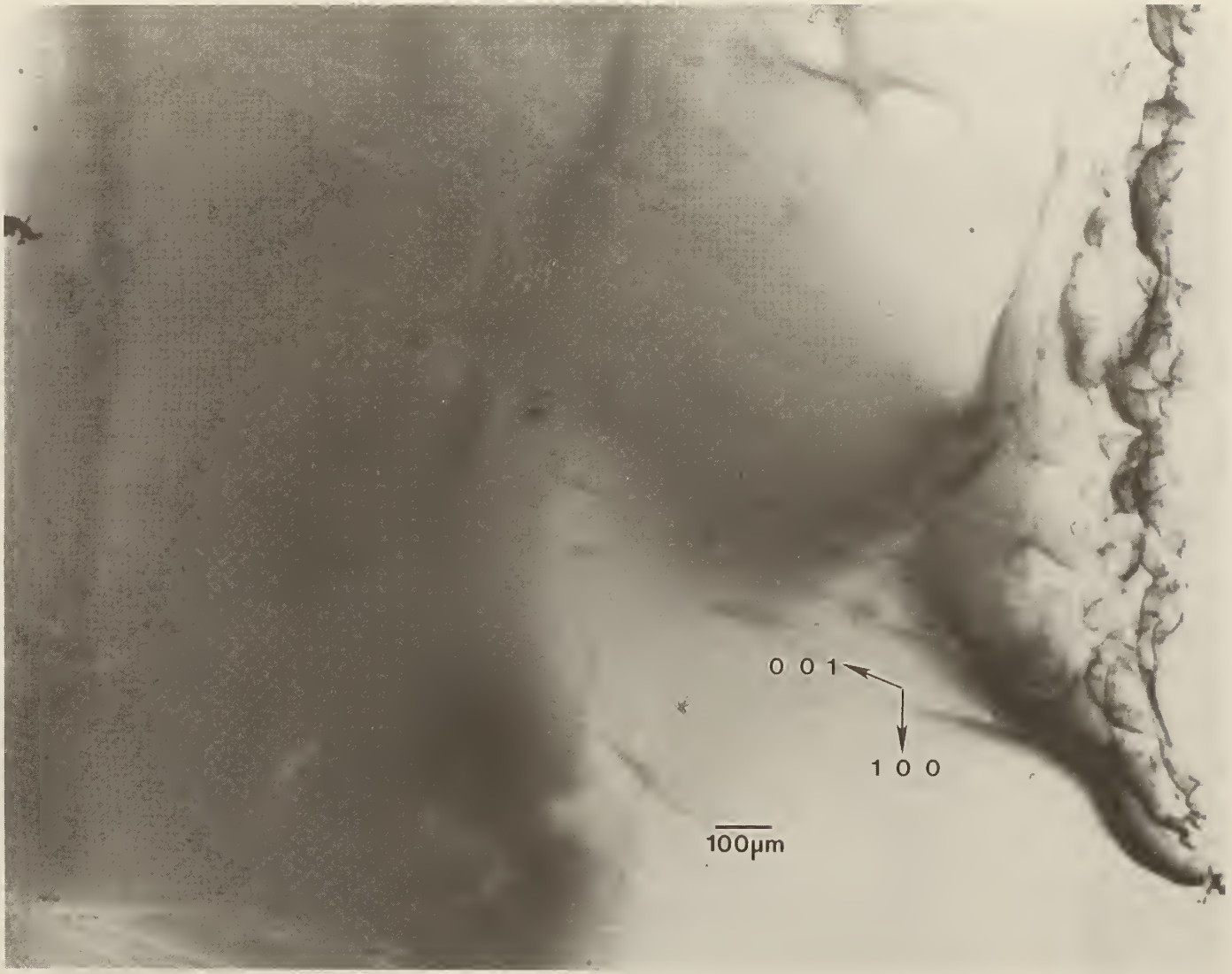

Figure 71. Enlargement of middle left-hand edge of figure 63, (001) diffraction. Darker areas diffract more strongly.

associated with irregularities at the granular interfaces, although radiographic effects from each layer are present.

The seed portion of this crystal takes up most of each image. Space growth was in the [001] direction along that one edge of the seed. The absence of a clear demarcation between the sseed and new growth in this region in most of the images is in contrast to the terrestrial growth of comparable material. The interface between the seed and the new growth is visible only in figure 60; defects in this grain do not appear to propagate into the new growth in the central portion of the disc. In the other grains, defects from the seed indeed appear to have propagated into the part grown in microgravity. Toward the edge of the disc, the irregularity observed in all of the grains is consistent both with rapid growth anticipated from the higher concentration gradients there and with the previous observation of defects before faceting becomes fully developed later in growth.

The last image, fig. 63, differs in shape along the growth edge from the others. It thus appears that new growth did not occur uniformly on all layers. On this one layer, growth appears to have been much slower than on the others, although this may represent initial meltback associated with the premature contact with the solution.

D. Gallium Arsenide

The terrestrial crystal of selenium-doped Bridgman-grown gallium arsenide diffracts over several degrees. A low resolution diffraction image, achieved by rocking the crystal 4^0 around a [11$\bar{2}$] axis during diffraction is shown in figure 72. An infrared image of the same crystal is shown in figure 73. The similarity of these two images is striking. The additional information in the full high-resolution diffraction images of this crystal, figures 74-77, is also striking by contrast. Enlargements of portions of these images are shown in figures 78-82.

The demarcation of the Czochralski seed from the new Bridgman growth is very clear in those images in which this region is in diffraction. The seed/growth boundary is delineated in two ways. First, toward the periphery of the boule it marks a smooth limit to diffraction, past which the lattice does not diffract under the same conditions. Thus, either the lattice constant, or orientation, or both differs in the new growth. Second, in the one region of the seed interface supporting diffraction from both sides, the mesoscopic structure of the growth is observed to be transformed at the interface. The cellular structure of the seed is characteristic of diffraction images of Czochralski-grown undoped gallium arsenide. In the new Bridgman growth, the formation of cells appears to be completely suppressed. Freedom from other demarca-

Figure 72. Low resolution (220) 8 keV diffraction image of approximately (220) surface of terrestrial GaAs crystal 119, in Bragg geometry. The sample was rocked through and angle of 4° during this exposure; the growth direction is [111]. Lighter areas diffract more strongly.

Figure 73. Infrared image of same crystal.

Figure 74. High-resolution (220) stationary diffraction image from approximately (220) surface of terrestrial GaAs crystal 119, in Bragg geometry. The growth direction is [111]. Lighter areas diffract more strongly.

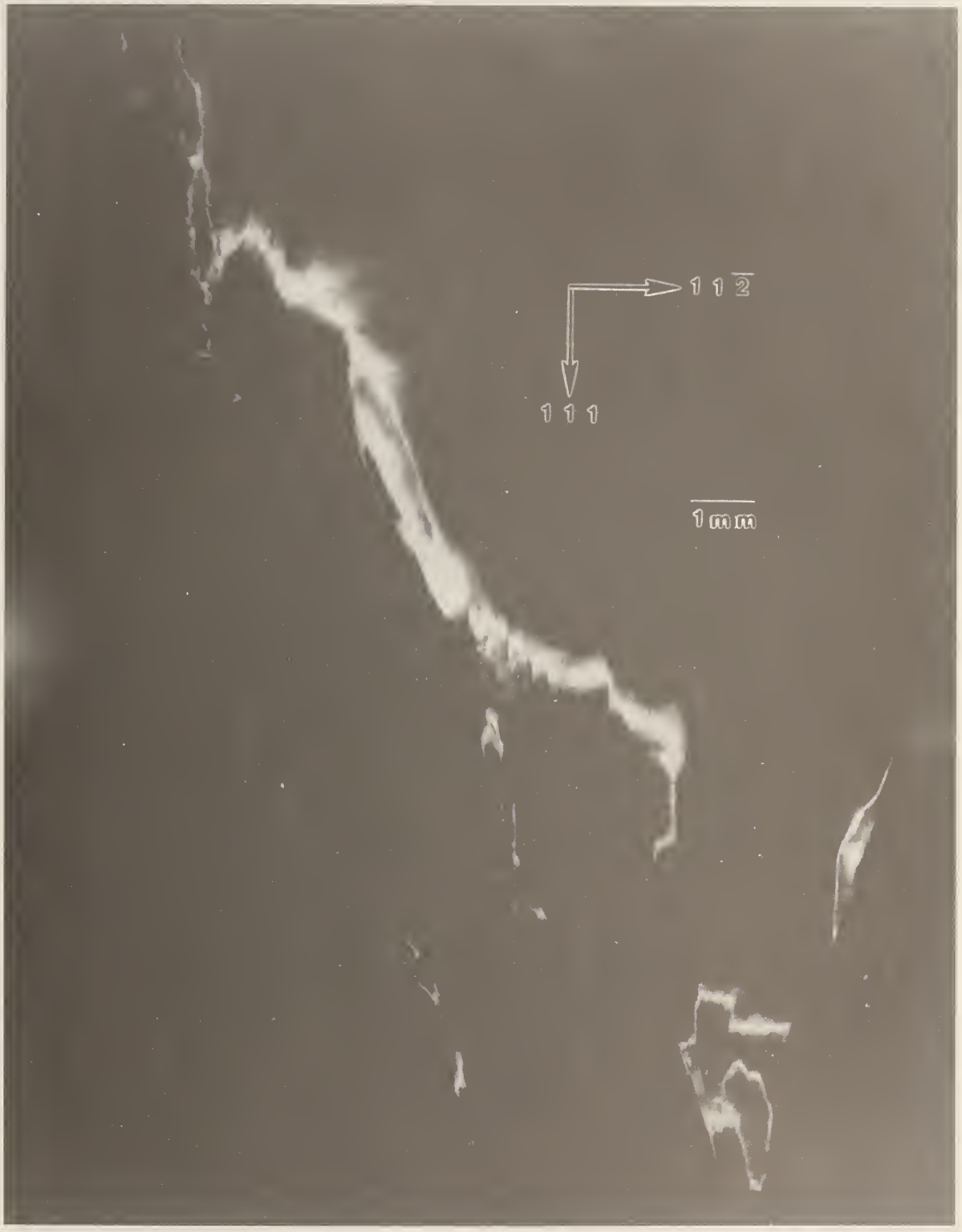

Figure 75. High-resolution (220) 8 keV diffraction image of approximately (220) surface of terrestrial GaAs crystal 119, in Bragg geometry. The angle of incidence is 3.9 arc minutes larger than in that for figure 38; the growth direction is [111]. Lighter areas diffract more strongly.

Figure 76. High-resolution (242) 10 keV diffraction image of approximately (220) surface of terrestrial GaAs crystal 119, in Bragg geometry. The growth direction is [111]. Lighter areas diffract more strongly.

Figure 77. High-resolution (242) 10 keV diffraction image of approximately (220) surface from GaAs crystal 199, in Bragg geometry. The angle of incidence is 19 arc seconds smaller than in that in figure 40; the growth direction is [111]. Lighter areas diffract more strongly.

Figure 78. Enlargement of figure 74, (220) diffraction, near the center of the seed/new growth interface. Darker areas diffract more strongly.

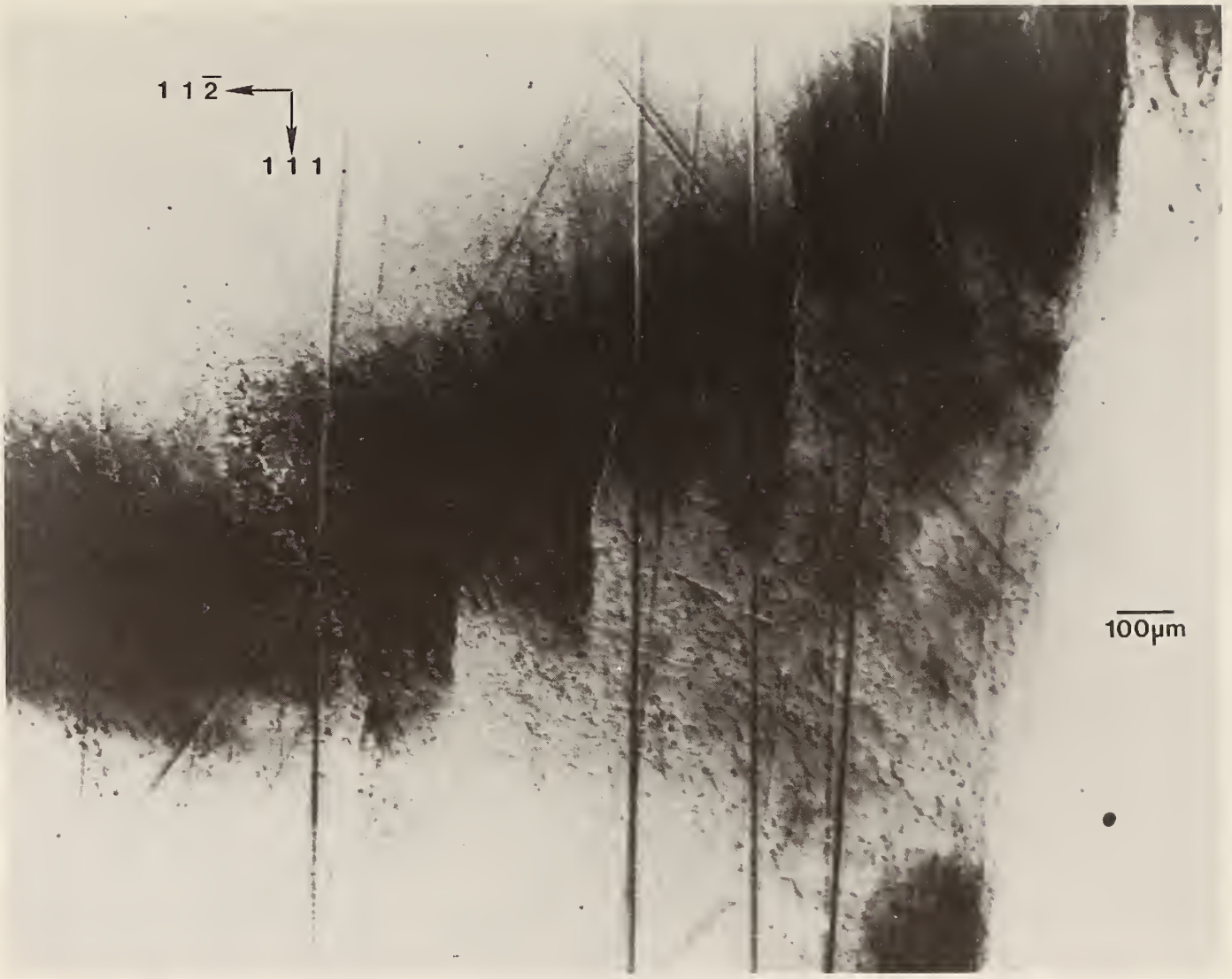

Figure 79. Enlargement of figure 75, (220) diffraction, further down the boule. Darker areas diffract more strongly.

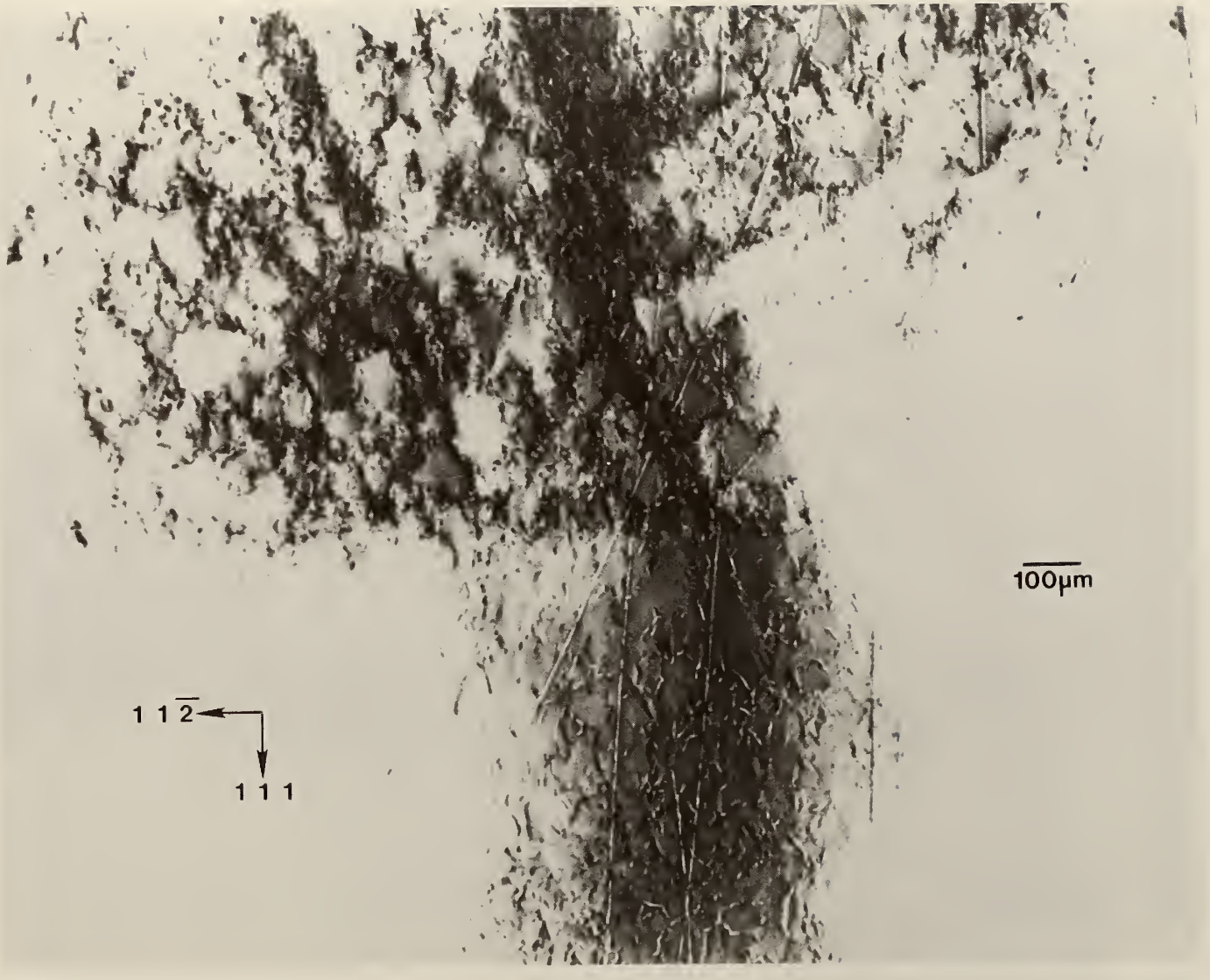

Figure 80. Enlargement of figure 76, (242) diffraction, near the center of the seed/new growth interface. Darker areas diffract more strongly.

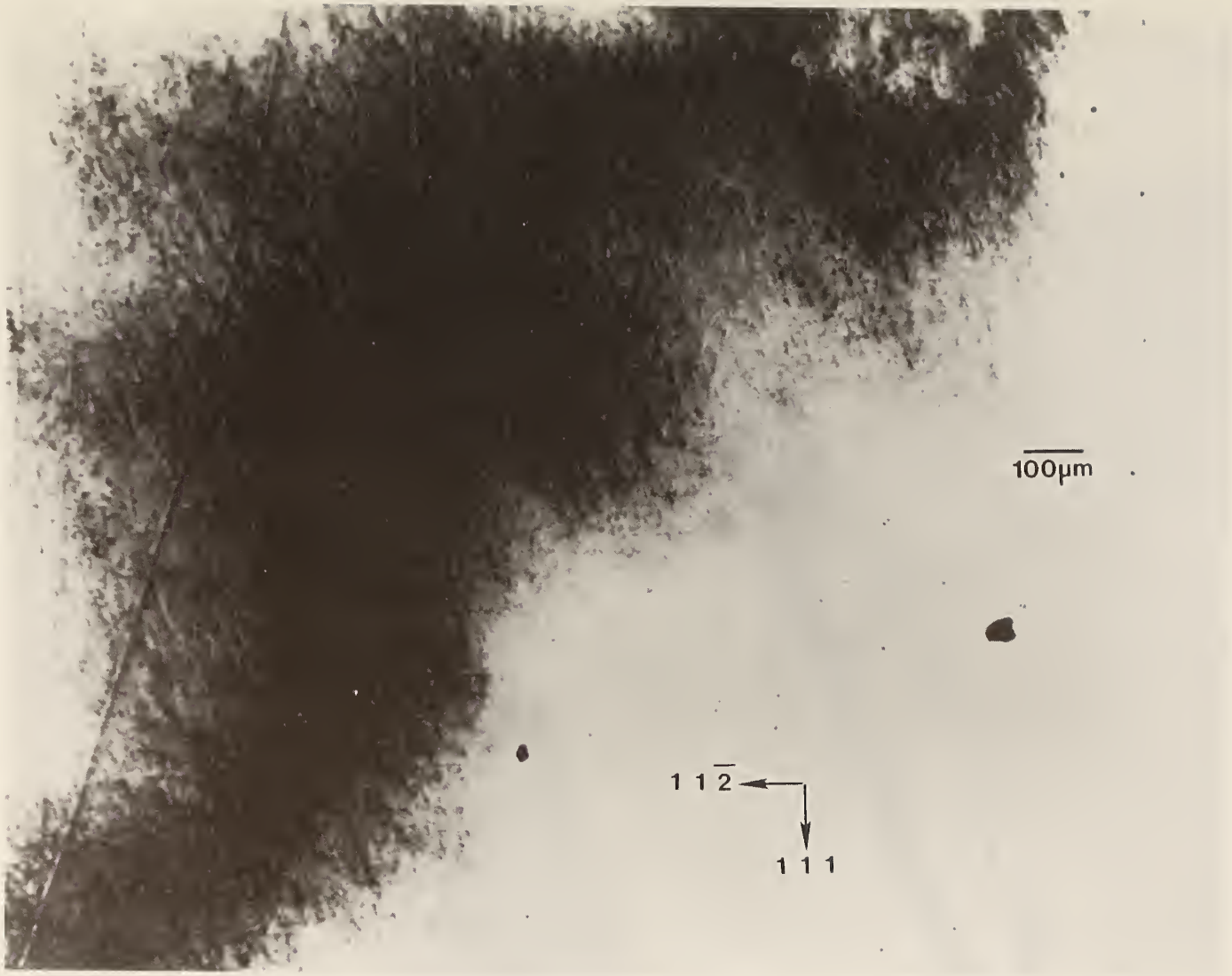

Figure 81. Enlargement of figure 77, (242) diffraction, further down the boule. Darker areas diffract more strongly.

Figure 82. Enlargement of figure 78, (242) diffraction, just past the region enlarged in figure 81. Darker areas diffract more strongly.

tion, however, indicates that, to the extent permitted by the lattice parameter match, the two lattices continue uninterrupted. The lattice parameter mismatch appears to set up a gradual warping of the crystal lattice. Further analysis of the features observed is precluded by the inability to observe diffraction in Laue geometry.

VII. SUMMARY OF INITIAL OBSERVATIONS

These results are summarized in the following sections. The three crystals of mercuric iodide, two of lead tin telluride, one triglycine sulfate crystal, and one gallium arsenide crystal show remarkable differences in their irregularities.

A. General Effects of Microgravity

Seven very different crystals do not provide a sample that is sufficiently large to form definitive conclusions. Nevertheless, our observations provide critical guidance for evaluation and crystal growth. The formation of pervasive multiple phases observed in two terrestrial crystals appears to have been greatly suppressed on growth of two comparable crystals in microgravity. The extent of space growth in a third crystal was too restricted to permit reliable interpretation, and its analysis was further complicated by the appearance of multiple grains in the seed.

Even more important, however, observation of the terrestrial specimens has led to new insight on the nature, distribution, and genesis of irregularity in each material. This insight does not yet resolve all outstanding questions, but permits us to pose the fundamental questions that we have identified in the preceding section. It provides guidance likely to lead to improved growth, both in space and on the ground.

B. Mercuric Iodide

Observation of a terrestrial specimen grown about the time of a Spacelab III crystal indicates that more than one phase is present. The features containing the additional phase(s), which appear to be globular in part and partly in the form of thin layers oriented along the {100} crystallographic directions of the matrix, dominating its mesoscopic structure, appear to have initiated a sharp lattice twist by 10 minutes of arc around an axis aligned with the growth direction and to have stiffened the two resulting subgrains. Formation of the additional phase(s) is suppressed both in the comparable Spacelab III crystal and a recently grown high purity terrestrial crystal. At the same time, the general regularity of the lattice of these latter crystals is lower than in the earlier terrestrial crystal. Superior performance of detectors made from these materials thus appears to be limited far more by

sharp discontinuities associated with additional phase(s) than by slow variation in the lattice.

New space growth experiments now assume even greater importance. Will use of new high purity material in space lead to still further enhancement of device properties? If so, will this be correlated finally with lattice uniformity on a scale of seconds of arc over a range of millimeters, which to date has proved to be less important than the formation of what now appear to be traps provided by features consisting of additional phase(s)? We thus find ourselves launched on a study of the fundamental questions, "What determines charge carrier mobility and lifetime in mercuric iodide?" and "How can they be improved through structural modification?"

C. Lead Tin Telluride

The mesoscopic structure of lead tin telluride appears also to be influenced strongly by the intrusion of additional phase material. But in this instance all available evidence points to identification of the additional phase(s) with a different alloy of the major constituents; the terrestrial sample displays subgrain structure, consistent with identification with additional lead tin telluride phase(s). Indeed, the presence of two phases has been predicted for systems with tellurium concentration very close to 50%.

Although the STS 61A crystal has grain structure that appears to be similar to that of the comparable terrestrial crystal, the formation of the subgrain variation characteristic of the terrestrial sample is suppressed in microgravity. This subgrain structure, associated with formation of a second lead tin telluride phase in the terrestrial crystal, thus appears to have been suppressed by reduction in gravity. This suppression is correlated with the predicted thermo-solutal stability in microgravity.

D. Triglycine Sulfate

Interpretation of the space-growth of triglycine sulfate is complicated by the inadvertent contact between the seed and the solution prior to space growth and by the layered structure that we observe in the seed. Defects in one of these layers appear not to have propagated in the central portion of the disc in microgravity, while defects in the other seed layers appear indeed to have propagated into the new growth. In addition, one of the seed layers appears to have grown at a rate slower than the others.

In the IML 1 mission scheduled, use of multifaceted natural seeds is planned. They will be characterized not only for various physical properties but also for defects and structural properties.

E. Gallium Arsenide

Although gallium arsenide has not yet been grown in space, the mesoscopic structure of a Bridgman-grown boule has been observed to differ from that of the Czochralski-grown seed. The Bridgman-grown lattice appears to be warped more than that of the Czochralski-grown seed. Neither observation is yet understood, and their resolution will require a sample thin enough to sustain anomalous transmission.

VIII. CURRENT LIMITATIONS AND IMPROVEMENT IN DIFFRACTION IMAGING TECHNIQUES

A. Advanced X-Ray Image Detectors

The foregoing sections have described how the techniques of synchrotron radiation diffraction imaging can be used to characterize the phenomena occurring in crystal growth. Most of the techniques applied to the four materials studied have been adapted from concepts developed in the classical laboratory experiments of x-ray topography performed between 1930 and 1960. The capability of laboratory techniques is rather limited. The relatively recent availability of synchrotron x-radiation has provided a new opportunity to improve the quality of the incident beam through improved x-ray optics which, in turn, has provided the wealth of microscopic detail now seen in the images as well as the realization of high resolution transmission video imaging in real time [32].

Much of the effort in establishing these now-routine techniques has concentrated on improving the parallelism and enlarging the size of the monochromatic incident beam to the point that the NIST x-ray imaging beamline at NSLS is the best facility for diffraction imaging in the world. However, as a direct result of our interaction and collaboration with NASA crystal growers certain areas of the imaging capability require improvement if the overall goals of the collaboration are to be met.

A concern expressed in the past by a number of crystal growers has been the turnaround time for acquiring the basic image data; i.e., the time that elapses before the images are ready for analysis. This can now be shortened by orders of magnitude. Serious effort has been devoted to this opportunity; the development that corrects this deficiency provides not only for hard copy images with the same resolution as images enlarged with ordinary magnification (10X) from film, but also speeds the acquisition of the image by up to an order of magnitude.

A natural choice of this development is to use image detectors currently available. There are three major types of such image detectors [33][34]. One is the combination of an image intensifier stage and either a charge-injection-device (CID) or charge-coupled-device (CCD) solid state image detector [35]. This type of detector is called an indirect image detector, because a phosphor screen must be placed in front of the detector to convert x-ray photons to visible photons. The second type is a

vidicon detector that receives x-ray photons directly [36][37] [38][39]. This is called a direct image detector. The third is a CCD detector, which should belong to the class of direct imaging detectors, although the majority of the applications to hard x-ray radiation favors the use of phosphors in front of the detector.

For the spatial resolution necessary to observe structural details even at the minimum level, the insertion of phosphors for the conversion of x-ray photons to visible photons is not desirable. Therefore, indirect image detectors cannot be used. Although vidicon detectors are used currently to follow image-changes as the incident or glancing angle of an x-ray beam is changed [40], they have never been tested in practice as a means of viewing isolated dislocations. We have used a high-quality GaAs crystal to test the practical applicability of a vidicon detector as a replacement for wet film technology. The vidicon detector produces images of reasonable resolution, but is poor in sensitivity at low photon flux levels. In other words, images from most crystals cannot be viewed using the vidicon detector with reasonable resolution, except for the images obtained in the reflection geometry. The images in reflection geometry do not provide much information on the microstructures in materials. We emphasize that the vidicon detector has been used throughout this work to locate diffraction images, as described in previous sections.

The next choice is obviously to adopt the CCD detector. Direct conversion has been considered by many to be sedulously avoided for fear of destroying the CCD array because it is subject to radiation damage. Prior developmental work, however, has shown that serious degradation does not ensue if the intensity of x-rays striking the CCD array is kept below 10^4 to 10^5 photons/mm^2/sec.

We have applied a CCD area detector to image the GaAs test crystal in transmission [41]. Figure 83 contains two forward (Q-beam) transmission diffraction images of the high-quality GaAs crystal, using 220 diffraction planes and 13.5 keV radiation. Figure 83a is a 100 second exposure of the CCD detector, while Figure 83b is a 150 second exposure of a nuclear plate (25 μm-thick emulsion). The same dislocations are seen in both images, but the CCD image indicates a better dynamic range than the image on the plate. The image size is 1 cm X 0.85 cm, and the pixel size is 20 μm X 20 μm.

This improvement not only eliminates film development but provides digital data without densitometry. It has single photon sensitivity, linear photometric response. The high sensitivity greatly reduces the exposure time compared to x-ray film and the linear photometric response gives higher contrast images than film which has a logarithmic response. The digital image data may be processed and enhanced by computer at the beamline. The unique

Figure 83. Transmission topographs of GaAs (a) with CCD detector and (b) a nuclear plate.

processed and enhanced by computer at the beamline. The unique feature of this CCD detector which accounts for its much higher resolution compared with other CCD applications in the x-ray field is the use of direct conversion of x-ray photons to charges accumulated in each pixel [41].

B. Higher Sensitivity Requirements

Our experience through collaboration with crystal growers has shown that there are three classes of sample crystals:

1. Samples which, because of growth conditions, preparation, handling, etc., do not allow us to pursue a detailed analysis of the microstructure in the raw data image. Transmission is usually impossible for this class. The images, however, may be helpful to the growers in their science.

2. Samples which are of a quality that requires many different (hkl) images, especially in transmission, revealing the microstructure in sufficient detail for detailed analysis.

3. Samples which are so perfect as to "test" the resolution limits of our instrumentation. This class of crystal has great value for the pursuits of x-ray physics but little additional analysis is usually required for the crystal grower.

Rarely do we get a class 3 crystal; most of the crystals provided have been class 1, as described in earlier sections. For an understanding of crystal growth mechanisms, samples of class 2 are desirable so that the relationships between crystal growth parameters and the resultant crystal imperfections can be studied in detail within the body of crystal boules at different local regions. As an example, a GaAs crystal which was grown in a laboratory is shown in Figure 84. The sample was sliced vertically along the growth direction of a boule grown with varying growth conditions in equal intervals. The changes in growth parameters are hardly discernible in an overall stationary image of diffraction, even in transmission. This crystal is of very high quality as evidenced by anomalous transmission images (the **O** and **H**-beam images) through a thickness of almost 1 mm. The major reason why such transient regions are not discernible is the lack of local strain sensitivity in obtaining those images. Had a diffraction image been obtained with more precise x-ray tuning in the specific region, the region corresponding to the change in growth conditions should have revealed a complex microstructure associated with such a change. This need for higher local sensitivity, higher spatial resolution and more precise sample manipulation, while viewing the image, certainly implies the inadequacy of the current routine way of recording images on film with the aid of a vidicon detector. We

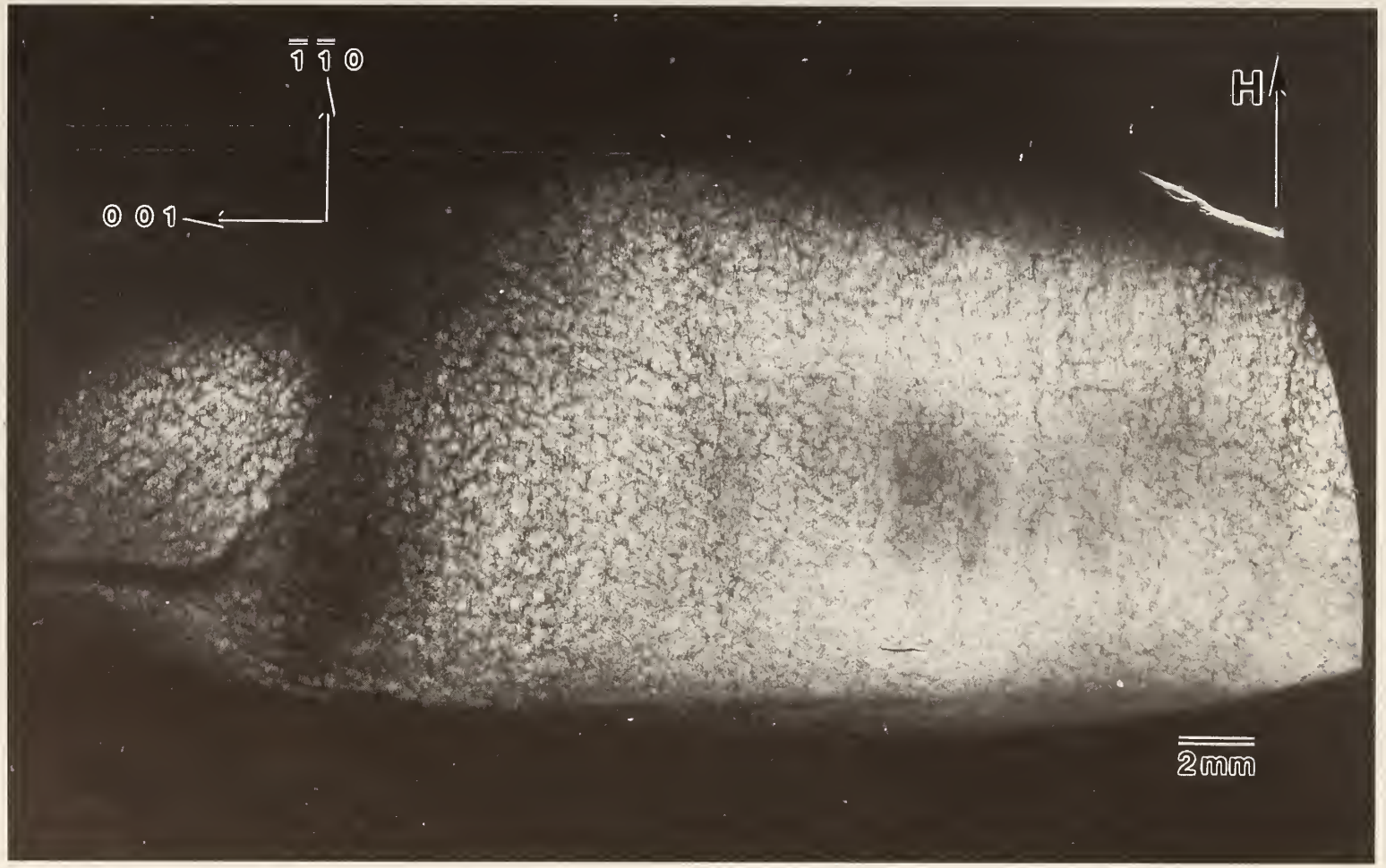

Figure 84. Topograph of GaAs crystal sliced along the growth direction of a boule grown with varying growth conditions in equal intervals. (220) symmetric transmission H-beam image at 10 kev.

need a new technique to "tune in" on local phenomena that are normally missed using the routine diffraction imaging techniques. The application of the direct imaging CCD combined with x-ray image magnification, which constitute the Hard X-Ray Microscope [6][42], has allowed us to make substantial progress in imaging these subtle details. This microscope provides a powerful tool for imaging not only in microradiography, but also in diffraction imaging, as described below. Figure 85 shows a microradiograph of a rather special specimen crystal consisting of a 0.38 mm-thick Si single crystal wafer upon which has been deposited patterns of lines and contact pads of Pd with a thickness of 0.15 μm. The image was obtained at a magnification of 79 with 12.25 keV x-rays [41][42][43]. At this magnification one CCD pixel represents 0.25 μm. The eleven evenly-spaced lines are 1 μm wide and 50 μm long, with a center-to-center spacing of 5 μm. The single line above the eleven lines is 0.6 μm wide. A sub-micrometer feature is clearly seen with this microscope. A blank image, taken before and after without the sample, is subtracted from the raw image data to produce Figure 85. This is another advantage of the CCD detector over film; the digital data may be further processed and analyzed quantitatively.

The substrate of the sample in Figure 85 is a single crystal and the Pd pattern is epitaxially coherent; diffraction images can be obtained and analyzed, as seen in previous sections. In transmission, two diffracted images appear: one in the forward direction of the incident beam, called the **O**-beam image, and the other in the Bragg diffracted direction, called the **H**-beam image. Without moving the microscope from the position set for microradiography, the **O**-beam image can be viewed on the monitor screen merely by rotating the sample. Figure 86 shows a microradiographic image of this sample to be compared with Figure 87 which is the **O**-beam image taken in transmission for the 220 diffraction with the microscope set for the same magnification, 22 X at 8.3 keV [41][42][43]. In dynamical diffraction, a strain field acts as a scattering center and produces a black and white image [6]. The black/white contrast is expected to be inverted in the **H**-beam image. This contrast inversion has been confirmed by moving the microscope to view the **H**-beam image. Therefore, there are interfacial strains around the features. The direction of the atomic shifts in these strained areas can be analyzed in detail in a quantitative way, since the mechanism of the x-ray microscope automatically allows it to act as a precise scattering angle analyzer.

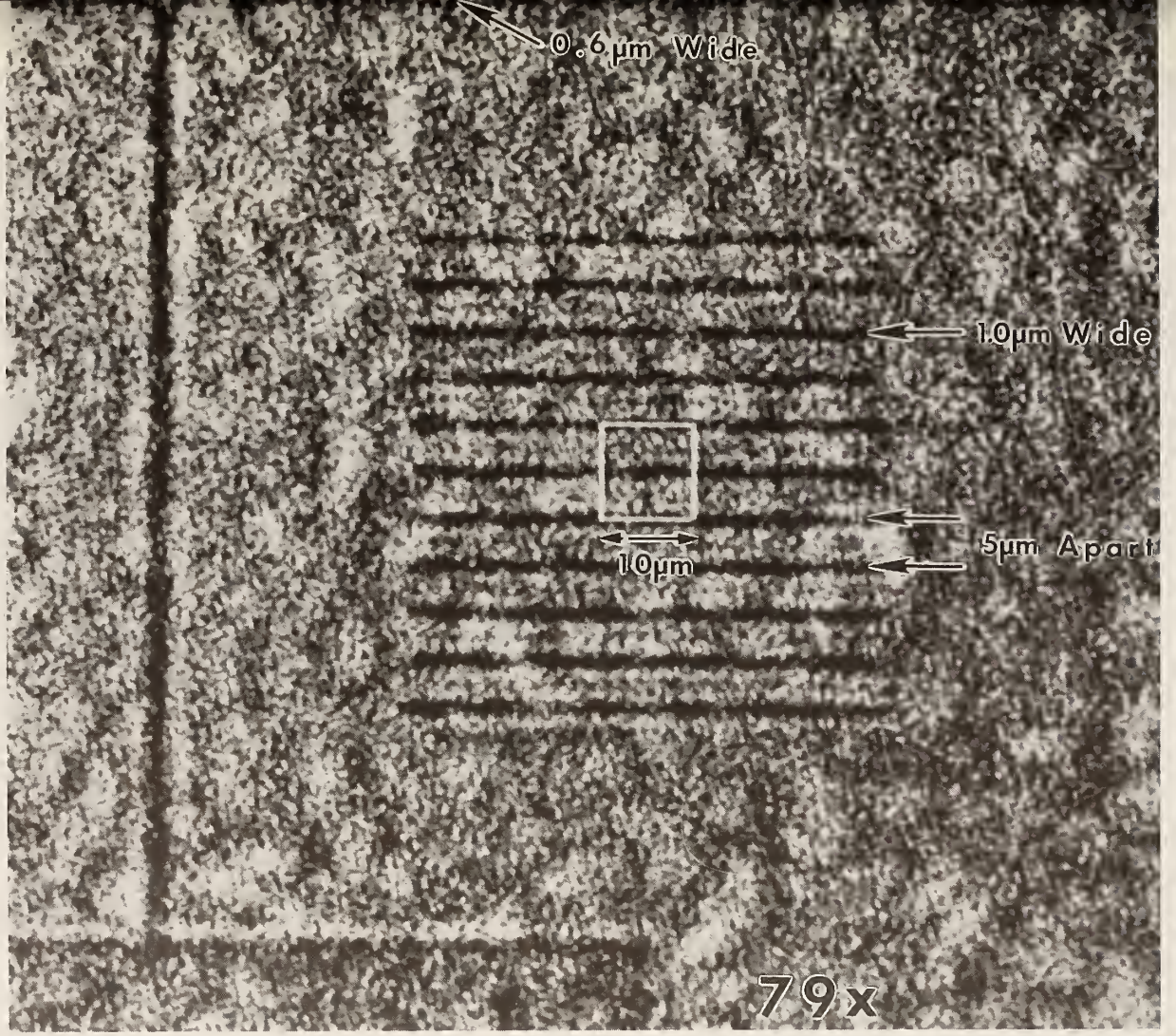

Figure 85. The radiographic image of a pattern of Pd lines on Si. This image was obtained with a magnification of 79 and a wavelength of 1.0 Å (12.3 keV). A single line, 0.6 μm wide, above eleven lines, 1 μm wide and 5 μm apart, is clearly visible. At this magnification, one CCD pixel represents 0.25 μm.

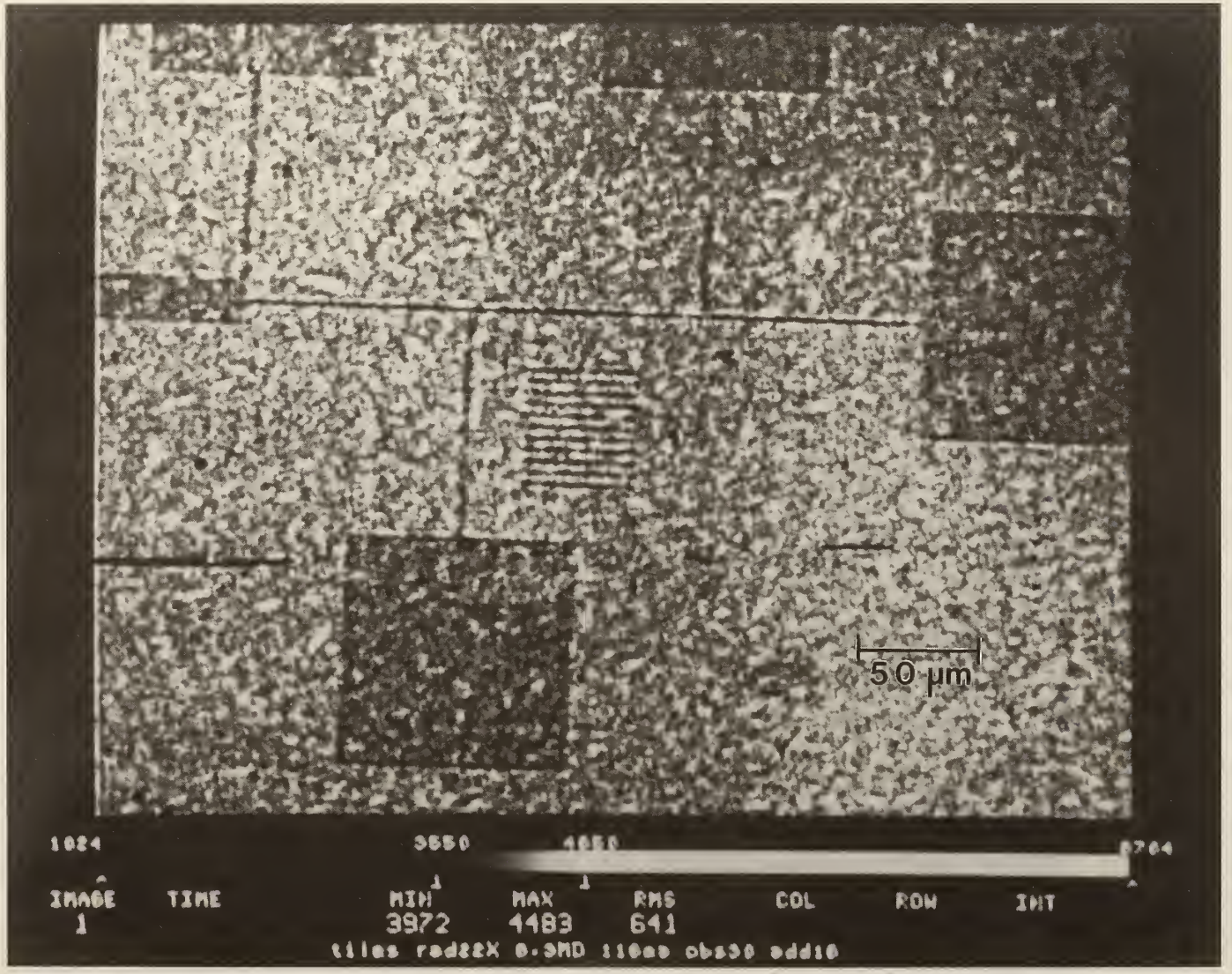

Figure 86. The radiographic image of another section of Pd pattern with the magnification of 22 X at 8.3 keV.

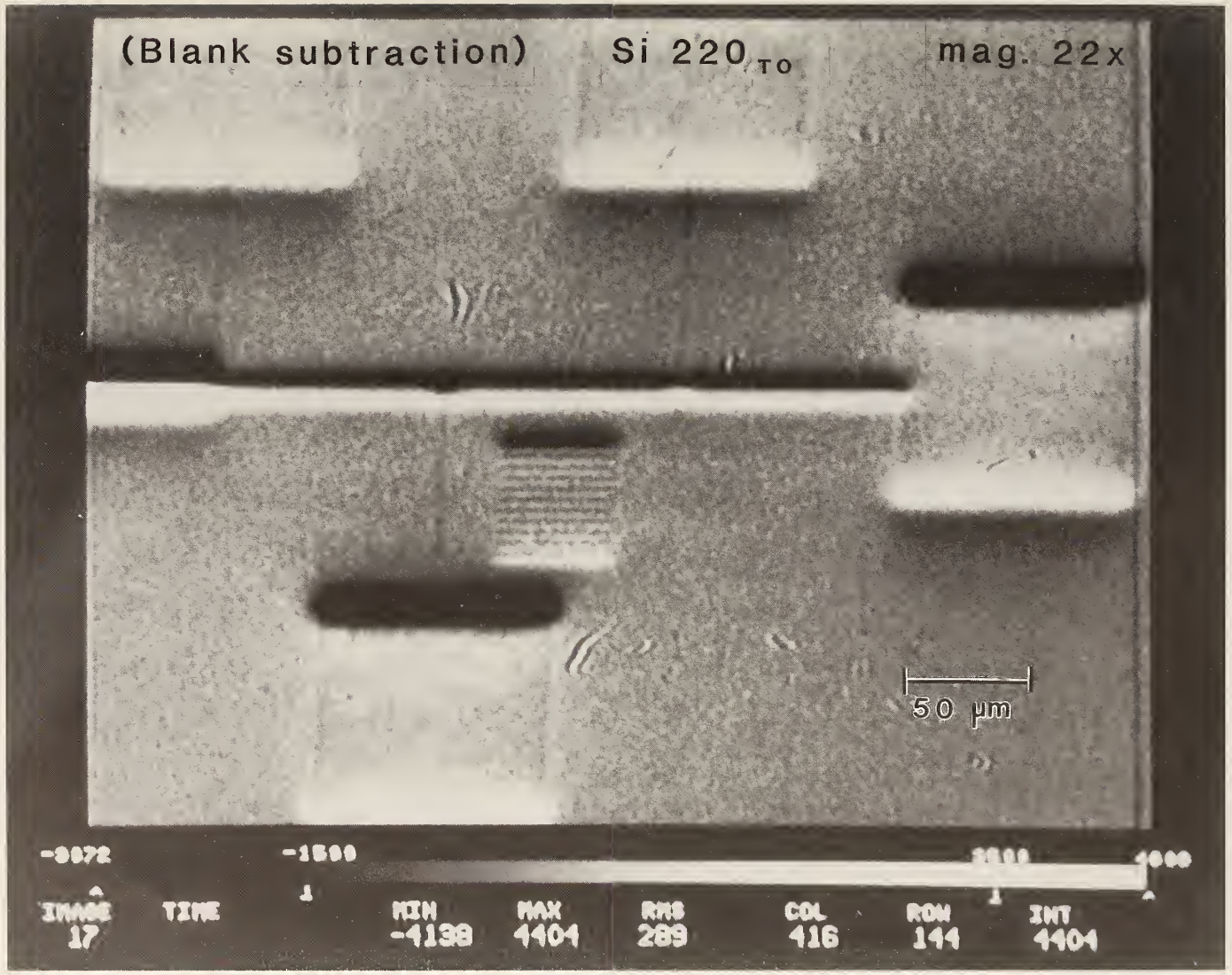

Figure 87. The O-beam image of the Pd pattern for the 220 diffraction in transmission with the same magnification of the microscope as the companion radiographic image in Figure 86.

C. Phase Contrast Microscopy -- Interface Problems

For many of the materials of interest the ultimate goal of crystal growth in microgravity as well as on earth is to provide substrate materials required for advanced microelectronic devices. This relationship and interaction of the substrate materials with device construction, such as epilayers, quantum wells and dopants, etc., is of great interest because device performance depends on these interactions. Crystals grown for general purposes and for the production of seed crystals, for example, have been observed to consists of layers which mimic the growth of epilayers. Device features used in microelectronics and photonics are prepared by a sequence of deposition of a few atoms at a time and doping in appropriate time intervals. These features are almost perfectly lattice-matched to each other and to the substrate. It is difficult to create images with good contrast from mutually coherent features consisting of similar materials.

Revealing these subtle features requires not only a higher degree of sensitivity but also delicate control and manipulation of the sample. To demonstrate such a need for crystal growth and fabrication science and engineering we show some results of imaging such device structures in a In(GaAs)P laser diode [41][42], in which many layers are produced by OMVPE (organometallic vapor phase epitaxy) and subsequent doping of different atoms, and are required to be highly lattice coherent (almost nonexistent mismatch in lattices) among themselves and with their substrates. It is extremely difficult to obtain images of the layers with good contrast in such a material using microradiography. In particular, most advanced microelectronic devices utilize materials composed of elements of high atomic numbers and do not permit x-rays to transmit through the unthinned sample. However, these materials are often highly perfect single crystals and, hence, x-rays can pass through more than one-half millimeter thick samples, almost regardless of x-ray energy, when the sample is set for Bragg diffraction. This penetration is possible due to one of those dynamical effects called anomalous transmission or the Borrmann effect [6][44][45]. Another feature of dynamical effects guarantees that those transmitted images represent true transverse cross sectional images of the layers [6].

Aided by micro-manipulation of angles and positions of the sample and a zooming capability, the x-ray microscope can view the diffraction image of particular layers or layer sections [41][42]. Figure 88 shows a 220 diffraction image in transmission in the Bragg diffracted direction (**H**-beam image) with a magnification of

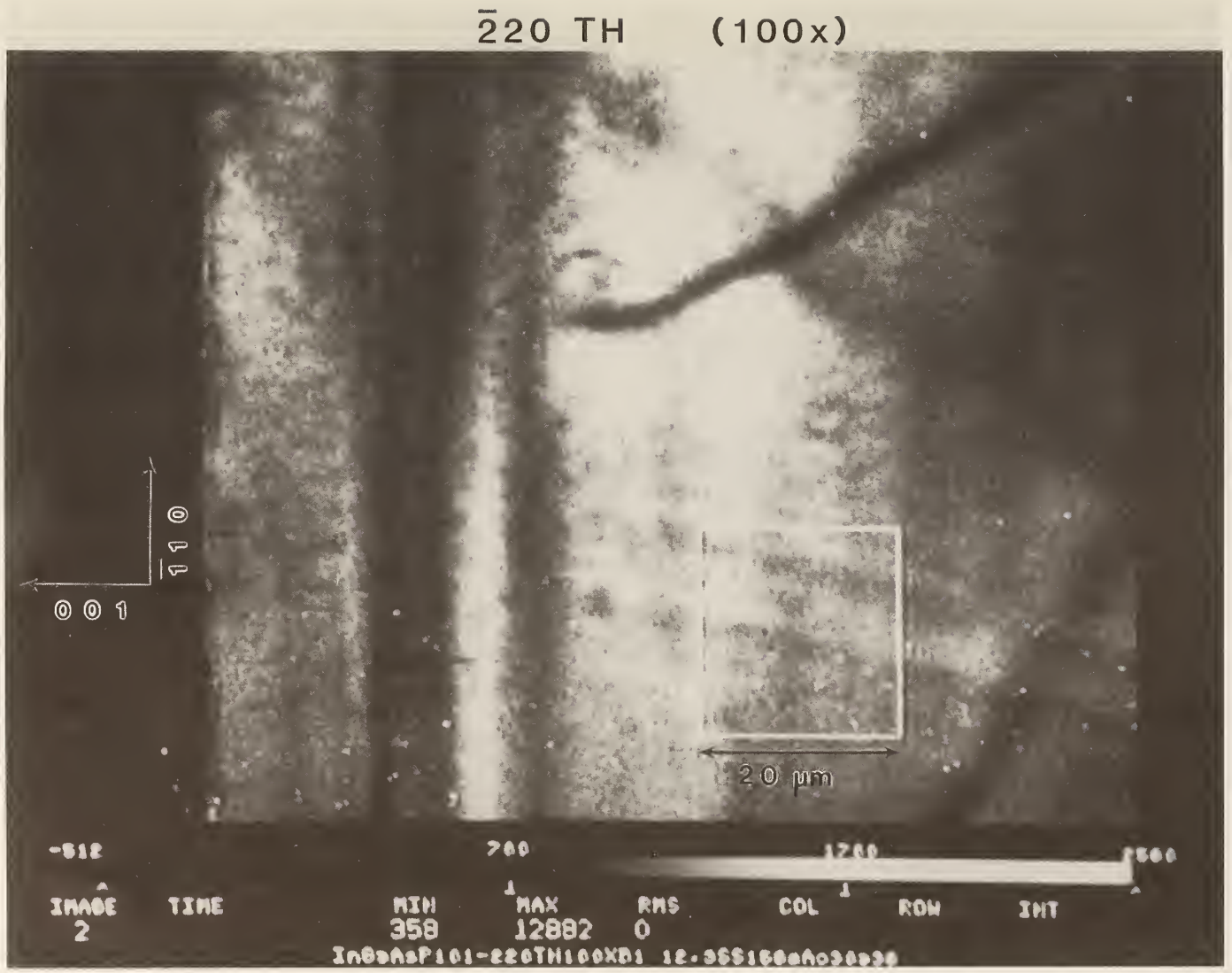

Figure 88 ($\bar{2}20$) transmission image in the Bragg diffracted direction (H-beam) with a magnification of 100 X at 12.3 keV.

100 X at 12.3 keV, precisely tuned to local features of two 1 μm thick layers near the surface of this device. Also visible are 2-3 μm thick layers located 20 ~ 50 μm below the surface (within the substrate crystal). These thicker layer images are broadened due to the interfacial strain observable under this diffraction condition, where the diffracting vector is parallel to the interfaces. These thicker images are "growth striations", well-known to crystal growers, and are produced when the substrate material was grown. Being magnified by the x-ray microscope, the striations appear in the shape of bands.

Two thin layer images are created by either local strains or lattice parameter changes, representing the 0.5-1 μm InP (or AlGaAs) layers doped differently on the InP substrate. These doped layers are part of the device mechanism. An enlarged portion of Figure 88 is reproduced in Figure 89 where A's show the discontinuous first layer nearest to the surface and B's are the segments of the second layer. The discontinuous and segmented images of these layers are indicative of the local variations of the precise Bragg angle for these layers. When the sample is rotated by less than 1 arc sec, new segments of the layers replace the existing images. This type of operation requires precise micromanipulation while magnified images are under view.

To summarize, recent experiments and accomplishments as part of this effort have advanced the x-ray imaging capability for crystal growth science and fabrication engineering. These improved measurement capabilities and techniques are ready to meet the goals and challenges of NASA's community of crystal growers when these techniques are accepted as readily available instruments and are accommodated into the routine practice of diffraction imaging. These advancements include increased spatial resolution in the real-time mode of operation, greatly improved turnaround time with on-line diagnostic and analysis capability, improved control and manipulation of the specimen crystal and the increased sensitivity, spatial resolution and data analysis capability of direct CCD imaging with image magnification, inherent in the hard x-ray microscope. The power of the x-ray microscope, using it as a phase contrast microscope, continues to be explored. One extremely promising application in diffraction imaging as well as microradiography is its use in producing the basic data for microtomographic reconstructions. We have shown its capability of producing two-dimensional images with 1 μm or less spatial resolution in microradiography and diffraction imaging [41][42][43]. A set of two-dimensional images is easily collected as a function of rotational angle. A tomographic image can be reconstructed from this set of high resolution two-dimensional images. To reconstruct a three-dimensional image with 1 μm spatial resolution, the increment of the sample rotational angle is, for example, roughly 0.5° for a cylindrical sample 100 μm in radius. Obviously, the

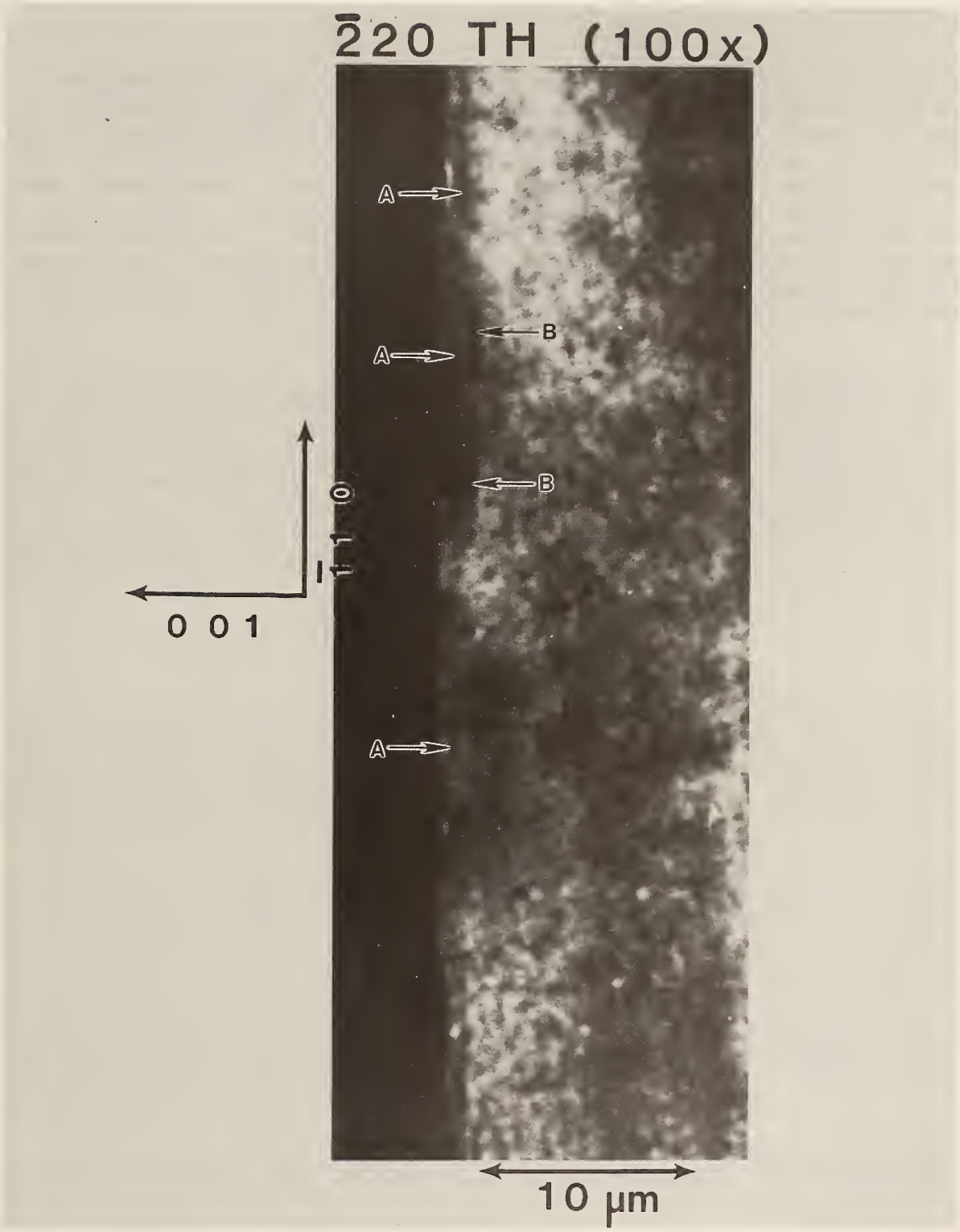

Figure 89. An enlarged portion of the image shown in Figure 74 where the A's show the discontinuous first layer and the B's are segments of the second layer.

larger the sample, the smaller the required angular increment. For the 3D tomographic image construction in diffraction imaging, care must be taken to use the direction of scattering vector, H, as a rotational axis. The micro-rotator currently in use can easily provide this capability with a well fixed rotational center controlled by a set of submicrometer translators. Algorithms are now available for tomographic reconstruction. A working microtomographic system capable of reaching one micrometer or less spatial resolution has become a reality with the hard radiation microscope described here.

IX. FUTURE ACTIVITY

A. Interest in Collaboration

The interest in high-resolution diffraction imaging among these NASA investigators is remarkable; the broad participation that they envision in the imaging experiments themselves is unprecedented. Direct participation of crystal growers in work on the beam line as well as in the analysis promises to increase the insight that is obtained over that possible with the *ex post facto* analysis, which has been characteristic of most previous work in high-resolution diffraction imaging.

B. The Prospects for Proteins

There appear to be strong grounds for the skepticism of many protein crystal growers with respect to the prospects for utility to them of high-resolution diffraction images. However, with proper attention at the outset, some, if not all, of the sources of concern identified may be circumvented.

Among the sources of concern most difficult to address are: 1) the mixture of kinematic and dynamical diffraction that we expect, and 2) the high level of irregularities that we also expect because it is characteristic of crystals of many types. Kinematic diffraction is likely to coexist with dynamical diffraction because of the optical thinness expected both from the crystal size and because of the small atomic number of the atoms in these crystals. It is not clear without trial whether or not the interpretational challenges presented by the irregularity and by the optical thinness can be met effectively.

Among the difficulties that may prove to be highly challenging, we anticipate the following: 1) the relevance of diffraction imaging to the desired order in these crystals, 2) changes in crystal regularity immediately following return to earth, 3) the presence of a mother liquor, 4) destruction by the x-ray beam, and 5) the relatively low scattering power of the atoms in these materials.

Because none of these difficulties is frivolous, and at least two of them may well prove to be insurmountable, we propose that special attention be directed to the identification of a material

and a particular sample that is likely to give us the best opportunity to circumvent the difficulties.

C. Crystal Preparation

We have noted the importance of four sample characteristics for fully successful analysis: thickness, surface orientation, surface condition, and density of irregularities. The analysis undertaken this first year was severely limited by the necessity to work with immediately available samples, which we recognized at the outset would not fulfill all of these conditions. It will clearly be important to continued success in future analyses to place special effort on the preparation and selection of suitable crystals.

Anomalous transmission through optically thick crystals is a function of their regularity. All six optically thick crystals that we examined as part of the effort this year were sufficiently thick that warping of the lattice during sample preparation was not likely to be a problem. This indeed proved to be an extremely important factor in the analysis that was carried out. Nevertheless, six of the seven crystals were too thick for observation of diffraction in Laue geometry, and this precluded a complete analysis. On the basis of this year's work, we anticipate that the information that would be provided by optimum analysis of comparable thin crystals would be worth the effort necessary to achieve satisfactory thinning.

The challenge here is not trivial, however. One must be careful not to distort the lattice in the thinning and subsequent mounting for imaging, particularly in the thinning of soft materials such as mercuric iodide, [22][26]. Because of the interesting irregularities in these materials, it seems likely that sample thickness less than a half millimeter, perhaps substantially less, is desirable; and warping and support then also become serious concerns.

Orientation close to a low-index lattice plane is also important to success in observing an optimum range of diffraction. Suitable orientation is not particularly challenging, but does require attention in the early stages of crystal preparation. Observation of several of the samples this year was limited by orientation that was far from ideal.

Feature-free surface treatment, both important and challenging, is not always achieved. The surfaces of all of the samples observed this year, however, were exemplary. None interfered in any way with the imaging analysis. This is strong testimony both to the interest and to the diligence of our collaborators.

Finally, success in the interpretation of diffraction images depends on the ability to distinguish the various irregularities, which places a limit on their density. This is a challenge particularly at the time of sample selection. Preliminary selection of the most promising materials through auxiliary structural information can dramatically increase efficiency in the exploitation of diffraction imaging.

D. Correlation with Auxiliary Data

Since high-resolution diffraction imaging analysis involves considerable effort, optimization of the knowledge gained through utilization of auxiliary data is important. This not only minimizes the special effort required for imaging, but increases the effective use of the other data and can lead ultimately to the deepest insight into the control of irregularity, which is a principal goal here. High-resolution diffraction imaging is not a suitable production line quality control tool. But the insight to which it contributes, in conjunction with other more readily obtainable data, can lead to the production of crystals with superior structure.

E. Crystal Selection Criteria

In summary, insight into the nature and genesis of irregularity through high-resolution diffraction imaging can be optimized through crystal selection along several lines: the nature of the crystal; collaboration with the crystal grower; and availability of auxiliary data. Wisdom is most likely to follow when attention is devoted to all of these areas.

In order to contribute to useful analysis, irregularities must be observed to vary under a range of conditions. This requires that crystals to be imaged are thin, suitably oriented, effectively polished, and free enough of irregularities that those remaining are isolated enough for analysis.

Since a high-resolution diffraction image is never unique and frequently not predictable, but typically varies strongly as the Bragg peak is traversed, imaging can be carried out so that the relative visibility of selected features is optimized. Participation of the crystal grower, first in the imaging and then in the interpretation, can contribute to the efficiency with which understanding achieved. Thus active collaboration with the crystal grower can play a central role in the success of the diffraction imaging.

Finally, success in diffraction imaging analysis can also be measured by the extent to which it ties together observations made by a variety of other characterization approaches. The presence of other data thus can contribute dimensions to the understanding achieved that can arise in no other way. Such data can serve to complement, to confirm, or to be confirmed by, the predictions based on diffraction imaging.

X. ACKNOWLEDGMENT

The extraordinarily interesting results of the initial year of collaboration described in this report would have not have been possible without the multifaceted support of the NASA Microgravity Sciences and Applications Division. Thanks to this strong NASA support, great strides have been taken in the sophistication with which several important crystal systems can be grown. Even more dramatic advances can now be anticipated with confidence.

XI. REFERENCES

[1.] L. van den Berg and W. F. Schnepple, "Growth of Mercuric Iodide in Spacelab III," 19th Int. SAMPE Tech. Conf. 754 (1987)

[2.] L. van den Berg and W. F. Schnepple, "Mercuric Iodide Crystal Growth in Space," Nucl. Inst. Meth. Phys. Res. **A283**, 335-338 (1989)

[3.] Lawrence J. DeLucas, Craig D. Smith, H. Wilson Smith, Senadhi Vijay-Kumar, Shobha E. Senadhi, Steven E. Ealick, Daniel C. Carter, Robert S. Snyder, Patricia C. Weber, F. Raymond Salemme, D. H. Ohlendorf, H. M. Einspahr, L. L. Clancy, Manuel A. Navia, Brian M. McKeever, T. L. Nagabhushan, George Nelson, A. McPherson, S. Koszelak, G. Taylor, D. Stammers, K. Powell, G. Darby, and Charles E. Bugg, "Protein Crystal Growth in Microgravity," Science **246**, 651-654 (1990)

[4.] W. Littke and C. John, Science **225**, 203 (1984)

[5.] Bruce Steiner, Masao Kuriyama, and Ronald C. Dobbyn, "Insight into the Genesis of Irregularity during Crystal Growth Achieved through High Sensitivity Monochromatic Synchrotron X-Radiation Diffraction Imaging (Topography)," Prog. Crystal Growth and Char., in press (1990)

[6.] M. Kuriyama, B. W. Steiner, and R. C. Dobbyn, "Dynamical Diffraction Imaging (Topography) with X-Ray Synchrotron Radiation," Ann. Rev. Mat. Sci. **19**, 183-207 (1989)

[7.] Bruce Steiner, Masao Kuriyama, Ronald C. Dobbyn, and Uri Laor, "Diffraction Imaging (Topography) with Monochromatic Synchrotron Radiation," J. Res. NBS **93**, 577-601 (1988)

[8.] Robert A. Schmitz, private communication (1990)

[9.] Bruce Steiner, Uri Laor, Masao Kuriyama, Gabrielle G. Long, and Ronald C. Dobbyn, "Diffraction Imaging of High Quality Bismuth Silicon Oxide with Monochromatic Synchrotron Radiation: Implication for Crystal Growth," J. Cryst. Growth **87**, 79 (1988)

[10.] Masao Kuriyama, Bruce Steiner, Ronald C. Dobbyn, Uri Laor, David Larson,and Margaret Brown, "Streaking Images That Appear Only in the Plane of Diffraction in Undoped GaAs Single Crystals: Diffraction Imaging (Topography) by Monochromatic Synchrotron Radiation," Phys. Rev. **B 38**, 12421 (1988)

[11.] B. Steiner, M. Kuriyama, R. C. Dobbyn, U. Laor, D. Larson, and M. Brown,"Structural Anomalies in Undoped Gallium Arsenide Observed in High Resolution Diffraction Imaging with Monochromatic Synchrotron Radiation," J. Appl. Phys. **66**, 559 (1989)

[12.] M. Schieber, C. Ortale, L. van den Berg, W. Schnepple, L. Keller, C.N. J. Wagner, W. Yelon, F. Ross, G. Georgeson, and F. Milstein, "Correlation between Mercuric Iodide Detector Performance and Crystalline Perfection," Nucl. Inst. Meth. Phys. Res. **A283**, 171-187 (1989)

[13.] Y. F. Nicolau and M. Dupuy, "Study of alpha HgI_2 Crystals Grown in Space by Differential Scanning Calorimetry, Scanning Cathodoluminescence Microscopy and Optical Microscopy," Nucl. Inst. Meth. Phys. Res. **A283**, 355-362 (1989)

[14.] Daniel Carter, private communication.

[15.] Robert Sweet, private communication.

[16.] W. J. Boettinger, P. W. Voorhees, R. C. Dobbyn, and H. E. Burdette, "A study of the Coarsening of Liquid-Solid Mixtures Using Synchrotron Radiation Microradiography," Met. Trans. A **18A**, 481-490 (1987).

[17.] G. R. Ricker, J. V. Vallerga, and D. R. Wood, "A Mercuric Iodide Detector System for X-Ray Astronomy," Nucl. Inst. Methods **213**, 133-144 (1983)

[18.] R. C. Whited and M. M. Schieber, "Cadmium Telluride and Mercuric Iodide Gamma Radiation Detectors," Nucl. Inst. Meth. **162**, 113-123 (1979)

[19.] R. C. Whited and L. van den Berg, "Native Defect Compensation in HgI_2 Crystals," IEEE Trans. Nucl. Sci. **24** 165-167 (1977)

[20.] M. Schieber, M. Roth, and W. F. Schnepple, "Crystal Growth and Applications of Mercuric Iodide," J. Cryst. Growth **65**, 353-364 (1983)

[21.] I. F. Nicolau and G. Rolland, "Deviation from Stoichiometry in alpha-HgI_2," Mat. Res. Bull. **16**, 759-770 (1981)

[22.] S. Gits and A. Authier, "Plastic Defects in Alpha-HgI_2 Single Crystals," J. Cryst. Growth **58**, 473-485 (1982)

[23.] T. E. Felter, R. H. Stulen, W. F. Schnepple, C. Ortale, and L. van den Berg, "Rutherford Backscattering and Auger Spectroscopy of Mercuric Iodide Detectors," J. Nucl. Materials (1988)

[24.] D. Wong, X. J. Bao, T. E. Schlesinger, R. B. James, A. Cheng, C. Ortale, and L. van den Berg, "Photoluminescence Variations Associated with the Deposition of Palladium Electrical Contacts on Detector-Grade Mercuric Iodide," Appl. Phys. Lett. **53**, 1536 (1988)

[25.] W. B. Yelon, R. W. Alkire, M. M. Schieber, and L. van den Berg, "Crystal Perfection of HgI_2," J. Appl. Phys. **52**, 4604 (1981)

[26.] S. Gits, "Characterization of Extended Defects in alpha-HgI_2 Single Crystals," Nucl. Inst. Methods **213**, 43-50 (1983)

[27.] Roger K. Crouch, Archibald L. Fripp, William J. Debnam, Fredrick M. Carlson, and Richard T. Simchick, "Results from a Compound Semiconductor Crystal Growth Experiment in a Low Gravity Environment," SAMPE ELectronics Materials and Processes Conf., Santa Clara, June 22-25, 1987

[28.] V. F. Miuskov, V. P. Konstantinova, and A. I. Gusev, "X-Ray Diffraction Investigation of Defects in Triglycine Sulfate Crystals," Kristallografiya **13**, 909-912 (1968); Soviet Phys. - Cryst. **13**, 791-794 (1969)

[29.] A. Izrael, J. F. Petroff, A. Authier, and Z. Malek, "X-Ray Topographic Study of Growth Defects in Triglycine Sulphate Crystals in Relation to their Growth Conditions," J. Cryst. Growth **16**, 131-141 (1972)

[30.] T. C. Harman, "Control of Imperfections in Crystals of $Pb_{1-x}Sn_xTe$, $Pb_{1-x}Sn_xSe$, and $PbS_{1-x}Se_x$", J. Nonmetals **1**, 183-194 (1973).

[31.] J. F. Butler and T. C. Harman, " Metallic Inclusions and Cellular Substructure in $Pb_{1-x}Sn_xTe$ Single Crystals," J. Electrochem. Soc. **116**, 260-263 (1969).

[32.] M. Kuriyama, W.J. Boettinger and G.G. Cohen, Ann. Rev. Mater. Sci **12** 23 (1982)

[33.] R.E. Green Jr: Advances in X-Ray Analysis 14 311 (1971) & **20** 211 (1977)

[34.] A. Rose and P.K. Weimer: Physics Today, September p. 24 (1989)

[35.] W.J. Boettinger, H.E. Burdette, M. Kuriyama and R.E. Green, Jr. Rev. Sci. Instrum. **47** 906 (1976)

[36.] J. Chikawa and I. Fujimoto: Appl. Phys. Lett. **13** 387 (1968)

[37.] J. Chikawa: "Real Time Radiologic Imaging: Medical and Industrial Applications" p. 209 (1980) ASTM Special Tech. Pub. 716, ASTM, Philadelphia

[38.] W. Hartman, G. Markevitz, V. Rettenmaia and H.J. Quaisser: Appl. Phys. Lett. **27** 308 (1975)

[39.] W. Hartman: "Real Time Radiologic Imaging: Medical and Industrial Applications" p. 201 (1980) ASTM Special Tech. Pub. 716, ASTM, Philadelphia

[40.] B. Steiner, U. Laor, M. Kuriyama, G.G. Long, R.C. Dobbyn: J. Cryst. Growth **87** 79 (1988)

[41.] M. Kuriyama, Nuclear Instrum. & Method (1990)

[42.] M. Kuriyama, R.C. Dobbyn and R.D. Spal: Rigaku Journal **19** (1990)

[43.] M. Kuriyama, R.C. Dobbyn, R.D. Spal, H.E. Burdette and D.R. Black, J. Res. NIST (1990)

[44.] G. Borrmann, Phys. Z. 42 157 (1941)

[45.] M. Kuriyama, Phys. Stat. Solid **24** 743 (1967)

APPENDIX: NASA Principal Investigations Engaged in Crystal Growth

Prof. G. J. Abbaschian
University of Florida, Gainesville

Prof. Elmer Anderson
University of Alabama, Huntsville

Prof. J. Barry Andrews
University of Alabama, Birmingham

Prof. Klaus J. Bachmann
North Carolina State University

Dr. Martin E. Barmatz
Jet Propulsion Laboratory

Prof. Robert J. Bayuzick
Vanderbilt University

Prof. Charles E. Bugg
University of Alabama, Birmingham

Prof. Frederick M. Carlson
Clarkson University

Dr. Daniel C. Carter
Marshall Space Flight Center

Dr. Ared Cezairliyan
National Institute of Standards and Technology

Dr. Larry DeLucas
The University of Alabama, Birmingham

Prof. Robert S. Feigelson
Stanford University

Prof. Merton C. Flemings
Massachusetts Institute of Technology

Dr. Archibald L. Fripp
Langley Research Center

Prof. Randall M. German
Rensselaer Polytechnic Institute

Mr. Thomas Glasgow
NASA Lewis Research Center

Prof. Martin E. Glicksman
Rensselaer Polytechnic Institute

Prof. Herman H. Hobbs
George Washington University

Prof. William Hofmeister
Vanderbilt University

Prof. William L. Johnson
California Institute of Technology

Prof. Carl C. Koch
North Carolina State University

Prof. Sindo Kou
University of Wisconsin

Prof. Ravindra B. Lal
Alabama A&M University

Dr. David J. Larson, Jr.
Grumman Aerospace Corporation

Dr. Sandor L. Lehoczky
Marshall Space Flight Center

Prof. Ponzy Lu
University of Pennsylvania

Prof. John L. Margrave
Rice University

Dr. David Matthiesen
GTE Laboratories

Dr. Mary Helen McCay
University of Tennessee Space Institute

Prof. Alexander McPherson, Jr.
University of California, Riverside

Prof. George F. Neilson
University of Arizona

Dr. R. R. Neurgaonkar
Rockwell International Science Center

Prof. John H. Perepezko
University of Wisconsin

Dr. Marc Lee Pusey
Marshall Space Flight Center

Prof. Chandra S. Ray
University of Missouri, Rolla

Dr. Franz Rosenberger
University of Alabama, Huntsville

Dr. Robert Schiffman
Intersonics

Dr. N. B. Singh
Westinghouse Research and Development Center

Prof. Julian Szekely
Massachusetts Institute of Technology

Dr. Frank R. Szofran
Marshall Space Flight Center

Dr. Eugene H. Trinh
Jet Propulsion Laboratory

Dr. Lodewijk van den Berg
EG&G Energy Measurements, Inc.

Dr. Marcus Vlasse
Marshall Space Flight Center

Prof. Donald Voet
University of Pennsylvania

Dr. Peter Voorhees
Northwestern University

Prof. Michael C. Weinberg
University of Arizona

Prof. Heribert Wiedemeier
Rensselaer Polytechnic Institute

Prof. William R. Wilcox
Clarkson University

Prof. August Witt
Massachusetts Institute of Technology

NIST-114A
(REV. 3-90)

U.S. DEPARTMENT OF COMMERCE
NATIONAL INSTITUTE OF STANDARDS AND TECHNOLOGY

BIBLIOGRAPHIC DATA SHEET

1. PUBLICATION OR REPORT NUMBER
NIST/TN-1287

2. PERFORMING ORGANIZATION REPORT NUMBER

3. PUBLICATION DATE
August 1991

4. TITLE AND SUBTITLE

High Resolution Diffraction Imaging of Crystals Grown in Microgravity and Closely Related Terrestrial Crystals

5. AUTHOR(S)

B. Steiner, R. Dobbyn, D. Black, H. Burdette, M. Kuriyama, R. Spal, L. van den Berg, A. Fripp, R. Simchick, R. Lal, A. Batra, D. Matthiesen, B. Ditchek

6. PERFORMING ORGANIZATION (IF JOINT OR OTHER THAN NIST, SEE INSTRUCTIONS)

U.S. DEPARTMENT OF COMMERCE
NATIONAL INSTITUTE OF STANDARDS AND TECHNOLOGY
GAITHERSBURG, MD 20899

7. CONTRACT/GRANT NUMBER

8. TYPE OF REPORT AND PERIOD COVERED
Final

9. SPONSORING ORGANIZATION NAME AND COMPLETE ADDRESS (STREET, CITY, STATE, ZIP)

National Aeronautics and Space Administration
Microgravity Science and Applications Division
Washington, DC 20546

10. SUPPLEMENTARY NOTES

11. ABSTRACT (A 200-WORD OR LESS FACTUAL SUMMARY OF MOST SIGNIFICANT INFORMATION. IF DOCUMENT INCLUDES A SIGNIFICANT BIBLIOGRAPHY OR LITERATURE SURVEY, MENTION IT HERE.)

This paper reports on irregularities found in three crystals grown in space, in four crystals grown entirely on the ground, and compares the two sets. Irregularities have been observed in mercuric iodide, lead tin telluride, triclycine sulfate, and gallium arsenide by high resolution synchrotron x-radiation diffraction imaging.

Radiation detectors made from mercuric iodide crystals grown in microgravity have been reported to perform far better than conventional detectors grown from the same material under full gravity. Effort is now underway to reproduce these "space" crystals, optimize their properties, and extend comparable superiority to other types of material.

12. KEY WORDS (6 TO 12 ENTRIES; ALPHABETICAL ORDER; CAPITALIZE ONLY PROPER NAMES; AND SEPARATE KEY WORDS BY SEMICOLONS)

crystal growth; gallium arsenide; lead tin telluride; mercuric iodide; microgravity; monochromatic synchrotron radiation diffraction imaging; TGS

13. AVAILABILITY

X	UNLIMITED
	FOR OFFICIAL DISTRIBUTION. DO NOT RELEASE TO NATIONAL TECHNICAL INFORMATION SERVICE (NTIS).
X	ORDER FROM SUPERINTENDENT OF DOCUMENTS, U.S. GOVERNMENT PRINTING OFFICE, WASHINGTON, DC 20402.
X	ORDER FROM NATIONAL TECHNICAL INFORMATION SERVICE (NTIS), SPRINGFIELD, VA 22161.

14. NUMBER OF PRINTED PAGES
162

15. PRICE

ELECTRONIC FORM

NIST Technical Publications

Periodical

Journal of Research of the National Institute of Standards and Technology—Reports NIST research and development in those disciplines of the physical and engineering sciences in which the Institute is active. These include physics, chemistry, engineering, mathematics, and computer sciences. Papers cover a broad range of subjects, with major emphasis on measurement methodology and the basic technology underlying standardization. Also included from time to time are survey articles on topics closely related to the Institute's technical and scientific programs. Issued six times a year.

Nonperiodicals

Monographs—Major contributions to the technical literature on various subjects related to the Institute's scientific and technical activities.

Handbooks—Recommended codes of engineering and industrial practice (including safety codes) developed in cooperation with interested industries, professional organizations, and regulatory bodies.

Special Publications—Include proceedings of conferences sponsored by NIST, NIST annual reports, and other special publications appropriate to this grouping such as wall charts, pocket cards, and bibliographies.

Applied Mathematics Series—Mathematical tables, manuals, and studies of special interest to physicists, engineers, chemists, biologists, mathematicians, computer programmers, and others engaged in scientific and technical work.

National Standard Reference Data Series—Provides quantitative data on the physical and chemical properties of materials, compiled from the world's literature and critically evaluated. Developed under a worldwide program coordinated by NIST under the authority of the National Standard Data Act (Public Law 90-396). NOTE: The Journal of Physical and Chemical Reference Data (JPCRD) is published bi-monthly for NIST by the American Chemical Society (ACS) and the American Institute of Physics (AIP). Subscriptions, reprints, and supplements are available from ACS, 1155 Sixteenth St., NW., Washington, DC 20056.

Building Science Series—Disseminates technical information developed at the Institute on building materials, components, systems, and whole structures. The series presents research results, test methods, and performance criteria related to the structural and environmental functions and the durability and safety characteristics of building elements and systems.

Technical Notes—Studies or reports which are complete in themselves but restrictive in their treatment of a subject. Analogous to monographs but not so comprehensive in scope or definitive in treatment of the subject area. Often serve as a vehicle for final reports of work performed at NIST under the sponsorship of other government agencies.

Voluntary Product Standards—Developed under procedures published by the Department of Commerce in Part 10, Title 15, of the Code of Federal Regulations. The standards establish nationally recognized requirements for products, and provide all concerned interests with a basis for common understanding of the characteristics of the products. NIST administers this program as a supplement to the activities of the private sector standardizing organizations.

Consumer Information Series—Practical information, based on NIST research and experience, covering areas of interest to the consumer. Easily understandable language and illustrations provide useful background knowledge for shopping in today's technological marketplace.

Order the **above** *NIST publications from: Superintendent of Documents, Government Printing Office, Washington, DC 20402.*

Order the **following** *NIST publications—FIPS and NISTIRs—from the National Technical Information Service, Springfield, VA 22161.*

Federal Information Processing Standards Publications (FIPS PUB)—Publications in this series collectively constitute the Federal Information Processing Standards Register. The Register serves as the official source of information in the Federal Government regarding standards issued by NIST pursuant to the Federal Property and Administrative Services Act of 1949 as amended, Public Law 89-306 (79 Stat. 1127), and as implemented by Executive Order 11717 (38 FR 12315, dated May 11, 1973) and Part 6 of Title 15 CFR (Code of Federal Regulations).

NIST Interagency Reports (NISTIR)—A special series of interim or final reports on work performed by NIST for outside sponsors (both government and non-government). In general, initial distribution is handled by the sponsor; public distribution is by the National Technical Information Service, Springfield, VA 22161, in paper copy or microfiche form.

U.S. Department of Commerce
National Institute of Standards and Technology
(formerly National Bureau of Standards)
Gaithersburg, MD 20899

Official Business
Penalty for Private Use $300